Electrical Characterization of Biological Elements by Atomic Force Microscopy

Ignacio Casuso Páramo

Electrical Characterization of Biological Elements by Atomic Force Microscopy

Ignacio Casuso Páramo

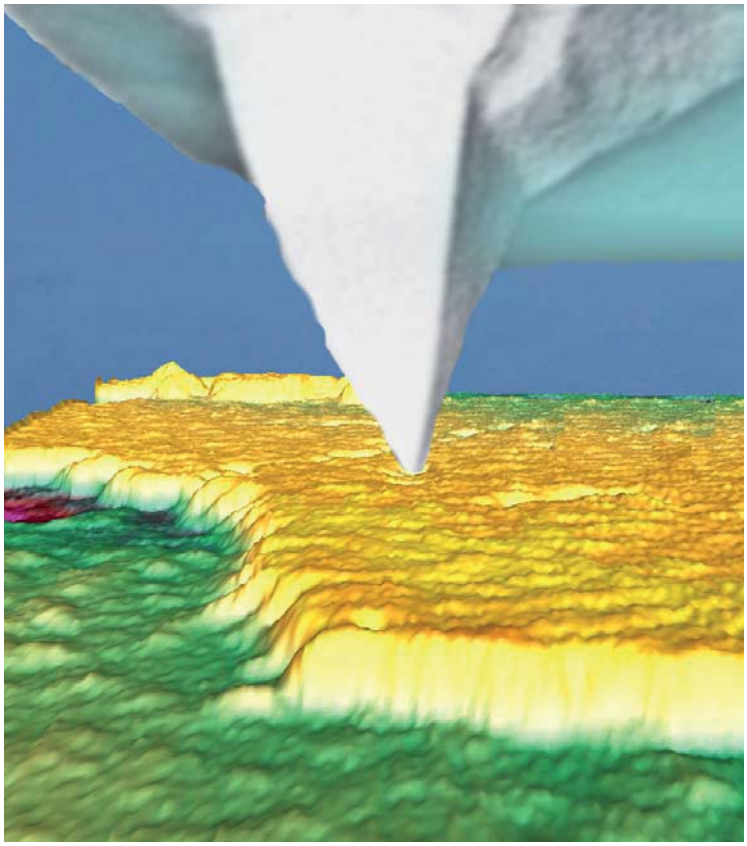

Departament d'Electronica

UNIVERSITAT DE BARCELONA

Universitat de Barcelona
Facultat de Física
Departament d'Electrònica

Electrical Characterization of Biological Elements by Atomic Force Microscopy

Memoria presentada para optar al título de Doctor en Ciencias Físicas

Programa de doctorado: Enginyeria i Tecnologies Electròniques
Bienio: 2002-2004

Autor: Ignacio Casuso Páramo
Director de tesis: Gabriel Gomila Lluch

El Dr. Gabriel Gomila Lluch, Profesor Agregado del Departament d'Electrònica de la Universitat de Barcelona

CERTIFICA:

que la memoria " Electrical Characterization of Biological Elements by Atomic Force Microscopy" que presenta el Sr. Ignacio Casuso Páramo para optar al grado de Doctor en Ciencias Físicas ha sido realizada bajo su dirección.

Barcelona, 10 de Enero de 2008

Dr. Gabriel Gomila Lluch

The cover image is a cartoon of an atomic force microscopy probe on a patch of purple membrane for electrical measurement, by *Ignacio Casuso*.

Resumen de la tesis

Una de las cualidades más significativas de los seres vivos es su gran capacidad para la detección de señales, solo gracias a la gran capacidad de discriminación, especificidad y sensitividad de las biomoléculas que componen los seres vivos la vida es posible. Siendo concientes de esta circunstancia es indudablemente tentador hacer uso de las propiedades biomoléculas para la fabricación biosensores, usando los biomoléculas los biosensores estarán dotados de las mismas altas capacidades de detección que las biomolecules mismas.

Gracias a los avances en la micro/nanofabricación y en biología molecular que han tenido lugar a lo largo de la última década las expectativas de aplicación de las biomoléculas en la fabricación de biosensores está en rápido aumento, y con ello la cantidad de actividad en el sector. De alta importancia ha sido la reducción de las dimensiones de los biosensores (miniaturización), ya que este hecho produce en los biosensores una mejor transducción de la actividad de las biomoléculas en señales procesables, y gracias a ese hecho cada vez un mayor número de biomoléculas pueden ser usadas para la fabricación de biosensores.

Es importante constatar que de todos los modos de transducción posibles para la fabricación de biosensores la transducción eléctrica proporciona la más directa integración de las biomoléculas en los biosensores. Desde un modo de vista técnico, el uso de la transducción eléctrica, posibilita que las biomoléculas puedan ser consideradas un componente del circuito eléctrico del biosensor, hecho que aumenta las posibilidades de miniaturización hasta escalas nanométricas, la escala misma de las propias biomoléculas, y de tal modo maximiza las prestaciones de futuros biosensores.

La tesis aquí presentada, consciente de las circunstancias científico-técnicas actuales previamente explicadas tiene como objetivo conseguir un avance en las técnicas de caracterización eléctrica cuantitativa de biomoléculas a la nanoescala para generar herramientas que puedan asistir tanto en el diseño como en el desarrollo de biosensores eléctricos.

La herramienta que ha sido seleccionada para llevar acabo el trabajo de la tesis ha sido el microscopio de fuerzas atómicas o AFM, esta técnica es capaz proporcionar a escalas nanométricas, y de manera simultanea, una caracterización topográficas y eléctrica, así mismo, el AFM puede operar en una amplia variedad de condiciones ambientales (vacío, gaseoso, líquido, y altas y bajas temperaturas) posibilitando el estudio de las propiedades eléctricas de las biomoléculas en una espectro de circunstancias, incluyendo soluciones fisiológicamente activas.

A pesar de la gran potencialidad del AFM para la caracterización eléctrica de biomoléculas su uso para este objetivo no es trivial, hecho que ha propiciado que hasta el momento el número de trabajos científicos en la materia sea limitado (<20). Este hecho es debido a la dificultad técnica de combinar la fragilidad de las biomoléculas, con la dureza y el gran tamaño de las puntas de AFM, así como con las elevadas fuerzas electrostáticas generadas por los potenciales aplicados. Ser capaz de combinar estos tres factores para maximizar la información eléctrica obtenida de las biomoléculas sin que su estructura sea destruida requiere una comprensión de los aspectos físicos y peculiaridades que gobiernan las medidas eléctricas de las biomoléculas con AFM para el desarrollo de protocolos operacionales de AFM.

Todos los trabajos encontrados en literatura han sido realizados con medidas DC, sin embargo también es posible realizar medidas eléctricas en AC. Es más no si no la suma de ambas contribuciones la que proporciona el comportamiento eléctrico de cualquier material, y de la biomoléculas en particular. La componente DC expresa el mecanismos de conducción y la componente AC las propiedades de polarización. En este trabajo de tesis nos adentramos en ambas disciplinas para ofrecer la máxima información eléctrica posible sobre las biomoléculas.

En el ámbito de las medidas DC se han desarrollado dos protocolos, uno de mapeo eléctrico y de medidas corriente-tensión en un solo punto (2).

Dada la fragilidad inherente a las biomoléculas no es posible utilizar el *modo de contacto*, modo estándar de mapeo eléctrico con AFM, con biomoléculas. El *modo de contacto* arrastra la punta sobre la muestra genera fuerzas de fricción suelen causar daños en las biomoléculas por las que pasa. Por lo tanto, es necesario encontrar un modo de mapeo que produzca una menor fricción. Una posibilidad que ha sido probada con éxito es el *modo de jumping*, la principales características del *modo de jumping* es realización del movimiento lateral de la punta fuera de contacto con la muestra, de esta manera se minimizan las fuerzas de fricción aplicadas en la muestra, y que después de cada movimiento lateral contacta la muestra con fuerza y por un tiempo programado. En esta tesis se demuestra que el *modo de jumping* es apropiado para el mapeo eléctrico de las biomoléculas y es capaz de identificar particularidades en la distribución espacial de la de la conducción de las biomoléculas.

El protocolo para la realización de medidas corriente-tensión en un solo punto de la biomolécula ha conseguido aumentar considerablemente la información eléctrica obtenida con respecto a las medidas corriente-tensión con AFM en biomoléculas presentes en literatura. El protocolo está basado en un aumento con respecto a las referencias en literatura de la rigidez de las sondas de AFM utilizadas, que han pasado de una constante de fuerzas de 2 N/m, a una constante de fuerzas de 40 N/m. Gracias a este aumento de la constante de fuerzas la deflexión de la sonda del AFM producida por campos electrostáticos aplicados se ve altamente reducida, y posibilita un aumento del potencial aplicado sin que este cause que la deflexión de la sonda del AFM dañe a la biomolécula, que es principal factor limitador del voltaje aplicado en los experimentos en literatura, de esta manera el potencial puede ser aumentado de 1 V a 9 V.

Sin embargo, el uso de sondas con constantes de fuerzas tan elevado no permite el uso de los procesos estándar para el posicionamiento vertical de la punta de AFM sobre la muestra, procesos que están basados en la monitorización de la deflexión de la sonda, y que en este caso, al ser tan rígida la sonda, no pueden ser realizados, ya que dañaría la muestra y la

medida eléctrica corriente-tensión quedaría invalidada. Una estrategia alternativa, que ha sido realizada en esta tesis, es posicionar verticalmente la punta usando una aproximación escalonada, donde en cada escalón se realiza medida eléctrica corriente-tensión. Esta estrategia permite caracterizar todo el rango deseado de posiciones en el eje Z con medidas corriente-tensión (punta está en el aire, punta a tocado ligeramente la biomolécula, y progresiva indentación de la punta en la biomolécula). Además, es posible determinar la distancia substrato-punta durante toda la medida gracias a la medida la deflexión de la sonda y del moviendo del posicionador vertical. La distancia substrato-punta no había sido previamente determinado en las medidas corriente-tensión en biomoléculas en literatura. Se hace notar que para el posicionamiento lateral de la punta en el plano XY el *modo dinámico* es utilizado tanto para sondas de 2 y 40 N/m, el *modo dinámico* oscila la punta continuamente, minimizando la fuerza de fricción.

Gracias las mejoras introducidas en el protocolo de adquisición de medidas corriente-tensión para biomolecules ha sido posible la observación por primera vez en un material biológico de una transición entre dos regimenes de transporte eléctrico por efecto túnel, en particular, entre el régimen de túnel directo y el régimen de Fowler-Nordheim o de injección, este hecho a posibilitado la la determinación directa del potencial de barrera Φ creado por la presencia de la biomolécula entre dos metales, y que está directamente relacionado con voltaje de transición entre ambos regimenes. Este hecho puede ser usado, siguiendo el modelo de Simmons para la conducción en sistemas Metal-Asilante-Metal, usando los valores de potencial de barrera Φ, y de distancia punta-substrato para extraer la masa efectiva m* de los electrones cuando atraviesan la biomolécula para una determinada distancia punta-substrato de compresión de la biomolécula (nunca antes medida en una muestra biológica).

En ámbito de las medidas AC en biomoléculas también se han desarrollado dos protocolos, uno dirigido al mapeo de la capacidad y con aplicación en la medida del espesor de capas no accesibles de

biomoléculas, y otro dirigido a la medida de la constante dieléctrica de la biomoléculas. Sin embargo, la obtención de medidas cuantitativas en AC requiere de la calibración de la sonda, que puede ser considerado como un tercer protocolo.

Las medidas AC realizadas en la tesis se basan en la variación de capacidad generada entre substrato conductor y sonda en respuesta a una variación de sus posiciones relativas. Para distancias substrato-punta inferiores a algunas decenas de nanometros se ha observado experimentalmente que la variación de capacidad está dominada por la variación de la capacidad entre substrato conductor y punta, y por lo tanto la variación observada es una medida directa de la propiedades locales del material presente entre punta y muestra. Sin embargo, dado que las dimensiones de las puntas de AFM son pequeñas y tienen radios de curvatura de 100 a 200 nm, las variaciones de capacidad son también extremadamente pequeñas (~ aF) y una alta resolución de medida en capacidad es necesaria. Este hecho complica las medidas AC ya que exige altos tiempos de promediado por píxel (~ 0.1 s), y esto aumenta la influencia de la deriva en la posición de la punta. Métodos de corrección de deriva son necesarios basados en la comparación de curvas de deflexión de la sonda del AFM con respecta a la posición vertical a baja y altas velocidades.

La calibración de la punta se realiza mediante una curva capacidad-Z, esta curva una vez comparada con un modelo de capacidad punta-substrato proporciona una parametrización de las dimensiones de la punta.

El mapeo en AC se realiza, igual que en DC, usando el *modo de Jumping*, como ya se ha comentado este modo permite minimizar la fuerza de fricción y controlar, además de la fuerza aplicada por la punta en cada píxel, el tiempo que permanece la punta en contacto con la muestra. Sin embargo, para tiempos tan largos como los requeridos para obtener suficiente resolución (~ 0.1 s) en capacidad para resolver la capacidad de la punta el sistema de AFM se vuelve inestable, por lo tanto es preferible

usar tiempos menores (~ 0.05 s), escanear repetidamente la misma línea y promediarlas.

Un hecho destacado con respecto a la capacidad entre la punta del AFM y el substrato conductor es su dependencia logarítmica, completamente diferente de la dependencia lineal del capacitor plano paralelo, y confiere al sistema punta de AFM-substrato algunos comportamientos singulares. Uno de estos comportamientos se observa en la variación vertical de la capacidad con respecto a Z que es independiente en primer orden de aproximación de la constante dieléctrica del material presente entre punta y substrato. Por lo tanto es solo dependiente de Z, este hecho puede ser utilizado en casos cuando una substrato conductor de un biosensor esta completamente cubierto por biomoléculas para determinar el grosor de la capa inferior y oculta de biomoléculas a partir de la medida de la variación relativa de capacidad al escanear la punta la topografía de la capas de biomoléculas superiores. Este hecho ha sido demostrado experimentalmente.

La capacidad entre punta y substrato si es dependiente del material presente entre punta y substrato si este material cambia (o la proporción de este) cambia. Este hecho puede ser aprovechado para medir la constante dieléctrica de una biomolécula. Para ello se ha desarrollado el *protocolo de Flying*, este protocolo consiste en desplazar la punta a distancia punta-substrato constante por el cima del borde una biomolécula, o de una colección de ellas. En el momento que la punta pase por encima del borde de la biomolécula la capacidad experimenta un salto, que si la punta esta calibrada y la distancia punta-substrato es conocida puede ser transformada en la constante dieléctrica de la biomolécula. Este hecho también ha sido demostrado experimentalmente.

Finalmente conviene aclarar que los protocolos desarrollados han sido concebidos con afán de globalidad y de aplicación a cualquier biomolécula, sin embargo han sido desarrollados en su totalidad en Membrana Púrpura PM, sin que este hecho les quite la generalidad de su

aplicación. La PM es una membrana celular proveniente de la halobacteria y que contiene un alto (75%) contenido en proteína. Los experimentos han sido realizados a temperatura ambiente en atmósfera de nitrógeno a 0% humedad, condiciones el las que la PM mantiene su actividad biológica y evita su degradación.

En global, el gran éxito de este trabajo ha sido la demostración de las excelentes características que el AFM prosee para convertirse en una herramienta adaptada para la asistencia de desarrollo de los biosensores eléctricos en su ruta hacia la miniaturización a la nanoescala.

Acknowledgements

I would like to dedicate this work of thesis first to my family and old times friends and secondly to Barcelona and all the people I have met in this wonderful city and with whom I have shared so many experiences with both in the lab and outside the lab. This work would not have been possible without the contribution of all the people present in the Nanobiolab, IBEC and Departament of Electrònica of the Universitat de Barcelona; I would especially like to acknowledge the support and extremely valuable help of my mentor Gabriel Gomila and of my closest hands-on labmate Laura Fumagalli with whom I have shared so many hours of work and pondering, of great importance has been also the contribution of Jordi Toset for its insights on the physics behind the AFM operation. I cannot forget Esteve Padròs from the Universitat Autònoma de Barcelona whose has made this work possible thanks to his kind contribution of biological sample and of its expertise. Finally, out of Barcelona, especially important have been the contributions of Ron Reifenberger from the Purdue University and Julio Gomez from the Universidad Autónoma de Madrid who have accepted me on their labs for several months stays, and only thanks to their advice and guidance this work of thesis have been possible.

INDEX

Chapter 1. Introduction

Chapter 2. The atomic force microscopy and the electrical characterization of biomolecules

Chapter 3. The set-up

Chapter 4. Development of atomic force microscopy protocols for the electrical characterization of biomolecules

Chapter 5. The test sample

Chapter 6. Direct current conductive atomic force microscopy mapping of the purple membrane

Chapter 7. Point contact current-voltage spectroscopy on purple membrane monolayers

Note: In the appendix additional information on biological terms such as enzyme, membrane protein, and topics such as protein polarizability or electron transport in proteins, and biological and physical aspects related to sensors is provided.

Chapter 1. Introduction

Summary: Chapter 1 frames the objective of this work of thesis. First, it provides a general view of the field of biosensors, and a focus on the motivation for electrical biosensing, indicating its advantages. It follows by highlighting the relation between miniaturization and the electrical biosensors, a fruitful relation which needs from new nanotools for its development. It is demonstrated that the scanning probe microscopies, and particularly the atomic force microscopy, is one of the best possible options for this task, once the required modification are performed.

1.1. Short introduction to biosensors

One general characteristic of living organisms is their great capability for signal detection; sensing their surrounding environment is critical for the survival of living organisms. This sensing efficiency is much higher than their man-made counterparts, the sensors, not only living organisms detect a much wider spectrum of signals, but do it with a precision the man-made sensors are far from achieving. An illustrative example can be found in gas detection (i.e. smell in living organisms terminology), smell is performed in superior organisms by a family of membrane proteins called olfactory receptors (ORs), in the case of the dog, ORs are able of differentiating between tens of thousands up to one million gaseous compounds at a high sensitivity of 10^{-17} M. On the other hand, the man-made gas sensors, based in the variation of the electrical properties of semiconductor in a response to gas exposure, are much more modest, and are limited to a detection spectrum of a few tens of gas compounds detectable at a sensibility of 10^{-4} M, thirteen orders of magnitude lower!

Being obvious that living organisms and the biomolecules in them provide far superior performance for sensing than their man-made equivalents it is tempting to harness the biomolecules to some generic biosensor that could thus be endowed with some of the most prominent properties of biomolecules: discrimination, specificity and sensitivity. But to harness the biomolecules it is required to establish an information transcription system that transcripts the activity of the biomolecules to the electronic circuitry for the information processing. Fig. 1a shows an scheme of a biosensor, and Fig. 1b a simplified diagram of the information processing pathway.

Only recently, on the last decade, the technical developments in the fields of micro/nanofabrication and molecular biology have yielded increasing expectations for a wider application of the biosensor concept to the medical and environmental technologies which has resulted in a boom of the activity in research and the development in the field of biosensors, due to the perspective of high returns of initial investment. The boom of the activity in biosensor can be clearly observed looking at the number of scientific publications per year on the topic of biosensors, number which can be obtained simply by introducing the string 'biosensor' in a scientific papers research engine, see Fig. 1c. Thanks to the new technologies that allow the reduction of the dimensions, biosensors are improving their speed, sensitivity, sample consumption, cost, parallel working, and portability [1,2,3]. These all excellent perspectives are still in development and due to the long development times of biosensors (~10 years) still only a handful of biosensors are present in the marke

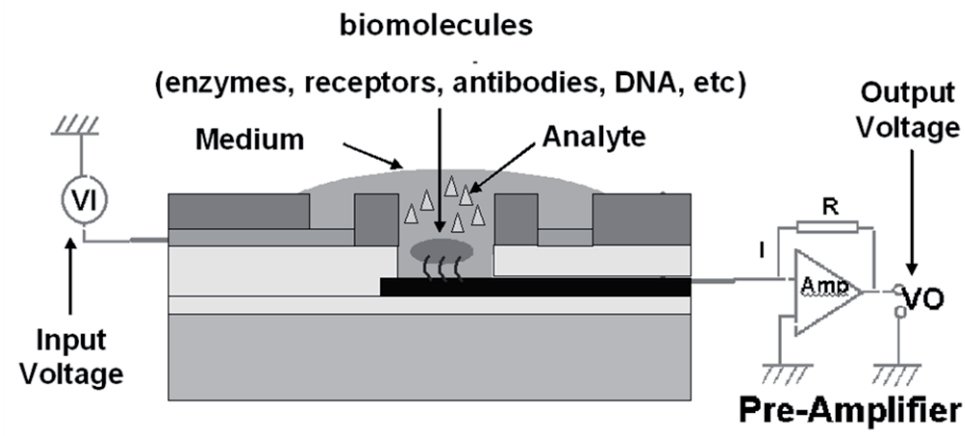

(a)

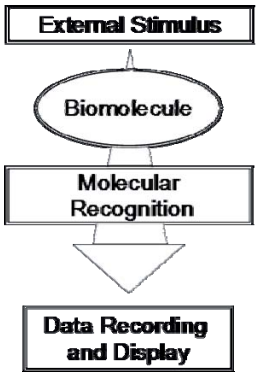

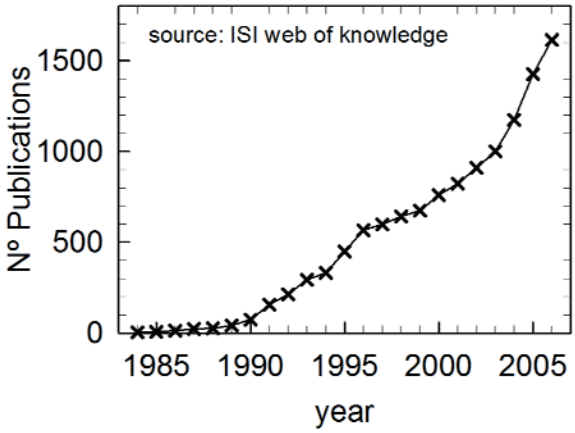

(b) (c)

Fig 1. (a) Cartoon showing the components of a biosensor. (b) Simplified diagram of the information pathway in a biosensor. (c) Evolution of the number publications per year of scientific articles that include the string 'biosensor' in the title and/or abstract.

1.2. Electrical biosensors

Electrical transduction techniques provide the most direct integration of biomolecules in a biosensor, this way biomolecules can be inserted directly in the circuitry of the biosensors, and in a technical sense, the biomolecules pass to be considered an additional component of the electronic set-up. The direct configuration of the biomolecules in the biosensor using electrical transduction entails a direct application of the recent advances in micro and nanoelectronics to biosensor technology miniaturization, and therefore to the performance benefits associated with miniaturization.

From all the available biomolecules, at the current time the electrical biosensors, almost exclusively make use of enzymes. Enzymes are the easiest possible biomolecule to perform electrical transduction with: enzymes are active electrochemical proteins where redox reactions occur, thus the activity of enzymes modifies chemically the surroundings, and this event may be used to easily monitor the biological activity of enzymes using electrochemical techniques. Thanks to use of enzymes biosensor technology has accomplished its higher successes.

Nevertheless, the dynamism of the research of electrical biosensors based on enzymes has kicked downstairs the use of other types of biomolecules for electrical biosensor technology. For instance, there is an ocean of possibilities to be explored in the study of biomolecules lacking from redox activity for its use in electrical biosensors. An increasing number of research groups is working in the implementation of non-redox biomolecules in electrical biosensors for which non-electrochemical transduction mechanisms are necessary: one recent application from *Varo and coworkers* [4,5] used bacteriorhodopsin to fabricate an electrical biological photoreceiver, see Fig. 2, on the other hand, *Dai and coworkers* [6] are working in the development of transductors that use nanotubes to transduce the activity of a variety of non-redox biomolecules. Nevertheless, the majority of researches run away from the

difficulties of electrical transduction towards safer approaches, mainly optical, which lack of the potential of development of electrical transduction but produce shorter term results. The success of non-redox optical biosensors technology of today for the early detection of prostate cancer with fluoresce microarrays [7], and the detection of the sepsis syndrome with a fiber optic evanescent wave [8], give us an indication of the potential of the non-redox electrical biosensor of tomorrow.

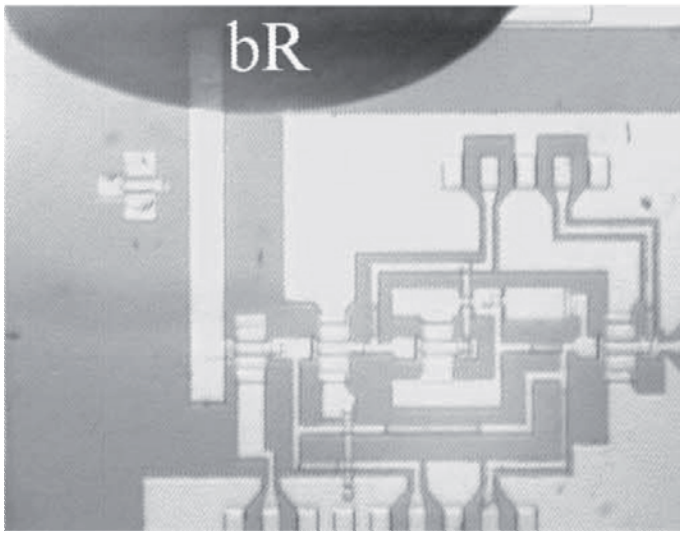

Fig. 2. Micrograph of an electrical biosensor based in the transduction of a non-redox protein, the bacterorhodopsin bR, from *Xu et al.* [5].

High efforts are required to develop biologically friendly technologies with enough sensitivity for an effective electrical monitoring of the subtle activity of non-redox biomolecules. The current trend towards the miniaturization of biosensors is improving the performance and taking the dimensions of the biosensors down to the nanoscale. The miniaturization of biosensors represents a great challenge which requires new knowledge and expertise on the functioning of the biological systems at such small scales, and how they interact with the circuit components that have the same scale as the biomolecules themselves. The task is difficult, but the reward is waiting.

1.3. Tools to assist the development of electrical biosensors

To achieve electrical biosensors in the micro/nanoscale, new tools able of characterizing electrically the biosensors at those small scales are required to assist the research, development and fabrication stages. Miniaturization is especially important for non-redox electrical biosensors fabrication where high levels of sensitivity are required to detect the biological activity. In the case of enzyme based electrical biosensors, the development of miniaturized electrical biosensors is not a vital need but a useful help which will improve their performance thanks to the improvements linked to the reduction of dimensions.

One important characteristic of the new tools is that they must be capable of performing electrical characterization at the nanoscale simultaneously to control the damage on the biomolecule, task not easy because the biomolecules are soft and of nanoscale dimensions whereas the probes used for the electrical measurements are stiff and of micrometric dimensions. Combining such different characteristics and controlling the damage on the samples is something that is a real challenge.

Another important characteristic of the new electrical tools is that they must be capable of working in liquid environments. Although there are some biomolecules that can work in dry environments, in most cases the functioning of biomolecules requires from liquid environments, and consequently the biosensors will in most cases be used in wet conditions or submerged in liquid solutions. It is therefore important that the tools can work in a variety of physical environments which includes the gaseous and liquid environments.

1.4. The scanning probe microscopy and the electrical characterization of biomolecules

One group of techniques that satisfies the criteria described in section 1.3 is the Scanning Probe Microscopy (SPM). The SPM consists in a sharp probe that moves in close proximity with the sample guided by a feedback system. The SPMs provide topographic information on the nanoscale structure of the sample in combination with other types of measurements including a variety of electrical characterizations. Using SPM it is possible to perform at the nanoscale: *conduction mapping*, *current-voltage curves*, *impedance mapping*, and *impedance spectroscopy*.

The SPM techniques have seldom been used for the electrical characterization of biological samples, at this time there is a lack of methodologies for this application. The standard methodologies used in the electrical characterization with SPM do not fit to its biological use because they tend to produce damage to the samples. The new needs for fabricating biosensors at the nanoscale are driving new attention to this field, new protocols are necessary to adapt the SPM techniques to the new technological requirements.

The family of the SPMs is divided mainly into two branches, each of one with different operational properties. Such difference comes from the different physical signal each branch uses to control the position of the probe. The two branches are termed Scanning Tunneling Microscopies (STM) and Atomic Force Microscopy (AFM)*:

* In this work of thesis, we deal with electron transport, therefore the techniques related to the ion transport like Scanning Ion Conductance Microscopy SICM and electrochemical ECM-AFM are not discussed here.

▪ The STM branch uses conductive probes to scan conductive samples, only thin layers of non-conductive materials can be present over the conductive substrate. The physical functioning of STM is based in the quantum tunneling of the electrons between the probe and the substrate when the distance between the probe and sample is only few nanometers. In these circumstances, the electron flow depends exponentially on the tip-substrate distance, and thus it can be used as a signal to control the vertical position of the probe. To obtain an image, the probe is scanned across the sample and at each point the vertical displacements of the probe is recorded, the combination of all the movements of the probe draws the topographic profile of the sample. The STM is capable of acquiring *current-voltage curves*, for this the scanning of the probe is stopped and the bias between substrate and probe ramped. STM is usually operated under ultra high vacuum, in these circumstances the STM easily achieve topographic atomic resolution, this high resolution is a consequence of the small area from which electrons are emitted at the end of the conducting probe, only a few atoms at the end of the tip of the probe. STM operation under air and liquid media is possible but with a drastic reduction of its performance.

▪ On the other hand, the AFMs operation is based in a force sensitive probe composed of a cantilever which holds a tip at the end. Thanks to the structure of the probe the force of interaction between the tip and the substrate is monitored and used by the AFM system to control the vertical position of the probe. The use of the force instead of the electric current as operational signal enables the AFMs to characterize any sample independently of its conductive nature. This fact is also very positive for the electrical characterization, because when conducting AFM probes are used it is possible to uncouple the electrical signal from the positioning of the probe, and thus have a better control of the position of the probe during the electrical measurement. The only drawback of AFM is that the lateral resolution is lower than the STM, instead of resolving atoms, i.e. angstrom

resolution, nanometers are generally resolved (only in special cases angstrom resolution is achieved). Nevertheless a nanometric resolution is enough for the electrical characterization of biomolecules because it allows easy location of the biomolecules where the electrical measurements want to be performed. Finally, as in the case of the STM, the AFM can be operated under ultra high vacuum, air and liquid environments.

The idea of using the SPM for the electrical study of biomolecules at the nanoscale is not new. In 1985, three years after STM invention in 1982 [9], it was shown that, under certain conditions, it was possible to perform STM imaging on biomolecules [10]. Since 1982, STM has been used to image the spatial distribution of the electron conduction through the biomolecules in a variety of liquid/wet environments. Numerous biomolecules that have been imaged taking advantage of the STM high spatial lateral resolution, and STM has been used for the differentiation of different areas of biomolecules [11], and for exploring the different conduction mechanisms of the electron transport through the biomolecules [12]. The drawback of STM is that a strict quantitative electrical analysis is not possible because the position of the probe cannot be uncoupled from the sample conduction, remaining the precise position of the probe during the electrical measurements unknown.

The electron conduction maps of STM were enough to satisfy the demand of electrical information from biomolecules for a long period of time, even if the conductive AFM started in 1992 [13], and it was not until the year 2000 that the AFM was first used to perform an electrical measurements in a DNA string, and it took until 2004 to perform the first electrical measurement using the AFM in a protein system [14,15]. Thanks to the use of AFM the electrical information is more quantitative, nowadays a total of 11 publications have been performed on DNA and 7 on proteins.

It is evident that there is some pulling technological force which has awakened the interest in the use of AFM for the electrical characterization

of biomolecules. Undoubtedly, one of the main factors is the activity in biosensors (Fig. 1a and Fig. 2), and their miniaturization. This idea of assisting the development of protein based electrical biosensors with electrical measurements with the AFM is clearly commented in both of the papers from Stamouli [14] and Zhao [15].

In spite of the increasing use of the AFM for the electrical characterization of biomolecules, the protocols for its application are not yet adapted to this task. As a matter of fact, the totality of the electrical measurements found in the literature is restricted to a strict range of AFM working conditions where the standard AFM methodologies do not damage the biomolecules. The adaptation of the AFM to the electrical characterization of biomolecules requires from a solid knowledge based expertise in the AFM technology. These modifications are not evident, otherwise they would have been previously developed, but the effort is worthy because it broadens the information spectrum for the electrical study of the biomolecules and their incorporation into electrical biosensors.

1.5. Objective of the thesis

The objective of this work of thesis can now be clearly drawn and stated as *'Advancing the electrical characterization of biomolecules at the nanoscale using the atomic force microscopy AFM for the acquisition of quantitative electrical information'*. This objective will be possible thanks to the understanding the physical aspects that govern the AFM electrical measurements on biomolecules, and will yield access to new types of electrical information that, once framed in theoretical models, will allow to play an active role in the future development of electrical biosensors.

1.6. References

1 J. S. Daniels and N. Pourmand, "Label-free impedance biosensors: Opportunities and challenges," Electroanalysis **19** (12), 1239-1257 (2007).

2 R. C. McGlennen, "Miniaturization technologies for molecular diagnostics," Clinical Chemistry **47** (3), 393-402 (2001).

3 A. Bange, H. B. Halsall, and W. R. Heineman, "Microfluidic immunosensor systems," Biosensors & Bioelectronics **20** (12), 2488-2503 (2005).

4 J. Shin, P. Bhattacharya, J. Xu et al., "Monolithically integrated bacteriorhodopsin-GaAs/GaAlAs phototransceiver," Opt Lett **29** (19), 2264-2266 (2004).

5 J. Xu, P. Bhattacharya, and G. Varo, "Monolithically integrated bacteriorhodopsin/semiconductor opto-electronic integrated circuit for a bio-photoreceiver," Biosens Bioelectron **19** (8), 885-892 (2004).

6 R. J. Chen, S. Bangsaruntip, K. A. Drouvalakis et al., "Noncovalent functionalization of carbon nanotubes for highly specific electronic biosensors," Proceedings of the National Academy of Sciences of the United States of America **100** (9), 4984-4989 (2003).

7 C. D. Chen, S. F. Cheng, L. K. Chau et al., "Sensing capability of the localized surface plasmon resonance of gold nanorods," Biosens Bioelectron **22** (6), 926-932 (2007).

8 E. A. James, K. Schmeltzer, and F. S. Ligler, "Detection of endotoxin using an evanescent wave fiber-optic biosensor," Applied Biochemistry and Biotechnology **60** (3), 189-202 (1996).

9 G. Binnig, H. Rohrer, C. Gerber et al., "Tunneling through a Controllable Vacuum Gap," Appl Phys Lett **40** (2), 178-180 (1982).

10 A. M. Baro, R. Miranda, J. Alaman et al., "Determination of Surface-Topography of Biological Specimens at High-Resolution

by Scanning Tunnelling Microscopy," Nature **315** (6016), 253-254 (1985).

11 A. Bandyopadhyay, K. Nittoh, Y. Wakayama et al., "Global tuning of local molecular phenomena: An alternative approach to bionanoelectronics," Journal of Physical Chemistry B **110** (42), 20852-20857 (2006).

12 P. B. Lukins and C. S. Barton, "Evidence for spatially-coherent trans-molecular electron tunnelling through two-dimensional arrays of Photosystem II core complexes," Chem Commun (5), 602-603 (2003).

13 D. Anselmetti, C. Gerber, B. Michel et al., "Compact, Combined Scanning Tunneling Force Microscope," Rev Sci Instrum **63** (5), 3003-3006 (1992).

14 A. Stamouli, J. W. M. Frenken, T. H. Oosterkamp et al., "The electron conduction of photosynthetic protein complexes embedded in a membrane," Febs Lett **560** (1-3), 109-114 (2004).

15 Y. Liu, M. K. Wang, F. Zhao et al., "The direct electron transfer of glucose oxidase and glucose biosensor based on carbon nanotubes/chitosan matrix," Biosens Bioelectron **21** (6), 984-988 (2005).

Chapter 2. The atomic force microscopy and the electrical characterization of biomolecules

Summary: In chapter 1 it was explained that the Atomic Force Microscopy (AFM) holds an intrinsic interest for its application to the electrical study of biomolecules at the nanoscale. In chapter 2 this idea is extended and investigated in detail. First, it is explained the basic technical fundaments for the understanding of application of the AFM to the electrical characterization of biomolecules, and the difficulties of such application, highlighting those aspects in where the AFM application can be improved and new AFM developments performed. Finally, we review in closer detail the results in the current literature.

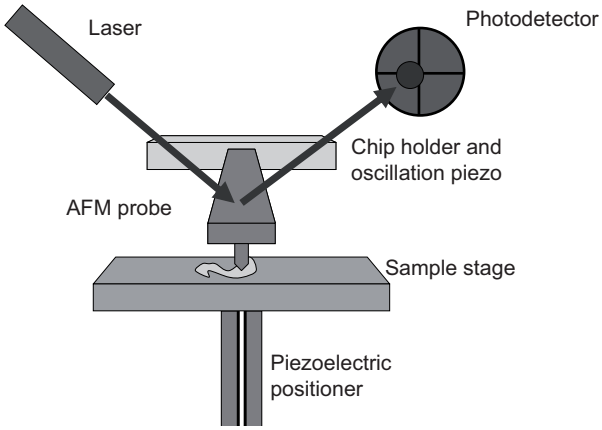

Fig. 1. Cartoon showing the basic components of an AFM set-up.

2.1. The must-know topics for the electrical characterization of biomolecules

The AFM is essentially a surface profilometer with lateral and vertical resolution ranging from subnanometer distances to few tens of nanometers. An AFM consists of five basic components (see Fig. 1): a sharp probe, a piezoelectric stage to raster the probe or the sample, a laser directed towards the probe, a photodetector to monitor probe deflection and measure the force applied to the sample, and a feedback system.

From this simple scheme, a host of operating methods and techniques to measure a variety of physical properties have been developed since the AFM invention in 1986 [1]. Typically, the spatial vertical resolution is higher than the lateral one by one or two orders of magnitude, and subnanometric lateral resolution is only obtained in special liquid conditions or under vacuum environment.

The AFM probes are commercially available. The probes consist of a sharp tip fabricated at the very end of a pliable cantilever that works as a Hookian spring. Cantilevers are generally made of Si or Si_3N_4 and can be purchased coated with various materials for electrical or magnetic measurements. The final tip radius is generally 20-50 nm in non-coated probes and 100-200 nm in coated probes.

The great value of AFM is its versatility. It can be operated in a variety of modes, environments (gases, liquids or vacuum) and temperatures; it is able to map the physical properties of the sample, and of single point spectroscopic measurements. Finally, it is especially useful for the electrical measurements because the probe position control system is independent from any electrical parameter.

Over the next subsections a host of AFM operating methods is described with special focus in its application for bioelectrical characterization.

2.1.1 Topographic atomic force microscopy modes

Contact mode is the basic operating mode of AFM, it works by maintaining the tip at a very short distance from the sample in the regime of Van der Walls force repulsion and controlling the applied force to the sample using the deflection of the cantilever that connected to the feedback loop maintains the force constant thanks to the vertical movement of the piezoelectric stage. The resulting vertical motion of the

scanner follows the topography of the sample and maps it simultaneously to any other measurement we may perform, see Fig 2. *Contact* mode produces a high applied lateral shear force on the sample and tends to damage soft samples such as biological material when operating in gaseous environments.

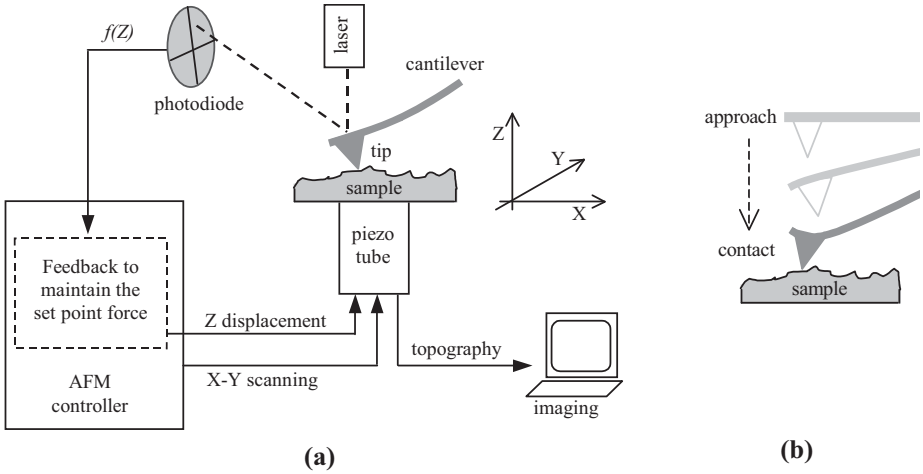

Fig. 2. (a) Simplified diagram of the AFM principle in *contact mode*. A constant deflection of the cantilever is maintained by a feedback loop to monitor the surface topography of the sample **(b)** contact mode approach.

Dynamic mode works by oscillating the cantilever which sustains the tip and performing the feedback on the amplitude of oscillation, see Fig 3. This methodology reduces the interaction between the tip and the sample, and enables that soft samples, as biological samples, can be imaged in gaseous environments without damaging them. Dynamic mode is not appropriate for electrical measurements because the continuous oscillation of the probe impossibilities a full control of the contact between sample and probe.

Jumping mode works by performing at each image point a cycle of tip retraction, lateral displacement and approach down to contact under force feedback control, see Fig. 4. This way lateral motion is performed at out

contact and the shear forces are reduced practically to zero, while simultaneously providing a good control of the contact with the sample, both the applied force and the time of contact are controlled. The control of the time in contact, not provided by the dynamic mode, enables that the electrical contact can stabilize and the measurement can be averaged over extended periods of time.

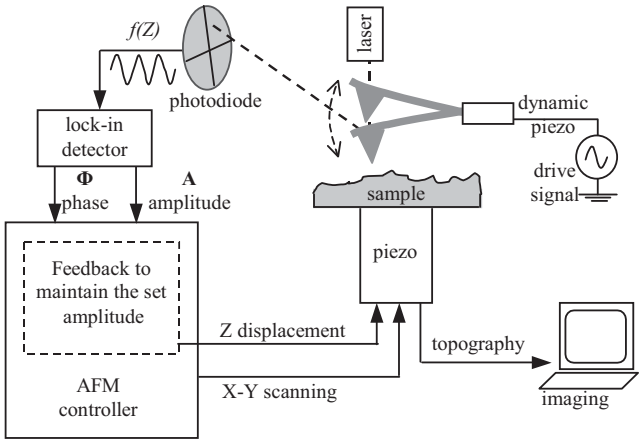

Fig. 3. Simplified diagram of the AFM principle in *dynamic mode*.

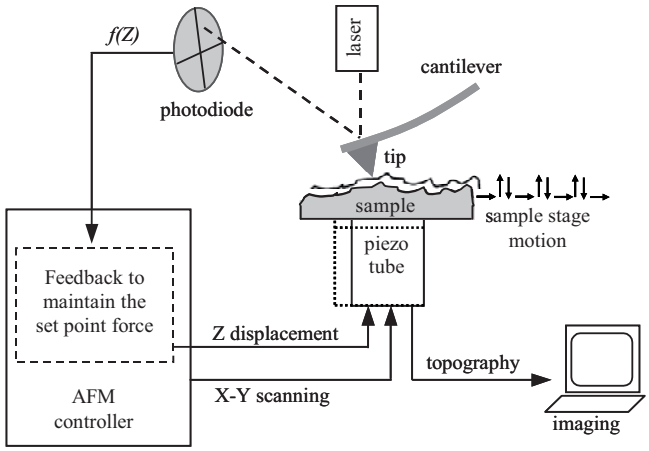

Fig. 4. Simplified diagram of the AFM principle in *jumping mode*.

2.1.2. Qualitative atomic force microscopy electrical characterization modes

Electrostatic modes. This group of techniques uses generally a double scan of the sample, they first record the topography using *dynamic* mode, and next scan at fixed distance from the sample the tip over the sample with an electric potential applied between tip and sample. This way it is possible to gather information on the distribution of some of the electrical properties of the sample. The electrical information is extracted from the oscillation of the probe which is influenced by the electrostatic forces generated by the sample. These techniques (*electrostatic force microscopy* and *kelvin prove microscopy*) provide good results, and are able to offer a clear contrast of the distribution of surface charges or dielectric areas over biological samples[2]. Nevertheless these methods only provide contrast, but the value of the electric potential in each area is not accessible, the oscillatory probe movement hinders a precise tip positioning.

Electrochemical AFM, SECM-AFM. This technique measures the DC current generated by electrochemical reactions which take place at or near the AFM probe, simultaneously AFM topographical information is also obtained. The contrast of the SECM-AFM images is obtained from the fact that when the probe is close to the substrate, the substrate perturbs the electrochemical kinetics at the probe, and this perturbation provides a qualitative electrochemical map of the activity regions of the sample with submicrometre-level precision. In order to improve the resolution, specific probes are in current development where an entire conducting probe is coated with an insulating material excepting the tip. These probes are not yet commercially available.

2.1.3. Quantitative electrical characterization: current sensing atomic force microscopy

The group of techniques of *current sensing AFM* (CS-AFM) *measurements* measures the transport of current through the sample. There are two versions; *conductive AFM* and *nanoscale impedance AFM*, both of the versions can be used to obtain quantitative electrical information of the samples, and both of them can be operated either in *contact* or *jumping* modes.

Conductive AFM (C-AFM), typically available with commercial equipment, probes the local current flowing though the conductive AFM tip when a bias is applied between tip and sample. Current detection is made by a transimpedance amplifier of different gains, depending on the current range, or a logarithmic amplifier when an extended range of current wants to be studied. It performs two types of measurements: a) *Point contact measurements*, where the tip is kept in contact with the surface at a fixed position and the current is measured while the bias of the conductive substrate is changed (*current-voltage spectroscopy or I-V curve*). In some cases the electrode is lateral and the substrate insulating. And b) *conduction mapping* of the sample, where the tip is scanned across the sample with the bias set at a constant value and the spatial variations of the current flow though the tip are registered, this provides a current map performed simultaneously to the topography acquisition.

Nanoscale impedance microscopy (NIM) is a technique that is not commercially available, and that was recently introduced by Shao et al.[3]. In the same way as C-AFM, it combines AFM with current measurements using two electrodes, one of them composed by the AFM probe and the other by the conducting substrate. NIM works by applying an input AC voltage signal at the substrate which generates an AC electric current that crosses the sample and arrives at the AFM probe, where it is measured. The interaction of the AC electrical signal and the sample is a source of information on the polarization mechanisms of the sample, the

important aspect of the information obtained is that it is extracted exclusively from the area of the sample that is between the AFM probe and the substrate, therefore it provides a local nanometric impedance characterization. Two types of measurements are possible, a) *frequency spectroscopy*, where the probe is in contact with the surface at a fixed position, and the input signal is scanned in frequency, thus enabling the study of the frequency behavior of the impedance, and b) *impedance mapping*, where the AFM tip is scanned across the sample mapping the impedance at each point at fixed voltage amplitude and frequency.

C-AFM and NIM characterizations combined can provide a set of information of great usefulness: a) The current-voltage characteristics of C-AFM determines the mechanism that governs the electron charge transport across the biomolecule, and b) the impedance measurements of NIM informs about the charge polarization of the sample. The combination of C-AFM and NIM measurements provides a full picture of the behavior of the charge in the sample. In electronics terms, the information C-AFM and NIM provide in combination is the equivalent to electrical data spreadsheet of the biomolecule, which would determine the way to integrate it into bio-hybrid electrical devices, for example a biosensor.

At the present time the CS-AFM techniques only can operate in gaseous and vacuum environments, important modifications would be necessary to adapt the techniques to the problems inherent to liquid operation as ionic currents or component degradation.

2.1.4. Problems that conventional current sensing atomic force microscopy finds for its application to biomolecules

Both types of conventional CS-AFM, C-AFM and NIM, present important problems for its application on biomolecules. Some of the problems are shared by both techniques but some are inherent to each one of them.

For the electrical mapping of biomolecules both C-AFM and NIM cope with the same problem, they require the tip to be in contact with the sample. In conventional AFM operation, the electrical mapping is performed in *contact mode*, but the use of *contact mode* generates high lateral shear forces on the sample that when applied on soft biological samples tend to produce irreversible damages invalidating the measurement. It is therefore necessary an adaptation of the conventional electrical mapping protocol for the case of biomolecules which is able to achieve a reduction of the applied shear force, and therefore avoids damaging the sample.

For C-AFM there is a specific problem for the acquisition of the *current-voltage spectroscopy,* or *I-V curves*, over biomolecules. The problem is that when the AFM tip is placed on top of the sample, and the *I-V curve* is acquired, the bias that is applied between the substrate and the AFM probe generates an attractive electrostatic force on the probe that bends the cantilever over the sample, creating a new a force on the sample. This force cannot be controlled using the feedback system of the AFM because the AFM feedback system 'mistakes' the electrostatic force with a variation of the topography of the sample during the *I-V curve* acquisition, and consequently moves up and down the probe. As a result, when a current-voltage spectroscopy is performed on biological samples these get compressed, if the bias is raised too high, the electrostatic force can easily damage the biomolecules we are characterizing.

The specific problem the NIM technique finds for its application to biomolecules is that the region we want to characterize, the region between the probe apex and the substrate C_{apex}, is extremely small, around 150 x 150 nm^2, and its capacitance, of the order of tens of *attoFarad,* which represents only a small fraction of the total capacitance measured in a NIM experiment of the order of 100 fF-1pF, and most of the measured capacitance is parasitic (also known as stray capacitance C_{stray}). This stray capacitance cannot be controlled due to its dependence on the spatial disposition of the components of the AFM set-up, which varies from measurement to measurement. Because C_{stray} is uncontrolled, and NIM measures the sum of C_{apex} and C_{stray}, the absolute value of C_{apex} cannot be known with NIM. Nevertheless NIM can measure the relative variations of capacitance either in time or space, but even if possible, this is not an easy task, probing the few *attoFarads* capacitance variation from the nanoscale apex of the probe over the parasitic background, from five to six orders of magnitude larger, is not evident, it requires very specialized instrumentation with extremely high resolution and a sophisticated calibration procedure to control the stray effects C_{stray} with sufficient precision in each measurement.

2.2. State of the art in the electrical characterization of biomolecules with the atomic force microscopy

In spite of the difficulties highlighted section 2.1, electrical measurements have been performed using the atomic force microscopy on biomolecules, the review of the state of the art will provide us the necessary perspectives from where develop our own work.

2.2.1 Types of samples

There are three types of biomolecules where the AFM has been used to study the electrical transport properties in gaseous enviroments: individual DNA strings, networks of DNA wires, and redox proteins (e.g. enzymes). All the studies in the scientific literature use exclusively C-AFM, and previously to this work of thesis, NIM had never been used for the electrical study of biomolecules.

The biggest impact has come from the study of the electron transport in **individual DNA strings**. There are 8 works published on the subject, and the main focus is the applicability of DNA strings as components for nanoelectronic circuits. These 8 works have been referenced a total of 256 times, most of the references (188) are referred to an early year 2000 publication by de Pablo et al. [4] in which poor electrical conductivity was observed for the DNA molecule. Two types of configurations have been used in the study of the DNA, (i) long DNA strings placed on top of insulating substrates and contacted on one side by a shadow-mask macroscopic electrode and on the other side by the conducting AFM probe [4,5,6,7], and (ii) short DNA strings inserted in self assembled monolayers (SAMs) placed over conducting substrates and contacted directly by the top with the AFM probe [8,9,10,11]. The experiments still have not fully clarified the conduction properties of the DNA, and the DNA seems to conduct only in some occasions. One of the possible sources of

discrepancy are the conditions in which the *point-contact I-V curve* measurements are performed in these experiments, it is possible that the applied force is not well controlled, and it has caused uncontrolled variations on the samples during the measurement, and thus on the electrical measurements.

The other area of research on DNA, the electrical conduction of **networks of DNA wires** with C-AFM has been investigated exclusively by the group of Kawai and coworkers, 3 works have been published on the subject, which have been referenced 23 times. The networks are made of wires of DNA formed by 15–25 DNA strings bundled together. The two first publications come from the years 2000 and 2001, where *point-contact I-V curve* measurements were performed on the DNA wires, and it was observed that networks produced a complex electrical activity [12 13]. Unfortunately, these experiments run into the typical weak point of C-AFM measurements on biomolecules, they completely ignore the effect of the electrostatic force applied on the samples, and the effect it may have in their measurements. This fact is especially problematic in the measurements from Kawai and coworkers where the bias applied is raised up to 10 V using *contact mode* and 0.12 N/m cantilevers are used, such conditions create forces up to 100 nN applied in an uncontrolled manner on the DNA wires (for technical details go to section 4.1). Therefore some of the electrical effects Kawai and coworkers observe could be directly related the electrostatic forces applied. In the third publication by Kawai and coworkers in the year 2005, with leading author *Terawaki*, the subject of the applied force is specifically considered, in this publication a new *conduction mapping* protocol, named *Point-Contact Current-Imaging Atomic Force Microscopy* (PCCI-AFM), is implemented, that is designed for performing *conduction mapping* of soft materials. The article shows nice conduction maps of the network of DNA wires, Fig 1b, and the dependence of the conduction on the ambient humidity [14].

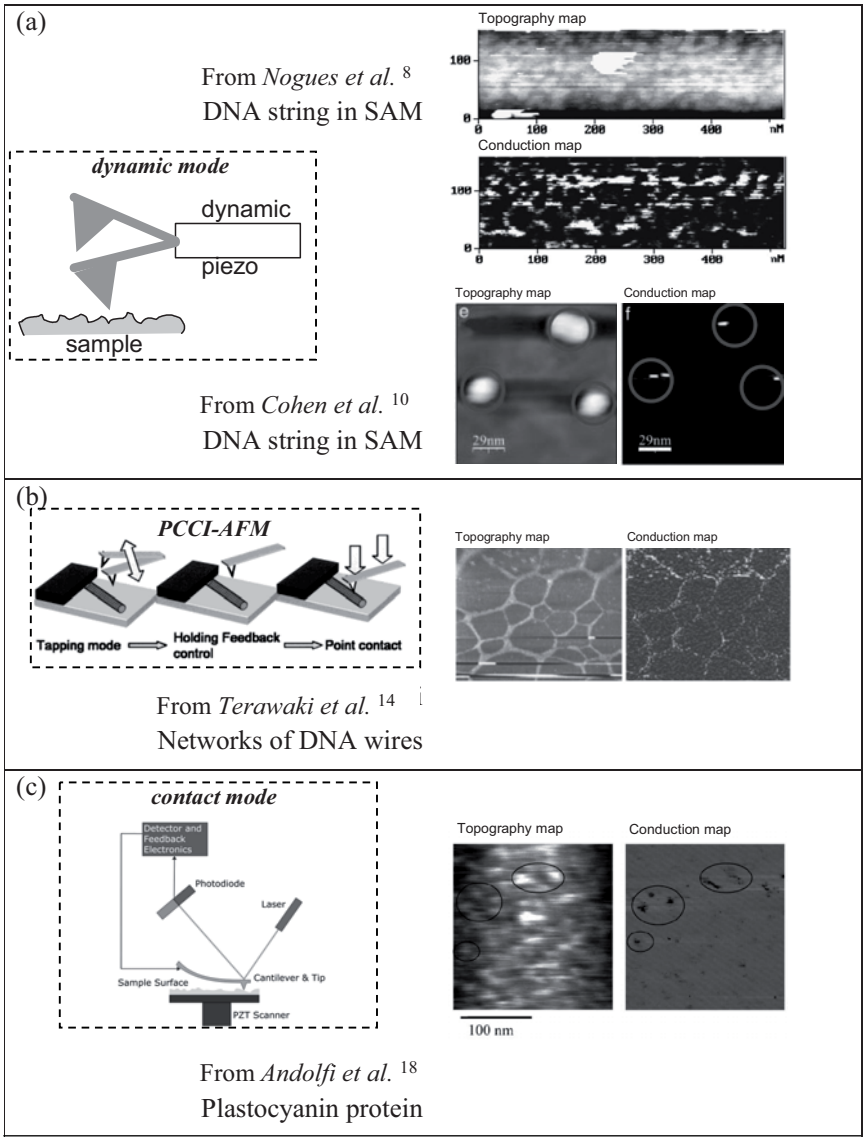

Fig 4. Conduction maps on biomolecules performed with different AFM techniques. Adjacent is the cartoon showing the functioning of the techniques (a) *dynamic mode*, (b) *PCCI-AFM* and (c) *contact mode*, the names of the authors of the imaged, and the type of sample used.

The newest line of research on electrical transport properties of biomolecules using the C-AFM of biomolecules are **redox proteins (enzymes)**. There are 5 works published, which mainly use *point-contact I-V curve* measurements, and have been referenced 46 times. The first of the papers was published in 2004 by *Stamouli et al.*[15], where the properties of photosynthetic protein complex were studied, and a strong anisotropy in the flow of current with respect the bias polarity was detected. Next followed: a study on the blue copper azurin by *Zao et al.* in 2004 [16], a study on the ferritin protein by *Xu et al.* [17] in 2005, and two studies from *Andolfi et al.* [18] [19] in 2005 and 2006 on the plastocyanin protein.

To date there has not been any works that use the AFM to study the electrical properties of non-redox proteins. From the comments of the authors on the C-AFM papers on enzymes, it was observed that these authors expected that the metal atoms present in their inner structure of enzymes increase the electron flow through the proteins, generating higher currents that are easier to detect. Nevertheless, these studies have revealed contrary to this belief, and they have shown that the metal atoms present in the enzymes do not play a significant role in increasing the current levels.

2.2.2. Types of AFM operation implemented

The *point-contact I-V curve* is the AFM measurement most performed in the electrical studies of biomolecules with AFM. All the published papers include at least one measurement of *point-contact I-V curves*. At most of the papers, the same methodology is used, the methodology is based in using AFM probes of spring constants between 1 and 5 N/m with *dynamic mode* to position the AFM probe in the XY plane on the desired measuring spot, next the oscillation of probe is stopped, and the AFM brought into contact to the top of the sample using *contact mode*, the final step is is sweeping the bias to perform an *I-V curve* on the sample. From all the papers in the literature only two

experiments change this methodology and substitute the *contact mode* by some other technique to bring the tip on the sample once the oscillation of the probe has been stopped: 1. Terawaki et al. used instead a fixed distance motion of the piezoelectric stage, whereas 2. Cohen et al. used a stepwise approach where an *I-V curve* is performed at each step.

From the 16 publications on the electrical study of biomolecules with AFM only 4 include *conduction maps*, the first one appearing in 2004. We note again that the main problem of *conduction maps* is that the lateral shear forces of the AFM probe motion tend to damage the samples. Three types of methodologies are found in the literature to perform *conduction maps*: *contact mode* used by *Andolfi et al*. on the plastocyanin protein [18], *dynamic mode* used by *Cohen at al.* and by *Nogues at al* on DNA molecules [8 9], and the specifically designed *PCCI-AFM* used by *Terawaki et al*. on networks of DNA wires [14]. As commented, the *PCCI-AFM* method combines *dynamic mode* with an approach of a predetermined distance in open feedback when the oscillation of the probe has been stopped.

The best results are clearly obtained with the *PCCI-AFM* method, see Fig. 4b, the conduction is well defined over the totality of the image, and the topography of the sample looks stable.

When *dynamic mode* is used to directly perform the *conduction maps*, the samples do not get damaged and look stable in time, but the quality of the *conduction map* is very poor, and it is easily observed that in Fig. 4a there is a difficulty in the acquisition of the electrical signal by the probe. This is a logical consequence of the oscillating movement of the probe during the electrical measurement, the electric signal measurement takes place only in the small period of time the tip is in contact with the sample, and the signal we measure is the average of the totality of the oscillation period, therefore the electric signal from the sample is weak. An additional difficulty found is that the signal is of bad quality, the continuous oscillation of the probe does not allow the electric

contact to stabilize, which introduces noise into the signal and further reduces the low current levels.

Finally, *contact mode* produces the worst results of all. The sample not only gets damaged during the measurement; sample dragging is evident in the image, Fig. 4c, but the *conduction maps* are unstable.

These 4 works are an illustrative example that in order to perform successful *conduction maps* of biomolecules it is necessary to implement AFM protocols that minimize the force transmitted to the biological samples and provide a good stable contact with them.

2.2.3. Theoretical data analysis

There are numerous theoretical studies on the electron transport of electrons in DNA and proteins. Nevertheless, theory and AFM experimental measurements have seldom been associated; for the DNA studies only *de Pablo et al.* [4] has included a theoretical discussion in the manuscript, whereas for proteins *Zhao et al*. [16], *Xu et al.* [17] and *Andolfi et al.* [19] include theoretical discussions.

The theoretical frameworks of DNA and proteins are different. The wire-like structure of DNA forces its theoretical study to be performed using computer calculations, whereas the bundle-like structure of proteins is more favourable for analytical expressions.

In the AFM publications of proteins, the theoretical framework used is sustained over the assumption that the presence of the biomolecule between the probe and the substrate creates an energy barrier between the AFM probe and the substrate that prevents the direct crossing of the electrons from the AFM probe to substrate, forcing the electrons to cross

through quantum tunnelling, in particular by direct coherent non-resonant tunnelling. The publications use a simple linear barrier model that allows the extraction of analytical expressions for the current flow, this way it is possible to estimate the height of the energy barrier by fitting the *I-V curves* acquired, the value height of the energy barrier has been measured to be 1-2 eV [16] [19]. But to the date, no data on effective electron mass on proteins has been provided to our knowledge.

We note that since no measurements with NIM have been performed on a biosample no theoretical results have been discussed.

2.2.4. Implications for future works

We have seen that two types of measurements have been used in the literature for the electrical characterization of biomolecules and both correspond to C-AFM applications. To date there has not been any application of NIM to the electrical characterization of biomolecules.

The first of the C-AFM measurements is *conduction mapping*, in this field *Terawaki et al.* have developed a technique that produces satisfactory results. Nevertheless, this is not the only AFM technique that can be used to achieve these results, commercial *jumping mode* has also good potential for performing *conduction mapping*, and its capabilities have not yet been fully explored in the electrical characterization of biomolecules. The next step will be establishing which are the uses and advantages of each of these two techniques with respect the *conduction mapping* of biomolecules.

The second of the C-AFM measurements is *point-contact I-V curves* measurements, but the protocols that have been used are missing some of information available in the *I-V curve* measurements. The reason for this is that (a) in order to avoid damaging the samples with the electrostatic

bending of the cantilever of the probe, the applied biases has been restricted to low values, and that (b) the distance between the AFM probe apex and the substrate during the *I-V curve* acquisition is not recorded, even if this parameter can be perfectly controlled using correctly the AFM system.

All together the review of the state of the art shows that the AFM characterization of biomolecules is at early stage for assisting the nanoscale electrical biosensor development, that much it is still to be done to improve the reliability, performance, and theoretical analysis. There are a whole range of applications to develop using the C-AFM, and whole new AFM electrical characterization field to start and develop; the NIM characterization of biomolecules. All these tasks have been worked out and are presented in the present work of thesis.

2.3. References

1 G. Binnig, C. F. Quate, and C. Gerber, "Atomic Force Microscope," Physical Review Letters **56** (9), 930-933 (1986).

2 H. F. Knapp, P. Mesquida, and A. Stemmer, "Imaging the surface potential of active purple membrane," Surface and Interface Analysis **33** (2), 108-112 (2002).

3 R. Shao, S. V. Kalinin, and D. A. Bonnell, "Local impedance imaging and spectroscopy of polycrystalline ZnO using contact atomic force microscopy," Appl Phys Lett **82** (12), 1869-1871 (2003).

4 P. J. de Pablo, F. Moreno-Herrero, J. Colchero et al., "Absence of dc-conductivity in lambda-DNA," Phys Rev Lett **85** (23), 4992-4995 (2000).

5 L. T. Cai, H. Tabata, and T. Kawai, "Probing electrical properties of oriented DNA by conducting atomic force microscopy," Nanotechnology **12** (3), 211-216 (2001).

6 K. Shimotani, T. Shigematsu, C. Manabe et al., "An advanced electric probing system: Measuring DNA derivatives," Journal of Chemical Physics **118** (17), 8016-8022 (2003).

7 C. Gomez-Navarro, P. J. de Pablo, and J. Gomez-Herrero, "Electrical properties of long molecules: single-walled carbon nanotubes and DNA," Int J Nanotechnol **2** (1-2), 90-102 (2005).

8 C. Nogues, S. R. Cohen, S. S. Daube et al., "Electrical properties of short DNA oligomers characterized by conducting atomic force microscopy," Physical Chemistry Chemical Physics **6** (18), 4459-4466 (2004).

9 H. Cohen, C. Nogues, R. Naaman et al., "Direct measurement of electrical transport through single DNA molecules of complex sequence," P Natl Acad Sci USA **102** (33), 11589-11593 (2005).

10 H. Cohen, C. Nogues, D. Ullien et al., "Electrical characterization of self-assembled single- and double-stranded DNA monolayers using conductive AFM," Faraday Discuss **131,** 367-376 (2006).

11 T. Heim, D. Deresmes, and D. Vuillaume, "Conductivity of DNA probed by conducting-atomic force microscopy: Effects of contact

electrode, DNA structure, and surface interactions," Journal of Applied Physics **96** (5), 2927-2936 (2004).

12 H. Lee, Y. Maeda, S. Tanaka et al., "Structure and electrical transport of self-assembled DNA networks on MICA surface using CP-AFM," Journal of the Korean Physical Society **39**, S345-S347 (2001).

13 J. H. Gu, S. Tanaka, Y. Otsuka et al., "Self-assembled dye-DNA network and its photoinduced electrical conductivity," Appl Phys Lett **80** (4), 688-690 (2002).

14 A. Terawaki, Y. Otsuka, H. Y. Lee et al., "Conductance measurement of a DNA network in nanoscale by point contact current imaging atomic force microscopy," Appl Phys Lett **86** (11), - (2005).

15 A. Stamouli, J. W. M. Frenken, T. H. Oosterkamp et al., "The electron conduction of photosynthetic protein complexes embedded in a membrane," Febs Lett **560** (1-3), 109-114 (2004).

16 J. W. Zhao, J. J. Davis, M. S. P. Sansom et al., "Exploring the electronic and mechanical properties of protein using conducting atomic force microscopy," J Am Chem Soc **126** (17), 5601-5609 (2004).

17 D. G. Xu, G. D. Watt, J. N. Harb et al., "Electrical conductivity of ferritin proteins by conductive AFM," Nano Lett **5** (4), 571-577 (2005).

18 L. Andolfi and S. Cannistraro, "Conductive atomic force microscopy study of plastocyanin molecules adsorbed on gold electrode," Surf Sci **598** (1-3), 68-77 (2005).

19 L. Andolfi, A. R. Bizzarri, and S. Cannistraro, "Electron tunneling in a metal-protein-metal junction investigated by scanning tunneling and conductive atomic force spectroscopies," Appl Phys Lett **89** (18), 183125 (2006).

Chapter 3. The set-up

Summary: The Atomic Force Microscopy AFM set-up used in this work of thesis is a commercial AFM set-up adapted to perform Conducting-AFM and Nanoscale Impedance Microscopy measurements on biomolecules on the best possible conditions. All the adaptations undertaken are discussed in detail in this chapter.

3.1. Description of the experimental set-up

The idea of the set-up is conceptually simple, it is basically composed of a standard commercial AFM system (from Nanotec Electronica S.L.) where the probe is connected to a preamplifier, and the sample holder is connected a function generator. In order to simplify the operation of the system, the electrical measurements are integrated with the rest of the AFM system, this is performed using the AFM controller Dulcinea^{TM} that is first set to generate the function going to the sample holder, and second to record the response measured by the preamplifier, see Fig. 1a. This way, the integration of all the signals possibilities the control of the totality of the system using a single software, in our case, we used the WSxM [1] provided by Nanotec Electronica S.L.

The set-up is designed to be capable of performing both DC and AC electric current measurement, where (a) the DC component measures the resistance to the current flow through the sample for an applied bias, and (b) the AC component, the dynamic response of the sample, in particular of the polarization. Both the preamplifier and AFM have been adapted for this task.

3.2. The preamplifier

The AC capabilities of commercial preamplifiers with respect their bandwidth, which typically goes from Hz to kHz, is rather limited. For AC characterization of samples is convenient to have access to the maximum possible range of frequencies. This way, the response of the polarization of the sample may be explored in a broader range of frequencies, and the system can be set to work at a frequency which is most appropriate for the experiment.

In order to increase the availability of bandwidth in our set-up, the group of Prof. Marco Sampietro from the Politecnico di Milano designed and built up a full custom preamplifier that now is protected under an international patent, WO 2005/062061 and whose details are discussed in Ref. [2]. The implementation of the developed amplifier on our set up has been mainly performed by Dr. Laura Fumagalli during her work of thesis[3].

The preamplifier provides for the DC component similar performance that DC preamplifiers present in commercial AFM set-ups. The gain is of ~1 GΩ over a ~100 Hz bandwidth, which reaches a maximum current level of ~10 nA and a low noise level flat at ~20 fA/√Hz. The minimum measurable current is then ~0.2 pA. But under full dynamic range operation it is observed a slightly higher quantization noise of ~0.3 pA, corresponding to the analog-to-digital converter (16bit ADC) least significant bit. The final DC performance of the set-up allows measuring a wide dynamic range of more than 4 orders of magnitude, from around ~0.3 pA up to 10 nA.

For the AC components, the preamplifier extends the upper limit of commercial bandwidth to the MHz range without affecting the noise level. The noise for low frequency is governed by the Nyquist noise (~10fA/√Hz) and only for frequencies superior to ~10kHz (or ~3kHz in

the case the preamplifier is plugged to the setup and stray capacitance is increased) the noise from the preamplifier dominates, and increases with the square of the frequency ν^2. The low level of noise achieved enables our AFM system to arrive to attoFarad capacitance sensitivities, but in order to get this resolution the signal must be averaged over a period of time. The factor by which resolution increases with time averaging is given by the square root of the sampling time $1/\sqrt{T}$. In our system, in order to achieve one aF resolution with 1 volt of AC signal applied the sampling time required per point is of ~1 second. This is a very important time reference, 1 aF resolution is required to resolve the capacitance variations between the apex of the AFM tip and the substrate in NIM operation.

Nevertheless, one second per pixel is a time scale between one and two orders of magnitude higher than the typical period of time per pixel used in standard AFM operation. Therefore there is a small mismatch between the period of time we need for our AC measurements and the operational periods of time of the AFM. This fact creates some difficulties, which will review over the next chapters, and where will show how to deal with them.

A photograph of the set-up and the working area where this work of thesis has been performed is shown in Fig. 1b. And in Fig. 1c the technical brochure for the preamplifier implemented is provided.

(a)

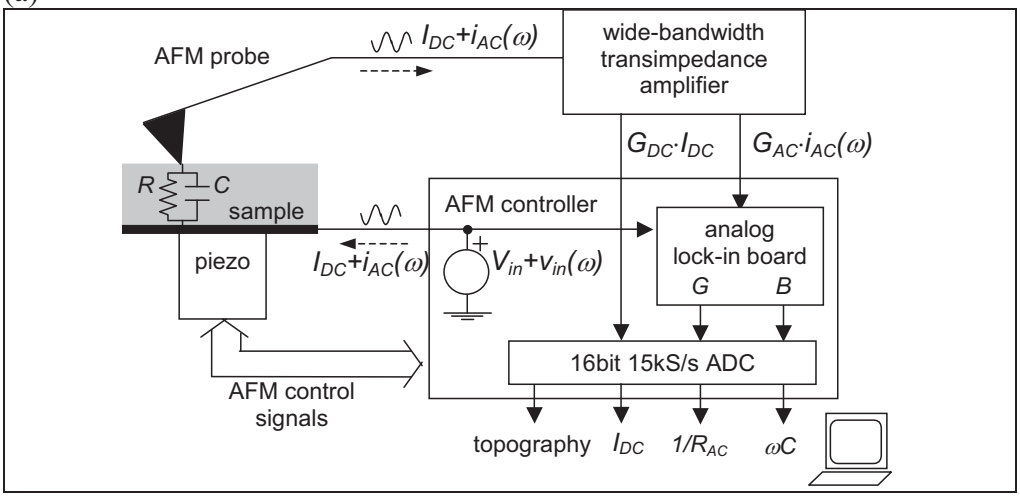

(b)

(c)

Parameter		Unit
Bandwidth		
BW_{dc}	[0 , 100]	Hz
BW_{ac}	[100 , 1M]	Hz
Gain		
$\lvert G_{dc} \rvert$	-0.9G	Ω
$\lvert G_{ac} \rvert$	40M	Ω
Input current noise flat level (for $f < f_c$)	~7	fA/√Hz
f_c	10k	Hz
Maximum current		
DC output	10n	A
AC output	8n	A
Input voltage offset	<1m	V
Output voltage offset		
DC output	-10m	V
AC output	-60m	V
Power supply	±15	V

Fig. 1. (a) The custom-made current-to-voltage amplifier, coupled to an analog lock-in board included in the AFM electronics, allows simultaneously imaging of the topography and of the admittance, either the real part G (conductance, G=1/R) and the imaginary part (susceptance, B=ωC), of the sample, (b) picture of the set-up with the AFM at the end, and (c) technical brochure of the preamplifier.

3.3. Adaptation of the commercial AFM set-up

In order to achieve the desired performance, the different components of the set-up, AFM, preamplifier and control system, must be integrated in the best conditions, at two levels, electronic and operational. On one side, the preamplifier from the Politecnico di Milano has to be integrated in the AFM set-up with the minimal introduction of electronic noise to the preamplifier. And on the other side, the control software, the WSxM from Nanotec, needs to be adapted to the operational requirements of the AC acquisition.

The adaptations performed for the integration of the set-up are listed and detailed:

1. One of the two analog lock-in amplifiers in the AFM controller Dulcinea^{TM}, originally designed for the control of the dynamic modes of the AFM, has been used for the handling of the AC signal after minor changes in the controller wire connexions, and calibrating the lock-in amplifier gains, once adapted the outgoing and the coming AC signals were convoluted, and the real Rac (resistance) and imaginary C (capacitance) of the samples could be measured. (task done by Nanobiolab team)

2. The piezoelectric tube that moves the piezoelectric stage was widened to allow a shielded wire to pass through to connect the stage with the AFM controller with minimal noise input. (task done by Nanotec)

3. A new removable sample holder was designed and built, the holder connects the piezoelectric stage with the sample and integrates a series resistance with the minimum possible conducting path to minimize the noise input and the stray capacitance. (task done by Politecnico di Milano)

4. A new tip holder was designed and built that enables a connection of the AFM tip with the preamplifier through shielded wire to minimize input noise. (task done by Nanotec)

5. The tip holder was shielded using a grounded metal sheet to minimize stray capacitance between the tip and the sample holder, the result was a reduction of stray capacitance from 200 to 40 fF. (task done by Nanobiolab team)

6. All the grounds of the components of the set-up were unified, this yielded an important reduction of the noise arriving to the preamplifier. (task done by Nanobiolab team)

7. The control software WSxM was modified. The averaging capability for the signal channels in *Jumping mode* was extended from only topography to the totality of the channels in the AFM controller. This way AC characterization was enabled in *Jumping mode*. This modification is now available as a general feature of the WSxM software. (task done by Nanotec)

8. The environmental control chamber of the commercial AFM system was connected to a source of dry N_2(g). The humidity and temperature of the atmosphere under which the experiment was performed was controlled using a commercial sensor (Rotronic Hydrowin3) that was installed in the AFM chamber. (task done by Nanobiolab team)

I would like personally thank the staff on Nanotec and our partners from Milano, and I cannot forget my lab-mate Laura Fumagalli without which all this would not had been possible.

3.4. Probes

Conductive probes used in C-AFM are standard AFM probes typically made of silicon or silicon nitride coated with a thin conductive film, usually of gold, platinum or doped diamond. The main requirements that a conductive probe has to meet in C-AFM are contamination

and wear resistance (to avoid peeling off of the conductive coating during scanning).

The best tips in terms of wear resistance currently available for current-sensing AFM are the doped diamond-coated probes [4,5,6] , as the one given in Fig. 2. The extremely hard conductive coating of these probes can resists for days of tip-surface contact experiments under high shear forces, thus offering the possibility of reliable electrical measurements. The internal resistance of doped diamond is of the order of several tens of kΩ, this does not represent a drawback in biological samples, which tend to have resistances above the MΩ that dominate the signal in C-AFM and NIM measurements.

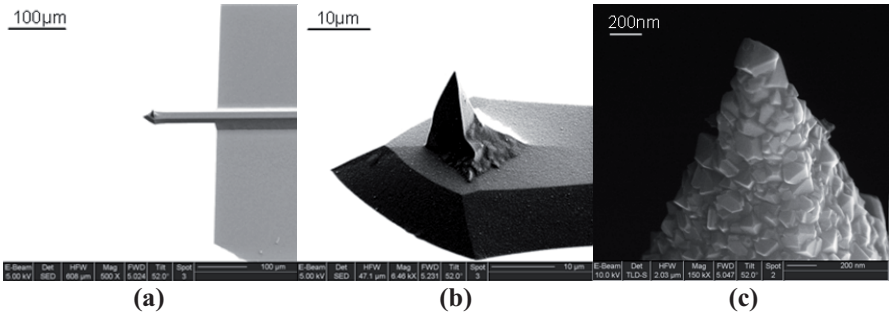

Fig. 2. Boron-doped diamond coated probes that are commercially available (Nanosensors) and suited to current-sensing AFM. SEM images with increasing magnification: **(a)** cantilever, **(b)** cone and **(c)** tip apex (nominal radius of 100-200nm).

An important feature of commercial conductive probes from the perspective of CS-AFM measurements is that the entire probe is covered with the conductive coating. This fact greatly affects the operation of the AFM in C-AFM and NIM measurements: In the case of C-AFM, the large coated area makes the cantilever of the probe very sensitive to electrostatic forces produced when a bias is applied between the probe and the conducting substrate, fact which, as has been previously discussed, caused problems in the C-AFM studies of soft materials, like biological samples, specially when *I-V curves* are performed. In the case of NIM measurements, the conductive coating induces significant

capacitance stray contributions C_{stray} in the NIM measurements, designing strategies to deal with such high parasitic capacitance contributions is a source of serious technical difficulties.

In particular, the probes used for this work of thesis were two types of conducting commercial boron doped diamond probes CDT-CONTR and CDT-FMR both from Nanosensors^{TM}, with nominal radius of 100-200 nm, and spring constants around 2.8 N/m and 40 N/m respectively.

3.5. References

[1] I. Horcas, R. Fernandez, J. M. Gomez-Rodriguez et al., "WSXM: A software for scanning probe microscopy and a tool for nanotechnology," Review of Scientific Instruments **78** (1), 013705 (2007).

[2] G. Ferrari and M. Sampietro, "Wide bandwidth transimpedance amplifier for extremely high sensitivity continuous measurements," Review Scientific Instruments **78**, 094703-094710 (2007).

[3] L Fumagalli, "Instrumentation for wide-bandwidth electrical characterization at the nanoscale using atomic force microscopy," Tesis, Polictecnico Milano (2006).

[4] S. J. Oshea, R. M. Atta, and M. E. Welland, "Characterization of Tips for Conducting Atomic-Force Microscopy," Review of Scientific Instruments **66** (3), 2508-2512 (1995).

[5] M. A. Lantz, S. J. O'Shea, and M. E. Welland, "Characterization of tips for conducting atomic force microscopy in ultrahigh vacuum," Review of Scientific Instruments **69** (4), 1757-1764 (1998).

[6] T. Trenkler, T. Hantschel, R. Stephenson et al., "Evaluating probes for "electrical" atomic force microscopy," Journal of Vacuum Science & Technology B **18** (1), 418-427 (2000).

Chapter 4. Development of atomic force microscopy protocols for the electrical characterization of biomolecules

Summary: In previous chapters it has been shown that the AFM represents an ideal tool for the electrical characterization of biomolecules at the nanoscale, and that has a great application for the development of electrical biosensors. It has also been shown that AFM has not been yet fully developed in what concerns the electrical characterization of biomolecules, which presents certain particularities due to the soft and fragile nature of biomolecules that have to be addressed specifically. Chapter 4 describes new strategies to push forward the application of the AFM to the electrical characterization, the strategies are explained in detail, and framed in the context of previously existing AFM methods.

4.1. Introduction

The AFM is overall a force-dependant technique, therefore to get the most out of its operation it is necessary to have a clear concept of the interplay of forces present during the measurements we perform, and especially on how these forces affect the magnitude we intend to study. Once we have a clear idea of the context in which the AFM measurement is going to be performed, it is necessary to select the best strategy for our measurement, parameters such as type of probe, operating protocol, or environmental conditions are important parameters which determine the success of the measurement.

4.2. New *I-V curve* protocol: *Dynamic&steps with stiff probes*

Description of the problem

Point contact current-voltage spectroscopy (*I-V curves*) has been the electrical measurement most used in the literature for the study of the electrical properties of biomolecules. The totality of the papers published report *I-V curves* as the main method to gain information on the electrical

properties of the samples under study. Therefore any improvement in the methodology to perform *I-V curves* has a high interest for the field of the AFM electrical studies of biomolecules.

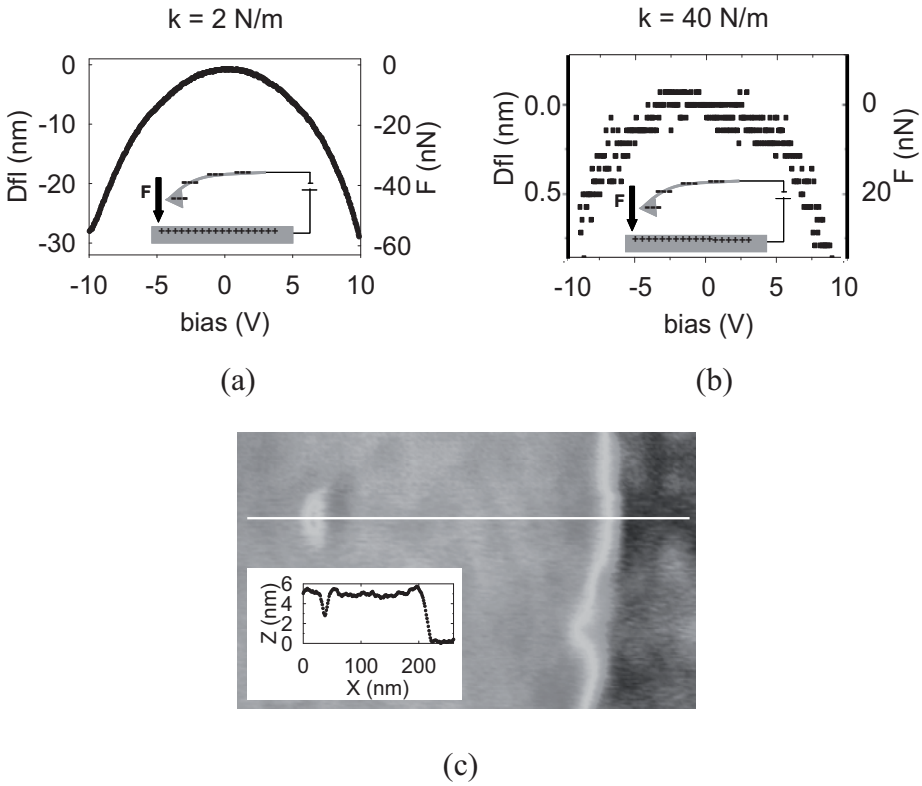

Fig. 1. (a) and (b), deflection of commercial AFM probes as a function of the applied bias for a cantilever of stiffness of (a) 2 N/m and (b) 40 N/m. (c) AFM tip indentation mark in biological membrane in a biological membrane due to excessive electrostatic loading.

The previous works typically used for the electrical *I-V curves* characterization of the biomolecules the following experimental conditions: conductive probes with spring constants between 1-3 N/m, and an applied bias range below 1 V. Thanks to this set of parameters, the authors of the previous works were capable of performing two standard

AFM operations over the biomolecules without causing damage to them, (a) to use *Dynamic mode* to position the AFM tip on the desired position of the XY plane, and once the desired spot has been found, (b) to use *Contact mode* to place on the Z axe the AFM probe on top of the sample. Next, once the AFM probe is correctly positioned, *I-V curves* were acquired.

The reason why the previous authors did not raise the bias over 1-2 V is understood looking at Fig. 1a. The figure shows the progressive bending in the air of a commercial conductive AFM probes with spring constants of 2 N/m as a function of the applied bias, it is observed that the probe suffers severe bending, and that when the bias reaches 9 V the bending reaches up 30 nm. Therefore in the case a biological sample was positioned below the AFM probe when the bias is raised, the cantilever bending would act exerting an intense force on the sample that would damage the sample. It is therefore logical for the authors which used 2 N/m probes to keep the applied bias below 1-2 V, otherwise their samples would have suffered physical damage during the *I-V curve* acquisition invalidated their measurements. By parameterizing the curves in Fig. 1a and 1b, the amount of force acting on the sample as a function of the applied bias can be roughly estimated in $F(pN) = 300 \cdot V^2$. Fig. 1c shows a practical example of cellular membrane damaged due to excessive electrostatic force loading, the shape of the AFM probe is clearly observed imprinted in the membrane.

Solution

The force transmitted to the sample below the tip can be reduced if the stiffness of the cantilever is increased, increasing the stiffness increases the amount of force the probe adsorbs as it bends, and therefore makes that less electrostatic force gets transmitted to the sample. This is clearly observed in Fig 1.b, where it is observed that the bending of a cantilever of spring constant of ~40 N/m is significantly smaller that the bending of the 2 N/m cantilever. Additionally, another factor which reduces the force applied on the sample by stiffer cantilevers is that

stiffer cantilevers have smaller cantilevers areas and this reduces the electrostatic force acting on the cantilever. Both factors combined has allowed us extending the bias range from 1 V up to 9 V by using stiff 40 N/m cantilevers.

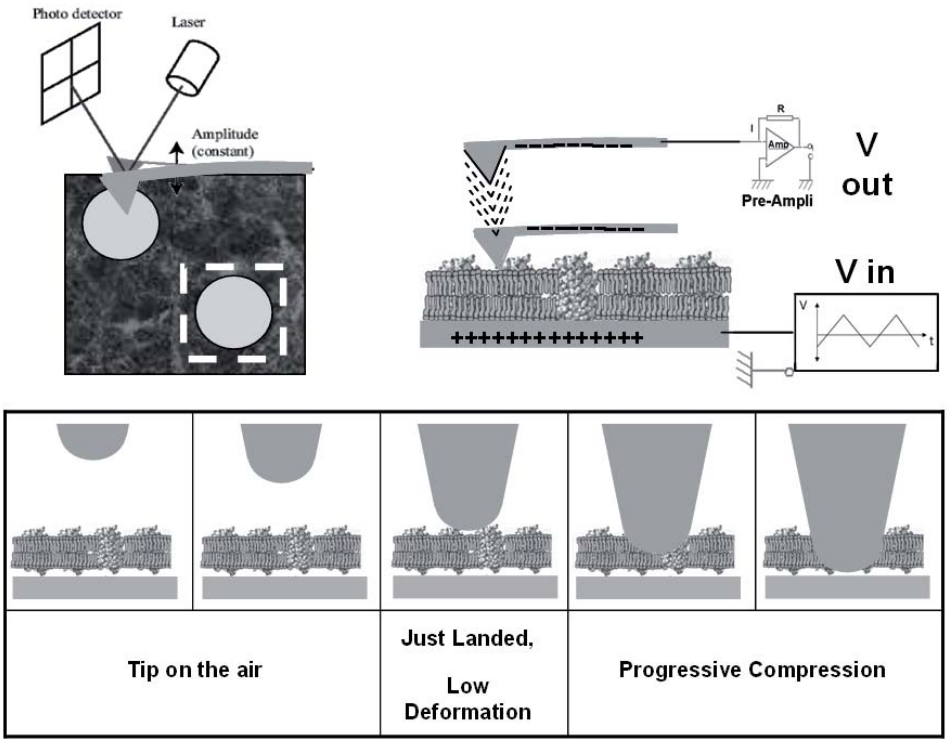

Fig. 2. Schematic representation of the protocol of *Dynamic&steps with stiff probes*. *Dynamic mode* is used to locate the measuring spot in the XY plane followed by a stepwise approach with an *I-V curve* in each step, the approach covers all the possible situation of the AFM probe in the Z axe.

Dynamic mode can also be used to position the AFM tip in the XY plane with the stiff cantilevers without damaging the biological samples. The only problem that hinders the direct use of 40 N/m cantilevers for

I-V curve acquisition is the positioning of the tip on the Z axe on top of the soft biological samples. If *contact mode* is used with a stiff cantilever, as it was used in the previous works to position the 1-3 N/m probes in the Z axe, the low sensitivity of the stiff cantilevers to the applied force would cause the application of intense forces on the sample, and, as a consequence, the uncontrolled damaging of the sample. The positioning of the tip in the Z axe requires from new strategies.

One possibility is the use of an open feedback stepwise approach independent from the sensitivity to the force of the stiff cantilevers where an *I-V curve* is performed at each step, this strategy, previously only used with 2 N/m cantilevers [1], works nicely with stiff cantilevers because the electrostatic cantilever bending at each step is greatly reduced, and thus enables to examine electrically step by step a set of Z positions covering all the possible tip locations (this is: tip in the air, tip just on top of the sample, and the progressive indentation of the tip in the sample), see Fig. 2. The great advantage of the techniques is that at each step the Z position can be directly related to the distance *L* between the tip and the gold substrate through the monitoring of the cantilever deflection and the piezo vertical displacement

Technical implementation

The experimental parameters we used for the implementation of the *dynamic&step*s *with stiff probes* protocol are: a Nanotec AFM, conductive diamond coated probes CDT-FMR Nanosensors^{TM} of nominal spring constant 40 N/m, an oscillation amplitude in *dynamic mode* of ~ 40 nm, a step height during the approach of 0.1 nm, a bias-range for the *I-V curve* acquisition at each step between -9 to 9 V, and a bias scan speed of 108 mV/ms both in the forward and backward senses. The programming of the protocol was performed with the 3D module present in the WSxM software [2]. The whole process resulted in a final vertical speed of approach between probe and sample of 0.35 nm/s.

Since this measuring method is inherently slow ("long" recording times are necessary to get the low electric current with enough precision, i.e. 0.35 nm/s of vertical Z speed) drift corrections procedures have to be implemented in order to get precise values for the vertical location of the tip. The problem of the drift is that when drift is present in an AFM system, the nominal values of the motion of the piezoelectric stage in the Z axe do not inform us of the real motion of the tip.

The drift motion tends to be linear with time, this way when the motion of the piezoelectric stage is performed at constant speed during a *dynamic&steps with stiff probes* protocol it is possible to apply a linear correction factor R to the nominal Z axe position. This way the real vertical Z axe position of the stage $Z_{real} = Z_{nominal} \bullet R$ can be obtained. R is defined by

$$R = 1 + \frac{V_{z,drift}}{V_{z,nominal}}$$

where $V_{z,nominal}$ and $V_{z,drift}$ are respectively the nominal vertical speed of the probe and the speed of the drift. The effect of the drift in the F-Z curves is represented in Fig. 3. When the drift approaches probe and substrate (+*drift*) the slope M_{+drift} of the cantilever deflection versus the nominal piezo Z position increases by a factor R^{+}. Inversely, when the drift withdraws probe and substrate (-*drift*) the slope M_{-drift} of the cantilever deflection versus the nominal piezo Z position decreases by a factor R^{-}.

The correcting factor R for the motion of the piezoelectric stage during the stepwise approach of the *dynamic&steps with stiff probes* protocol can be extracted using one F-Z curve performed at fast speed (for example, 2000 nm/s) on an uncompressive substrate and using it as a reference for drift free motion. For fast speed F-Z curves $V_{z,nominal} >> V_{z,drift}$, thus R equal to 1, and the final real Z axe position Z_{real} is by all means free of drift and equal to $Z_{nominal}$. Next, the R during the

stepwise approach of the *dynamic&steps with stiff probes* protocol can be extracted from the ratio of the slope $M_{+/-drift}$ of the stepwise approach and the slope M_{0drift} free of drift of the fast F-Z curve,

$$R = \frac{M_{+/-drift}}{M_{0drift}},$$

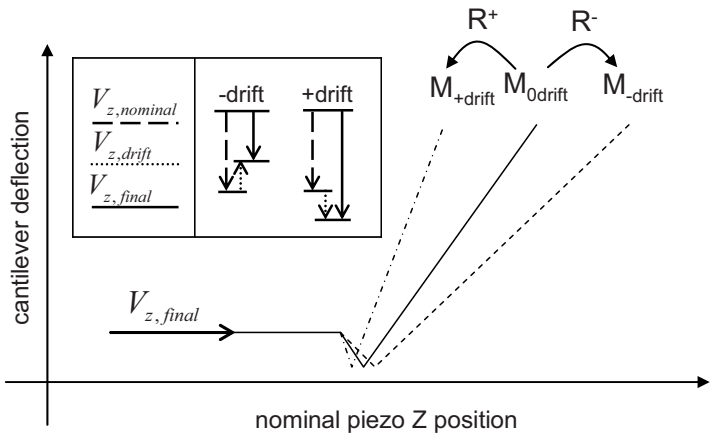

Fig 3. Scheme showing the effect of the drift in the final vertical movement of the probe and on the F-Z curves. The inbox shows the situation in speed vectors. The schematic F-Z curve shows that when the drift approaches probe and substrate (+*drift*), the slope M_{+drift} of the cantilever deflection as a function of the nominal piezo Z position (when the probe in contact) increases with respect the situation when no drift in present M_{0drift}. Inversely, the opposite situation is found when the drift withdraws the probe from the substrate (–*drift*), $M_{-drift} < M_{0drift}$.

Once the drift is corrected, the tip-substrate (inter-electrode) distance *L* at each of the steps of the approach can be simply obtained from the thickness of the biomolecule, t_{bm} (measured in dynamic mode), the variation in the piezo displacement, Δz_p and the cantilever deflection, Δd with respect the first contact with the membrane. The value of *L* is

then extracted as $L = t_{bm} - |\Delta z_p| + |\Delta d|$. The point of first contact with the biomolecule is typically easily identified by a reduction of the electrostatic cantilever bending and a sudden increase in the current flow through the tip at high applied bias. The overall procedure provides the inter-electrode distance with an estimated uncertainty below 0.5 nm.

4.3. New DC and AC *conductive mapping* protocol. *Jumping Mode*

Description of the problem

Biological material is delicate and when nanometric AFM tip is scanning its surface it can easily get damaged. It is therefore necessary to look for alternative techniques to electrically map biological samples. A full review of *conductive mapping* protocols and its effect on the conductive mapping of biomolecules was provided in Section 2.2.

Section 2.2 concluded that the standard method for mapping the electrical properties in AFM, i.e. *contact mode*, cannot be applied on biological materials due to the high shear forces it generated on the samples that causes damage to them. We also observed that the *Dynamic mode* does not damage the biomolecules, but that quality of the *conduction maps* it generated is not satisfactory. Only the *PCCI-AFM* methodology provides satisfactory results, but this technique has the problem that it is not commercial, and, at this time, its use is restricted to T. Kawai and coworkers.

Solution

Jumping mode JM [3] is a wonderful alternative for the *conductive mapping* of biological samples, and soft samples in general. During JM imaging the shear forces applied to the sample are minimized thanks to the lateral displacement of the tip out of contact. The probe is only brought in contact with the sample once the lateral motion has been

stopped. The full JM cycle is *"tip removal / lateral displacement / approach using the contact mode* feedback", see Fig. 4.

JM presents two other important advantages with respect *contact mode*: (a) The electrical data for each pixel of the *conduction map* exclusively comes from a single position of the sample, contrary to standard *contact mode* where the data comes from a period of time during which the probe is continuously moving. And (b) the drift of the laser spot on the photodiode is corrected at each point, an offset is applied at each point when the probe is out of contact, that ensures a constant force applied at all points of the scanning. In *contact mode* the drift of the system cannot be corrected causing that applied force changes during the image acquisition, fact especially important on soft samples and with long acquisition times as the ones required for NIM images.

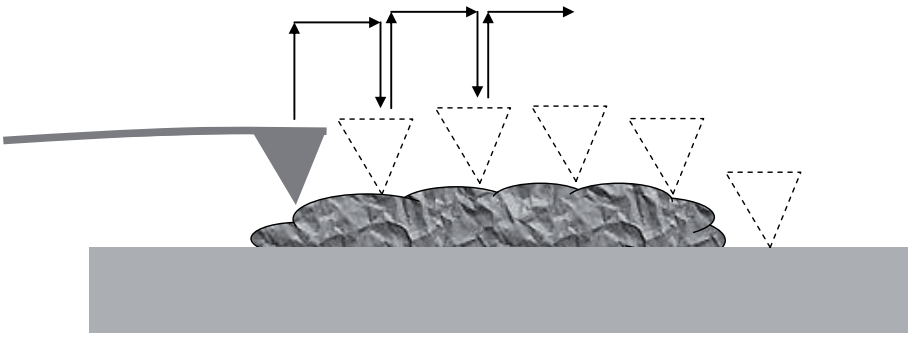

Fig. 4. Scheme of operation of Jumping Mode, the lateral displacement of the tip is performed out of contact which minimizes the shear forces applied to the sample. The probe is only brought in contact with the sample once the lateral motion has been stopped. The full JM cycle is *"tip removal / lateral displacement / approach using the contact mode* feedback". Jumping Mode can be used for conductive mapping either with C-AFM or NIM.

The contact time *T* of the AFM probe with the sample is together with the applied force, one of the two fundamental parameters for CS-AFM electrical measurements. For C-AFM, during the first milliseconds after

the tip gets in contact with the sample during a *Jumping mode* cycle, the tip suffers certain mechanical instability that introduces noise in the DC current, this effect can be minimized extending the contact time to allow the damping of the mechanical tip vibrations, the best results are obtained when the DC current acquisition is performed on the last part of the contact time period. In the case of AC measurements (NIM), the sampling time equals the contact time *T*, and therefore the contact time is related to the resolution of the impedance measurements, and, as previously commented in section 3.2, produces an improvement by a factor of $1/\sqrt{T}$ in the minimal detectable impedance change.

Nevertheless, there is an absolute limit for the contact time *T* in JM operation, the feedback system of JM becomes unstable for times superior to ~0.15 s, therefore when acquisition times > 0.15 s per pixel are required, the only possibility is repeating the same scan over the same line, this way, performing consecutive scans, the resolution can be improved until the desired value is reached.

One important aspect that has to be kept in mind is that the *contact mode* that is used to position the probe over the sample during the JM measurement transmits all the electrostatic force present between the probe and the substrate to the sample (as explained in section 2.1.4 for *I-V curves* in contact mode). This fact limits the applied voltage that can used for JM *conductive mapping* on biological samples to values < 1 V to avoid damaging the samples.

Technical implementation

The general experimental parameters used for the implementation of the *Jumping Mode conduction mapping* are: a Nanotec AFM, conductive diamond coated probes CDT-CONTR Nanosensors^{TM} with nominal spring constant of 2.5 N/m, fast mode offset correction to continuously correct the effect of drift on the applied force, and jumping

heights of 100 to 200 nm. All the parameters were controlled with Jumping Mode module present in the WSxM software [2].

The contact times *T* for C-AFM and NIM are very different, C-AFM probe stabilization requires of contact times *T* of ~10 ms to obtain good quality images, whereas NIM requires much longer contact times of ~140 ms to reach enough resolution to resolve the impedance changes in the samples, this is a few aF resolution. These long contact times had never before been used in JM, as this is the first implementation of NIM in JM.

4.4. Capacitance Flying

Description of the problem

In section 2.1.2 the *electrostatic modes* where introduced. The concept of the *Capacitance Flying* protocol works in a similar way to these *electrostatic modes,* and shares with them the objective of detecting the spatial variations in the electric fields generated by changes in the electric properties of the samples. The *electrostatic modes* are highly efficient in detecting the presence electric field variations over the sample; they easily generate an image in which areas of the sample with different intensities of electric field are visualized. Nevertheless, the *electrostatic modes* do not provide quantitative information on the field intensities nor in their changes. This is the space *Capacitance Flying protocol* aims to fill, the *Capacitance Flying protocol* aims to achieve quantitative field measurements, and consequently the quantification the physical properties governing the electrical behavior of the samples, and its distribution in the sample.

Capacitance Flying protocol moves the AFM tip over the sample at a constant tip-substrate (inter-electrode) distance *L*, and makes use of NIM to measure the capacitance variations that take place between the AFM tip and the substrate (generally flat). Thanks to the fact the

measurement is performed at constant *L*, the measurement is equivalent to a capacitor inside which different dielectric objects are introduced and removed. *Capacitance Flying protocol* only works in a quantitative way when *L* is known, otherwise no quantitative information can be extracted from the measurement. We note that previous STM works have already used capacitance variation measurements at constant Z position to observe dielectric constant variations [4], nevertheless the fact the probe position is unknown in STM measurements has avoided any quantitative measurement.

The *Capacitance Flying protocol* requires a high level of AFM expertise because it is necessary combining the measurement of small local capacitance variations which require long acquisition times with correcting the drift and controlling the tip-substrate distance *L* when the probe is flying over the sample, and there is no physical contact to reference to the probe *Z* position.

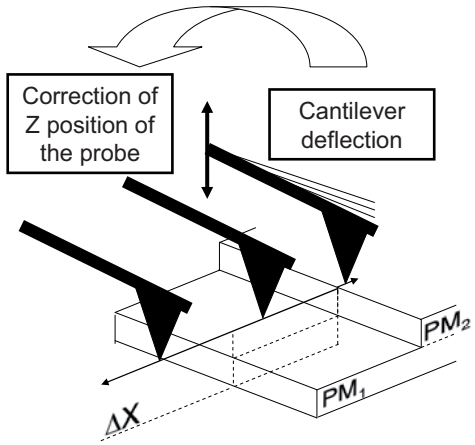

Fig. 5. Scheme of basic operation of the *Capacitance flying protocol*. The AFM probe moves in open feedback along a scan line where a small 'nano-clift' is present. The probe only touches the sample at the 'nanoclift' that produces a deflection in the cantilever, this deflection is then used to correct the *Z* position of the probe for the next Flying scan. In order to produce the less possible damage to the sample and the probe, the *Z* position during the scan is set to brush past the 'nano-clift', in a situation where the cantilever deflection is minimal but noticeable.

The small capacitance variations that take place in the measurement can only be detected if the AFM set-up is used to its maximum performance. First, it is necessary to maximize the signal, for this the probe-substrate distance *L* must be reduced to values below a few tens of nanometers, we have experimentally observed that in these circumstances the local tip-substrate capacitance variations can be observed with the set-up because it is in this range that local variations dominate the total capacitance variation. Second, the time of acquisition per pixel must be sufficiently large to arrive to aF resolution, which has been experimentally observed to produce sufficient contrast to perform the quantitative analysis of the data.

Solution

To achieve small inter-electrode *L* distances we make use of stiff cantilever to reduce the dependence of the probe bending to the forces acting on it (the same concept used in the *dynamic&steps* protocol). This process has allowed us to position the probe less than 5 nm away from the sample without collapsing.

Also as in the *dynamic&steps* protocol we use *dynamic mode* to position the AFM tip on over the desired position on the XY plane where the capacitance measurement is to be performed.

The problem that has to be solved is that when the tip is in the air we lack of any interacting force that can be used as a reference by the AFM feedback systems to position the tip in the *Z* axe. Therefore an alternative way to control the *Z* position of the tip during the flying of the tip must be searched. An option is to use only one reference point per scan line, the best one is when the tip reaches the end of the scan line. This can be performed using a sort of topographic ‘nanoclift’ on the sample, if the ‘nanoclift’ is placed at the end of the scan line, and we make the tip brush past the ‘nanoclift’, the *Z* position of the probe can be known, we will know when the tip touches the ‘nanoclift’ by the deflection of the

cantilever. This event can be used as reference to recalibrate vertical *Z* position of the probe and maintain it always in a brush past situation where the cantilever deflection is minimal but noticeable, see Fig. 5. This methodologhy achieves scanning a soft material at constant height *L* with a stiff cantilever without causing damage to the area of the sample we are characterizing.

The way to proceed is the following:

- For the probe to fly parallel to the substrate a scan direction that is transversal to the slope of the substrate is selected.

- Position the probe using *dynamic mode* and locate a scan line on a sample that has the required characteristics to perform the measurement so a 'nanoclift' is present at the end of the scan line.

- Stop the oscillation of the probe maintaining the scan motion.

- Modify the tip-substrate distance *L* until a small deflection is observed at the end of the scan line. During these scans the NIM measurement is performed.

- Activate again the *dynamic mode* to image the area where the measurement has been performed and this way control any possible undesired damage to the sample during the measurement.

To finish this section I would like to leave record of a better alternative for performing the *Capacitance Flying protocol* that came to my mind when there was no time to experimentally perform it during my PhD period. The idea is to substitute the 'nano-clift' by a better reference, the *dynamic mode*. The basic idea is the same as previously described, but instead of using a 'nanocliff' at the end of each scan line, the dynamic mode would be activated exclusively at the end of the scan line, this way the Z position could be equally referenced, and it would be avoided the need of special topographic features in the sample, and furthermore tip contamination would be reduced.

This new *Capacitance Flying protocol* requires from the development of specific software, given that none of the current control AFM software packages offers this option. As commented, this new methodology was not implemented in this work of thesis because of the finite time of the doctoral period, and remains as an open topic of research.

Technical implementation

The experimental parameters we used for the implementation of the *dynamic&steps with stiff probes* protocol are: a Nanotec AFM, conductive diamond coated probes CDT-FMR Nanosensors^{TM} of nominal 40 N/m spring constant, an oscillation amplitude in *dynamic mode* of ~ 40 nm, an AC voltage of 3 V, and scan speed of ~ 5 s per scan cycle (forward and backward motions). In order to achieve enough capacitance resolution the same line is scanned several times, typically from 5 to 10.

4.5. Capacitive probe calibration

Description of the problem

As commented, the NIM technique measures the variation of impedance between the AFM probe and the substrate during the scanning of the probe over the sample. This capacitance variation depends on two factors, (a) the electrical properties of the material between the tip and the substrate, and (b) the dimensions and position of the probe, see Fig 6a. These two factors must be uncoupled if it is desired to achieve a quantitative characterization of the impedance distribution of the sample. Therefore, factor (b), the capacitance variation produced by the dimensions and position of the probe, must be well characterized to be subtracted from the total capacitance measurement.

Solution

NIM measurements measure the impedance in the volume in-between the tip and the substrate, this measurement can only be obtained if distance between the tip of the probe and the substrate L is below tens of nanometres, region where the total capacitance variations is dominated by the capacitance variation between the tip apex of the probe and the substrate.

In order to extract quantitative information from the measurement of the tip apex capacitance the dimensions of the tip apex must be calibrated, To parametrize the tip apex a possibility is to model the tip apex as a cone that ends in a sphere (see Fig. 6b). This structure is defined by two parameters, the radius of the sphere R and the opening angle of the cone θ. This model allows for an analytical expression for the capacitance of tip apex on a flat metallic substrate, which was deduced by Hudlet et al. [5]:

$$C_{apex}(z) = 2\pi\varepsilon_0 R \ln\left[1 + \frac{R\left(1-\sin(\theta)\right)}{L}\right] + K(R) \qquad (Eq.1)$$

where ε_0 is the dielectric permeability of vacuum and $K(R)$ residual parameter that depends on R.

Now it is necessary to measure the model parameters, this can be performed using a simple experimental protocol. It consists of displacing the tip vertically in the Z axe (movement typically termed *force curve F-Z* in AFM terminology) and measure the variation of the capacitance along the Z axe. The data acquired can be fitted with *Eq*.1, and R and θ extracted.

The quality of the fitting indicates the correctness of the model in the description of the electromagnetic field distributions between the tip of the probe and the substrate. If the fitting is within the range of

experimental error for a *Z* range of several hundreds nanometers, it would mean the model is correct within the range of experimental error.

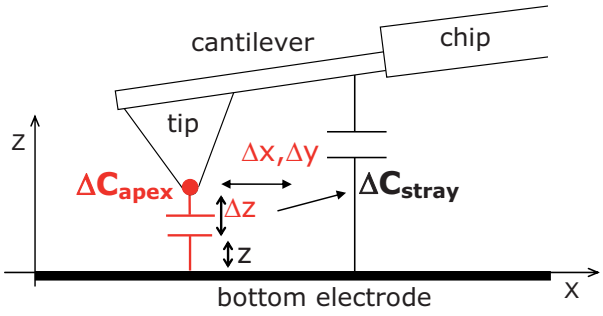

(a)

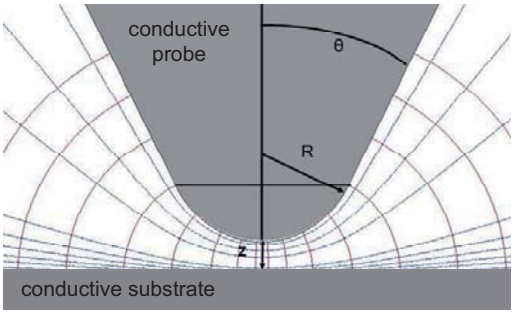

(b)

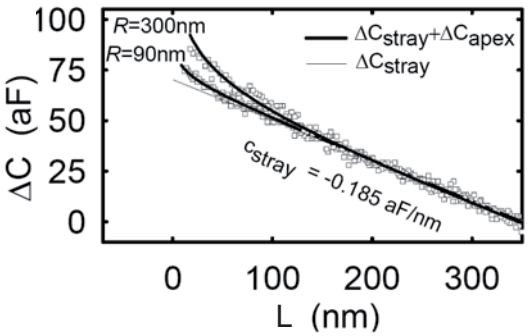

(c)

Fig 6. (a) Components of capacitance of an AFM probe with a conductive substrate. (b) Distribution of the electric field lines at the tip of the AFM probe, and (c) plot of the system capacitance variation as a function of the vertical position of the AFM probe for two different probes, the tip apex capacitance variation becomes significant for *L* below few tens of nanometers, the fittings of the curves to *Eq*.1 is also shown and the extracted tip apex radii R specified.

The apex capacitance C_{apex} is parallel to the much higher stray capacitance C_{stray} relative to the interaction of the substrate with all the rest of components of the AFM, i.e. the μm-sized tip and cantilever, the mm-sized chip, and the cm-sized probe holder and cables. For our set-up, $C_{apex} < 40$ aF whereas $C_{stray} \sim 40$ fF. Nevertheless, when the AFM probe moves a few nanometers in Z the variation of C_{stray} is of the order of ~aF, the same order of the variations of C_{apex}, and must be corrected from the measurement. The good news is that C_{stray} follows a linear variation with slope M_{stray} in all the space directions including the Z axe, this enables, once the linear dependence is characterized, for which we use the region $L > 100$ nm where C_{apex} is insignificant, to easily account for C_{stray} in the measurement adding a linear component $M_{stray} \cdot L$ to *Eq. 1*:

$$C_{total}(z) = 2\pi\varepsilon_0 R \ln\left[1 + \frac{R(1-\sin(\theta))}{L}\right] + K(R) + M_{stray} \cdot L \qquad (Eq.2)$$

Fig. 6c shows the total capacitance variation for two different AFM probes as a function of the tip-substrate distance L with no sample present between the tip and the substrate. The fitting of E*q. 2* to the experimental curves has produced fittings within the range of experimental error. In the fittings θ has been manually set to θ=30º leaving as only free parameter R, it is important to clarify that the important thing for the calibration of the tip apex is obtaining a correct parametrization of the evolution of $C_{apex}(z)$, not the precise angle θ and radius R of the tip. The results show that the two probes present different $C_{apex}(z)$ evolutions which are characterized by values of R of 300 and 90 nm. As commented, M_{stray} is determined from the slope of the region $L > 100$ nm.

Technical implementation

The *Capacitive probe calibration* must be performed during all the types of NIM measurements (*jumping mapping* or *capacitance flying*)

to obtain quantitative measurements, and in the same technical conditions as these NIM measurements.

One aspect that must be taken into account is that, as the rest of capacitance related protocols, because of the slowness of the capacitance measurement, drift correction is necessary. The same strategy as explained in the *dynamic&step*s *with stiff probes* and *Capacitance Flying* protocols can be used to correct the drift in the capacitance probe calibration using a F-Z curve performed at high Z speed.

4.6. References

1 H. Cohen, C. Nogues, D. Ullien et al., "Electrical characterization of self-assembled single- and double-stranded DNA monolayers using conductive AFM," Faraday Discuss **131,** 367-376 (2006).

2 I. Horcas, R. Fernandez, J. M. Gomez-Rodriguez et al., "WSXM: A software for scanning probe microscopy and a tool for nanotechnology," Review of Scientific Instruments **78** (1), - (2007).

3 P. J. de Pablo, J. Colchero, J. Gomez-Herrero et al., "Jumping mode scanning force microscopy," Appl Phys Lett **73** (22), 3300-3302 (1998).

4 C. C. Williams, J. Slinkman, W. P. Hough et al., "Lateral Dopant Profiling on a 100 Nm Scale by Scanning Capacitance Microscopy," Journal of Vacuum Science & Technology a-Vacuum Surfaces and Films **8** (2), 895-898 (1990).

5 S. Hudlet, M. Saint Jean, C. Guthmann et al., "Evaluation of the capacitive force between an atomic force microscopy tip and a metallic surface," European Physical Journal B **2** (1), 5-10 (1998).

Chapter 5. The test sample

Summary: In previous chapters the motivation for our research has been explained, together with the technological adaptations and developments performed. In chapter 5 we focus on the sample that will be used to put into practice all aspects commented in the previous chapters. The sample selected is a protein system, the purple membrane. Chapter 5 provides the elements that have lead to the selection of this samples, a full picture of the scientific background, and the previous electrical studies on the sample. Furthermore, the good conditions of the sample used for our research are verified, and the structure of the sample at the nanoscale studied using high resolution Atomic Force Microscopy.

5.1. Requirements of the samples

In order to perform our work of thesis on the development of electrical characterization techniques using the AFM the use of an appropriate sample is a very important factor. The sample must not be an impediment nor a difficulty, but a tool that helps us in our developments. For these the sample must satisfy some requirements:

- The samples should be as flat as possible to minimize possible uncertainties in the electrical AFM measurements related to topography. If the sample is too rough, the AFM tip will touch the sample with different regions of the tip depending on the area of the sample on which it is, and this fact could produce uncontrolled variations in the electrical measurements. This does not mean that rough samples cannot be studied electrically with the AFM, but it brings an additional difficulty that at this stage of AFM technical development is better to minimize.

- The sample should provide repetitive measurements, this means that it must be easy to prepare, handle and to be able to withstand long days of measurements without degrading, so the same conditions are found every time we repeat the measurements.

- The sample should have a good background of knowledge, this way the interpretation of the results will be simplified and it can be more easily framed in the existing literature.

- The sample should be of scientific and technical significance. It is important that the electrical characterization at the nanoscale of the sample finds applications for other members of the scientific community, which will help to extend the impact of the findings and to consolidate the technology and knowledge developed.

5.2. The purple membrane

The purple membrane PM is a two dimensional crystal lattice composed of a lipid bilayer and a single protein species, the bacteriorhodopsin (bR), see Fig. 1, which acts as a light-driven proton pump across the Holobacterium Salinarum (H. Sal.) cell membrane. PM is currently the best known membrane-protein system. bR´s atomic-level configuration was established in 1999 and the lipid composition is known in detail. The bR belongs to the seven transmembrane proteins (7TM) whose great importance is discussed in the Appendix, it is composed of seven α-helixes surrounding a retinol aldehyde covalently linked to an α-helix by a weak covalent bond, the Shiff base. The assembling of the bR proteins in the cell membrane is a highly ordered two hierarchic level structure. The lower level is composed by the clustering of three bR proteins in triangular structure, named the trimer, and the higher level is composed by the arrangement of the trimers in the membrane, which form a close packed hexagonal lattice in the natural state of the bacteria which is referred to as *wild type PM.*

The bR is a very efficient light energy harvesting biomolecule, when it works it creates an electrochemical gradient across the H. Sal. Cellular

membrane that is used for the storage of energy. Of central importance to the functioning of the bR is the retinol 'antenna' attached to the aminoacid structure near the middle of the protein. The retinol absorbs the incoming photon and sets in motion (the photocycle) a sequence of electronic and conformational changes in within the protein which result in the release of a proton by the extracellular sides of the protein[1], see Fig. 1b. The protein then returns to its ground state through a few more conformational states.

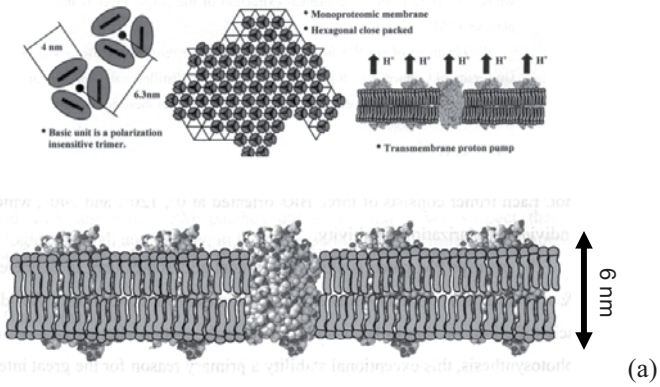

(a)

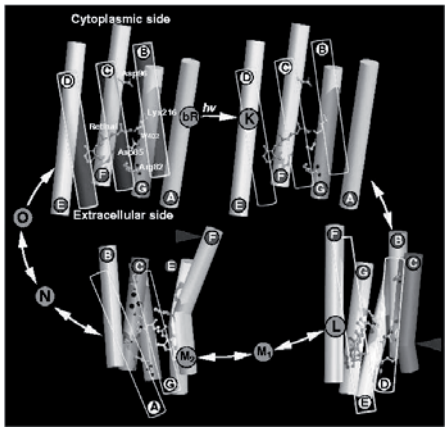

(b)

Fig. 1. (a) Cartoon of PM composed of bR trimmers aggregated into an hexagonal extended lattice in cell membrane the lipid bilayer. (b) Scheme of the structural changes that take place in the bR during its photocycle. Image from *Membrane Protein & Kinetic Crystallography Group @ Göteborg University.*

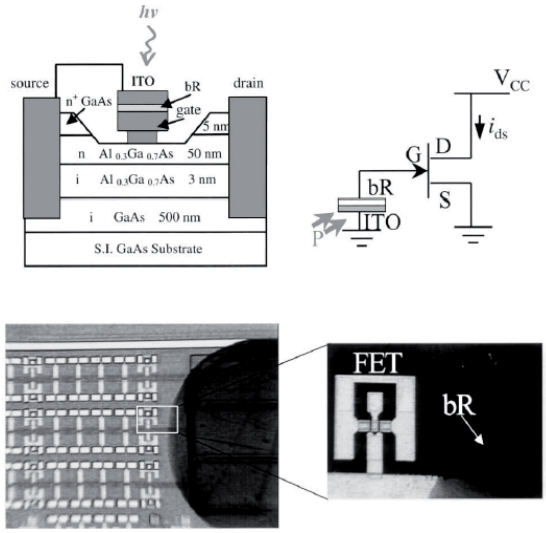

Fig. 2. Image from *Xu et al.* [7]. High-speed bR based photoreceiver

The bR is very stable, it is able to work in a wide range of conditions producing small changes in the photocyle: wide temperature range [2] [3], low and high pHs [4], and even in the absence of water [5].

One of the two most practical properties of the PM is that the PM is easily and extensively produced thanks to its bacterial origin, and that in solution the PM does not form vesicles, it is in a open sheet structure, which enormously facilitates the deposition of multiple layers of PM if required. All together the PM is an ideal candidate for both technical bio-applications and the scientific study of the 7TM proteins. Focusing in the technical application, the PM has shown a promising potential for building artificial retinas, optical information storage materials, and photoelectric energy conversion devices [6] [7] [8]. As previously commented in section 1.2, in the last years the PM has also started to be used for the development of nanoscale bioelectronic devices [9], which highlights the importance of developing techniques for electrically characterizing the PM at the nanoscale.

Another good property of the PM linked to its bacterial origin is that it is easily modified both genetically, chemically or physically. The number of variants of the PM is at this time very large. One of the most interesting variants of the PM from the point of view of the electrical studies could be the *bleached PM.* In this membrane the light sensitive retinol aldehyde molecule has been removed using a bleaching process, this causes, not only the lost of light sensitivity, but a restructuring of the membrane which has been observed both using NMR [10] and AFM [11] measurements. In particular the structure of the trimer is almost unchanged, but the long range lattice is lost. This is fact represents an interesting point of electrical study because it is well known from solid physics that periodicity has a great on effect on electrical properties of solid bodies.

The PM is thus a sample that fulfils all our requirements of relevancy, easy lab handling, and AFM friendly, and has a high implicit interest for its electrical study at the nanoscale. Nevertheless, it does not exist any electrical study of PM at the nanoscale. Fact which highlights the novelty and difficulties of the studies performed in this PhD work.

5.3. Obtaining the purple membrane

Halobacterium salinarum bacteria grow WT PM patches in their cellular membrane in the presence of high salt concentration solutions and a low luminosity environment. The patches can be released from the bacteria membrane by disrupting the bacteria using the increment of inner osmotic pressure produced by a lowering of the salt concentration in the solution, next filtering is used to separate the PM patches from the rest of the organic material floating around in the solution [12], and is finally stored in MilliQ water. We have typically used PM concentrations around 10^{-7} M.

To obtain bleached PM from WT PM, a 15 μM WT PM suspensions is mixed reacted with hydroxylamine (in a medium containing sodium phosphate 150 mM, hydroxylamine 1 M, and pH 7.0) and at the same time intensely shined with light with a luminance of 300 lux.

These processes have been performed by Prof. Esteve Padròs and his team from the Biophysics unit of the Department of Biochemistry and molecular biology of the Medicine Faculty of the Universitat Autònoma de Barcelona UAB.

5.4. Purple membrane characterization

5.4.1. Functional characterization by light absorbance

The optical activity of WT and the bleached types of PM can be characterized using the adsorption spectra of a beam of light shined through suspensions containing the membranes. Fig. 2 shows the results, there is a shift in the adsorption spectra following the bleaching of the PM patched in solution, which evidences the lost of the retinol molecule from the bR structure. The measurements were performed using a Varian Cary3-Bio spectrophotometer by Prof. Padròs and his team. In particular, the absorption maximum of PM (λ_{max} = 568 nm) disappears completely indicating full bleaching, and a new absorption maximum about λ_{max} = 360 nm appears.

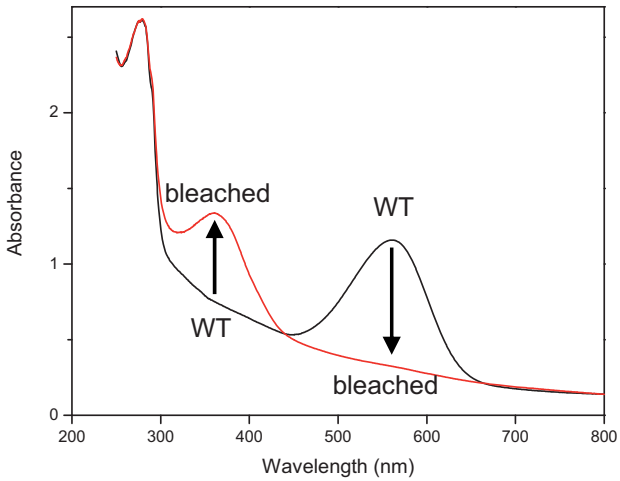

Fig. 3. Absorption spectra of the purple membrane recorded for Wild Type and bleached membrane suspensions. The absorption maximum of PM (λ_{max} = 568 nm) completely disappears indicating full bleaching, and a new absorption maximum at λ_{max} = 360 nm appears.

5.4.2. High resolution structural characterization of the purple membrane by atomic force microscopy

Prior to study electrically the PM samples, high resolution imaging of the samples using the AFM was performed to ensure that the state of samples at the nanoscale is the one expected. The methodology to perform this measurement is nowadays pretty standard (although not easy at all). Measurements are performed in an ionic solution to shield the long range electrostatic forces [13], and thus enhance the topographic resolution, the probes that are used have soft cantilevers and sharp AFM tips to enhance the lateral sensitivity to the repulsion forces from the bR proteins. For the sample preparation, we followed the protocol from Müller et al. [13], a) the PM patches were adsorbed on a freshly cleaved mica substrate, b) the solution was formed by dissolving both $MgCl_2$ and KCl p.a grade salts (Panreac Quimica SA) to a concentration of 50 mM and a pH buffer obtained by Trizma Base and Trizma HCl (Sigma Chemie AG, Buchs, Switzerland) to a final pH of 7.6. As AFM system

was used the same Nanotec Electronica S.L system used in the rest of the thesis but using the liquid cell module instead of the electrical module. Finally, the selected AFM probes were Olympus Biolever® probes with nominal force constant 0.03 N/m.

Figs. 4a and 4b show the raw high resolution topographic AFM images of the PM samples, WT and bleached PM. As expected only the WT PM shows a homogenous long range periodical structure. In the case of the WT PM the lattice shows the characteristic close packed hexagonal expected for the PM, whose unit cell is formed by the bR trimer, and which creates a very high density of bR protein in the membrane, 75 % of bR and only with 25 % lipids. The size of the trimers is observed to be about 6 nm and its dimensions are homogenous through out the membrane. As a conclusion the topographical AFM characterization demonstrates the good state of the sample we will use for the electrical studies and characterizes its nanoscale structure.

Fig. 5 shows topographical PM images in higher detail after image processing for noise removal using averaging. The larger image results from a three-fold averaging. The inset image results from the averaging of the unit cell of bR trimer, thanks to the averaging of ~40 unit cells it is possible to observe the inner planar 120º rotation symmetry of the bR trimer which is formed by aminoacid loop protrusions connecting the different transmembrane α-helixes that compose the bR protein.

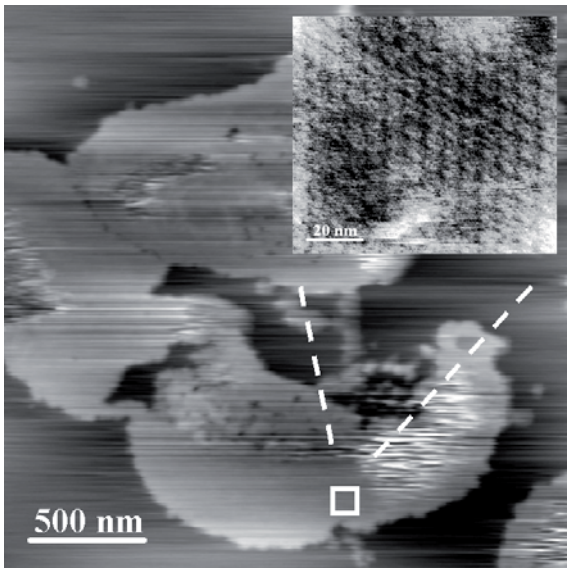

(a)

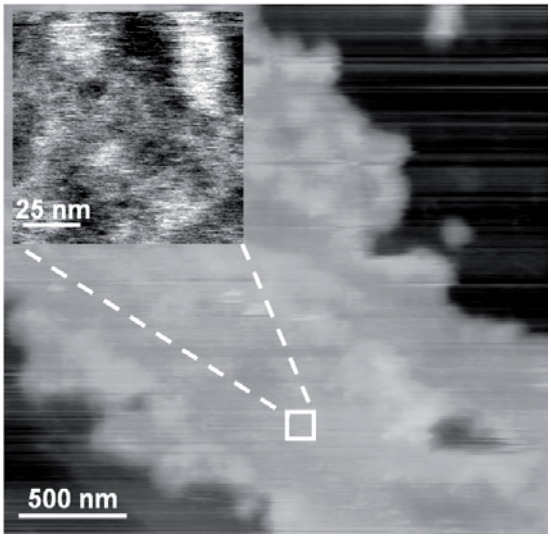

(b)

Fig. 4. (a) and (b) high resolution AFM topographs of PM containing respectively bR and bO, (a) clearly shows the hexagonal arrangement of the bR trimers in the membrane in contrast to (b) where no crystalline assembly of proteins is observed.

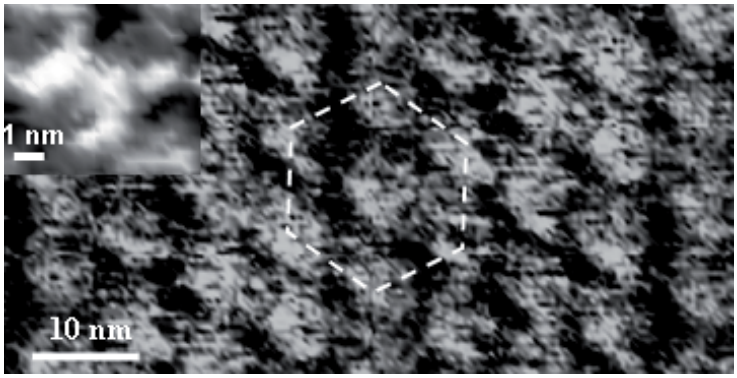

Fig. 5. Processed topographical AFM images of the PM containing bR. The larger image results from three-fold averaging to decrease noise. While the inset results from ~30 averages of the unit cell, the bR trimer, inner features of the bR trimer are observed formed by aminoacid loops connecting the α-helixes that compose the bR protein structured in a planar 120º rotation symmetry.

5.5. Preparation of the purple membrane for electrical atomic force microscopy experiments

To prepare the sample for electrical measurements a drop of 10^{-7} M PM suspension is placed on top a conductive substrate, where it is let to rest for about 15 minutes, so the PM patches in the suspension, which can be imagined as 'wet leaves' in water, have time to gently adsorb on the gold surface, and sometimes bend upon themselves or pile up forming stacks, that altogether tend to form steps of PM patches. Next the drop is removed by a N_2(g) flow and immediately introduced in the AFM chamber under dry N_2(g) for AFM characterization.

The conductive substrate selected is gold on mica. This substrate has two advantages, first it is very flat which assures that the topography observed corresponds to the PM patches and not any feature of the underlying substrate, and second the gold is an ideal material both for biological material handling and for microfabrication; gold is an inert material which avoids any degradation of the PM patches deposited on the

electrode and also a standard material in microfabrication, therefore highly appropriate from the point of view of the device fabrication. Fig. 6 shows a topographical characterization of a PM patch deposition, it is observed that several PM layers pile up in some regions.

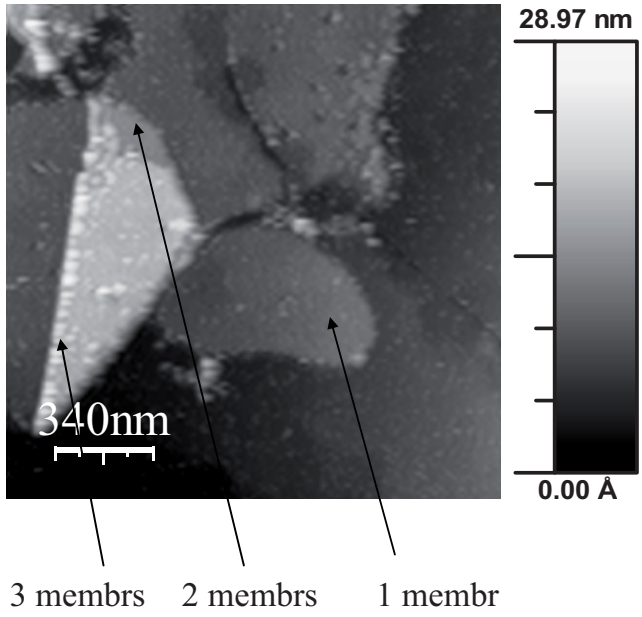

Fig 6. Topographic images of a PM patch in N_2(g) deposited on gold on mica performed in dynamic mode with probes with cantilevers of 2 N/m. The image shows that the PM patches pile up and, in this case, forms a pile of up to three PM membranes.

5.6. Literature on the electrical characterization of the purple membrane and comparison with the focus of this work of thesis

Although to date the purple membrane has not been electrically studied at the nanoscale, some studies have been performed at larger scales. In particular, there are three AC current studies performed on multilayered deposit of PM tens microns thick and several millimetres wide [14] [15] [16], and there is one DC current study using sub-millimetre electrodes on a PM deposit hundreds on microns wide of one monolayer thick with small gaps in between the PM patches [17].

The studies of AC spectroscopy on PM are performed using commercial spectrometers and with the sample at 60 % relative humidity. They have showed that in the range of frequencies from 10^{-2} to 10^{5} Hz the variation of the polarization/dielectric response is small, and only for higher frequencies (10^{6} to 10^{8} Hz) there is an adsorption peak in the polarization of the PM (caused by the resonance of the dipoles in the PM with the applied field). With respect to the range of frequencies from 10^{-2} to 10^{5} Hz, the value of (real part of) relative dielectric constant shows a value of 7 [14]. This information can be combined with measurements of capacitance in capacitors filled with PM [16], these measurements have shown that when the PM is dried there is a reduction of the dielectric constant of PM conglomerate inside the capacitor by a factor of ~1.4 times over a broad range of frequency, combining both measurements the dielectric constant of dried PM can be estimated to be 7/1.4 = 5. Currently in the literature there is not a direct measurement of this value.

On the other hand, the study of DC current-voltage *I-V curves* on PM membranes at 60 % humidity using sub-millimetre electrodes show that in the case WT PM monolayer the electron current flow is sensitive to sample illumination, event which does not take place in the bleached PM, where the retinal is not present, and this sensibility of the electron flow to the illumination does not appear. The authors associate this result to the

fact that only the WT PM can isomerate the retinal (conformational change of the bacteriorhodopsin caused by the adsorption of a photon of light), and conclude the retinal plays a role in the current flow through the PM. The work also uses a simple derivation of the current density per bR trimer dividing the total measured current by the area of the electrode, a value of ~ $3x10^{-19}$A is obtained.

In comparison with the existing literature, the electrical characterization of the PM by AFM carried out in this work of thesis will take the electrical studies to the nanoscale, this way, not only the study is performed at the natural scale of the membranes (they are 5 nm thick and the trimers ~ 6 nm wide), but the uncertainties associated with the macroscale are avoided, in particular, the averaging over large irregular areas, and uncontrolled presence of water between the PM layers of the PM deposits are avoided.

5.7. References

[1] R. Neutze, E. Pebay-Peyroula, K. Edman et al., "Bacteriorhodopsin: a high-resolution structural view of vectorial proton transport," Biochimica Et Biophysica Acta-Biomembranes **1565** (2), 144-167 (2002).

[2] O. Kensch, T. Restle, B. M. Wohrl et al., "Temperature-dependent equilibrium between the open and closed conformation of the p66 subunit of HIV-1 reverse transcriptase revealed by site-directed spin labelling," Journal of Molecular Biology **301** (4), 1029-1039 (2000).

[3] Y. Yokoyama, M. Sonoyama, and S. Mitaku, "Inhomogeneous stability of bacteriorhodopsin in purple membrane against photobleaching at high temperature," Proteins-Structure Function and Bioinformatics **54** (3), 442-454 (2004).

[4] L. P. Wang, Z. S. Shen, J. W. Wang et al., "The pH-dependence of photochemical intermediates of O and P in bacteriorhodopsin by continuous light," Biochemical and Biophysical Research Communications **343** (3), 899-903 (2006).

[5] G. Varo and L. Keszthelyi, "Photoelectric Signals from Dried Oriented Purple Membranes of Halobacterium-Halobium," Biophysical Journal **43** (1), 47-51 (1983).

[6] T. Miyasaka, K. Koyama, and I. Itoh, "Quantum Conversion and Image Detection by a Bacteriorhodopsin-Based Artificial Photoreceptor," Science **255** (5042), 342-344 (1992).

[7] J. Xu, P. Bhattacharya, and G. Varo, "Monolithically integrated bacteriorhodopsin/semiconductor opto-electronic integrated circuit for a bio-photoreceiver," Biosens Bioelectron **19** (8), 885-892 (2004).

[8] Q. Li, J. A. Stuart, R. R. Birge et al., "Photoelectric response of polarization sensitive bacteriorhodopsin films," Biosens Bioelectron **19** (8), 869-874 (2004).

[9] K. Bradley, A. Davis, J. C. P. Gabriel et al., "Integration of cell membranes and nanotube transistors," Nano Letters **5** (5), 841-845 (2005).

[10] S. Yamaguchi, S. Tuzi, M. Tanio et al., "Irreversible conformational change of bacterio-opsin induced by binding of retinal during its reconstitution to bacteriorhodopsin, as studied by C-13 NMR," Journal of Biochemistry **127** (5), 861-869 (2000).

[11] C. Moller, G. Buldt, N. A. Dencher et al., "Reversible loss of crystallinity on photobleaching purple membrane in the presence of hydroxylamine," Journal of Molecular Biology **301** (4), 869-879 (2000).

[12] Oesterhe.D and Stoecken.W, "Functions of a New Photoreceptor Membrane," Proceedings of the National Academy of Sciences of the United States of America **70** (10), 2853-2857 (1973).

[13] D. J. Muller, D. Fotiadis, S. Scheuring et al., "Electrostatically balanced subnanometer imaging of biological specimens by atomic force microscope," Biophysical Journal **76** (2), 1101-1111 (1999).

[14] I. Ermolina, A. Lewis, and Y. Feldman, "Dielectric properties of the bR membrane," Journal of Physical Chemistry B **107** (51), 14537-14544 (2003).

[15] P. Berntsen, R. Bergman, H. Jansson et al., "Dielectric and calorimetric studies of hydrated purple membrane," Biophysical Journal **89** (5), 3120-3128 (2005).

[16] J. A. Rupley, L. Siemankowski, G. Careri et al., "Two-Dimensional Protonic Percolation on Lightly Hydrated Purple Membrane," Proceedings of the National Academy of Sciences of the United States of America **85** (23), 9022-9025 (1988).

[17] Y. D. Jin, N. Friedman, M. Sheves et al., "Bacteriorhodopsin (bR) as an electronic conduction medium: Current transport through bR-containing monolayers," Proceedings of the National Academy of Sciences of the United States of America **103** (23), 8601-8606 (2006).

Chapter 6. Direct Current conductive atomic force microscopy mapping of the purple membrane

Summary: In previous chapters we have examined the importance of the electrical characterization of biomolecules with the AFM, have reviewed the state of the art, and have explained new AFM strategies to extend the range of the electrical information accessible through AFM operation. Now it is time to put the theory into practice, and use the protocols developed into our selected protein system, the purple membrane PM. Chapter 6 is dedicated to a simple but fundamental application, the direct current conductive AFM mapping of biomolecules, in this case of the PM.

6.1. Introduction

In chapter 2 it was commented that conventional conductive maps with C-AFM are obtained in contact mode, and this generates high lateral shear forces that tend to irreversibly damage soft samples, like biomembranes. In section 4.3, a new alternative was proposed to substitute contact mode, we proposed avoiding this problem by performing the conductive maps in Jumping mode (JM), rather than in contact mode, because in JM the AFM tip is laterally displaced when out of contact and thus minimizes the shear forces applied on the sample, and furthermore JM also grants mechanical stabilization of the contact prior to the electrical measurement by controlling the contact time, thus improving reproducibility of the measurement.

6.2. Technical details

Please refer to section 5.4 for the preparation of the PM (bR and bO) for the AFM measurement.

For the main operation aspects of C-AFM (DC) conductive mapping in JM please refer to section 4.3. The particular measurements shown in this chapter have been obtained with 3 nN maximum normal force, 100 mV applied voltage and 12 ms contact time (the acquisition takes place only during the last 0.1 ms).

One of the most important technical aspects refers to the contamination of the AFM probe. When performing current imaging of biological material contamination becomes a serious problem because biological material is pretty loose and easily gets adhered to the probe and avoids that the current flows through the tip creating an insulating coating at the tip apex. Controlling the contamination is a key aspect for a successful C-AFM conductive mapping on the PM, the first measure one must take is to reduce as much as possible the applied force, this greatly reduces the probability of getting the tip contaminated. But unfortunately, even if a small applied force is used, the long hours (typically > 5 h) that a AFM session lasts cause that the tip typically stops conducting at least a couple of times. Therefore to be able to finish the experiment it becomes critical to count with some strategy to clean the tip from the biological contamination. Ideally the cleaning should be performed in the same site where the experiment is being performed to be able to continue with the characterization of the PM patches we were studying, if the AFM probe is macroscopically removed from the working site, we will not be able to place it back, and we will have to start over with a new patch.

For the probes of 2-3 N/m spring constant and on PM patches on dry environment, it has been found that is possible to remove the contamination from the probe up and down over a PM patch without touching the patch but remaining a few nanometers away, in these conditions the contamination passes from the probe to the PM patch. Evidently this operation must be performed on a PM path which we are not studying.

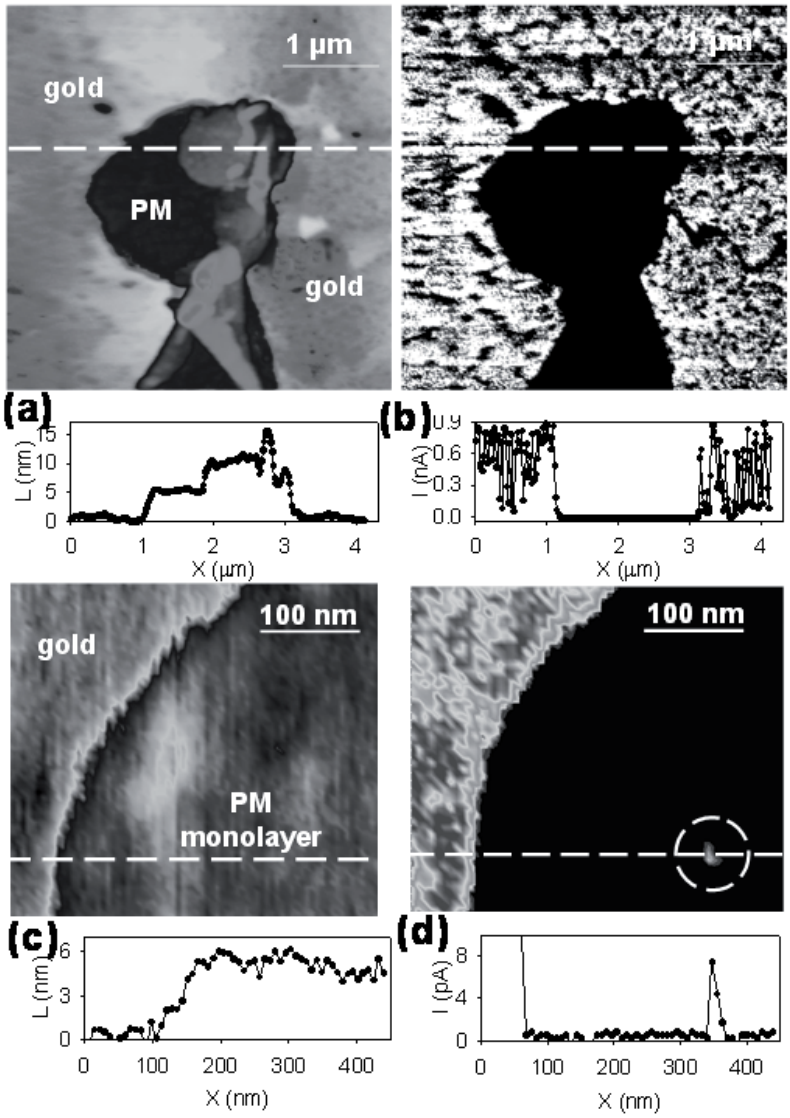

Fig. 1. Conduction mapping of Purple Membrane patches using Jumping Mode showing both the conduction and topography images simultaneously acquired, and the signalled profiles. (a) and (b) have been acquired on a multilayered PM patch, and (c) and (d) on a PM monolayer. Clear contrast is observed between the PM and the surrounding conducting gold. In a few of the PM monolayers (~ 5 %) isolated conducting pinholes are observed which are not related to topography.

6.3. Findings

The use of JM has allowed us performing conductive mappings of patches of PM. Fig. 1 shows simultaneous topographic (1a, 1c) and conductive images (1b, 1d) of a multilayer pile of PM patches (1a, 1b) and a single monolayer (1c, 1d).

The topography shows the expected ~ 5 nm thickness for the monolayer membranes, both for the first monolayer in contact with the substrate and subsequence monolayers placed on top of other monolayers. The quality of the images is good, and shows the same definition as the images obtained on the PM patches using *dynamic mode* and shown in the Fig. 6 of chapter 5.

In the long hours of work using jumping C-AFM we have verified that under low applied force and low enough bias the jumping C-AFM does not damage the membrane. Fig. 2 shows an example at this respect. The two images show the topography of the same area of a patch continuously scanned for more than one hour at 100 mV bias applied and 3 nN force. This result shows that jumping C-AFM does not produce alterations to the membrane.

The conduction images show that the PM presents a highly homogeneous insulating nature, and clear contrast is observed between the conductive bare gold areas and the PM patches. Contrast is also observed within the bare gold area, this contrast is clearly identified in the topographic image to be related to the presence of small remainings from the PM deposition (< 1 nm high) over the gold surface, where remainings from the deposition are present the current flow is reduced.

On the vast majority of the area of PM patches the electron current levels are lower than 0.3 pA, i.e. lower than the setup resolution. This fact sets a lower limit to the local resistance of the tip-PM monolayer, which can be estimated to be higher than 0.3 TΩ at 100 mV.

Thanks to the stable imaging achieved it is possible to perform a wide survey of the conduction on statistically significant number of PM patches.

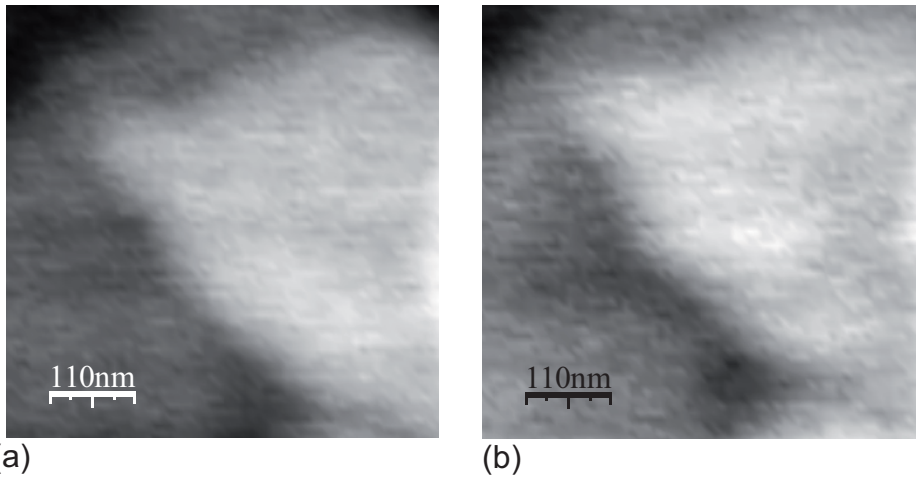

Fig. 2. (a) Topography of a purple membrane patch deposited on gold. Two layers of membranes are observed as well as the gold which is colored in sea blue. The sample was scanned using jumping C-AFM with an applied force of 3 nN and a bias of 100 mV. (b) Same area of Fig. 1 after several hours of continuous scanning. No damage to the sample is observed, it shows that jumping C-AFM does not produce alterations to the membrane. Digital drift correction was applied to avoid uncontrolled drift.

After studying a few tens of PM monolayers containing bR it has been detected that some bR containing PM monolayers present conductive pinholes on its surface with conductions levels of ~ 5 pA at 100 mV and lateral dimensions of ~ 10 nm, see Fig. 1d. Importantly, the conduction defects are stable, and consecutive scans find the conductive defects always at the same position, and are not related to any significant topographic feature. The percentage of PM patches that present these conductive defects is small of only about 5%, nevertheless its existence is significant, and even if the origin of these defects is still unknown, the finding of the conducting defects with the use of *conduction mapping* in JM represents a solid prove of the capability of the technique to retrieve

information on the distribution of the inner conduction properties of biomolecules at the nanoscale. All this performed without causing damage to the sample.

In the case of the bO containing PM monolayers no such conductive pinholes have been found, although it must be commented that the number of conductive maps of bO PM has been much smaller. Nevertheless, the important fact is that both types of membranes presented high insulating and homogeneous electrical behaviour, and that the C-AFM in jumping mode is able of detecting inner conductive features of the biological samples at the nanoscale.

Chapter 7. Point contact current-voltage spectroscopy on purple membrane monolayers

Summary: In chapter 6 we showed that the PM monolayer presents an extremely insulating nature that is highly homogeneous across its surface. In chapter 7 we try to gain further insight in the conduction properties of the PM by means of *point contact current-voltage spectroscopy* (*I-V curves*) using the *dynamic&steps with stiff probes* protocol.

7.1. Technical details

The studies on the conduction properties have been performed using the technologies and methodologies explained in previous chapters. The PM was biologically prepared as described in section 5.3 and deposited for the AFM measurement using the description from section 5.4. With respect to the *dynamic&steps with stiff probes* protocol, the description of the methodology can be found in section 4.2, in the particular case of the study of the PM monolayer, the protocol has been operated using a bias range from - 9 V to + 9 V in forward and backward sense, scanned at a rate of 108 mV/ms with a step height of 0.1 nm.

One particular aspect of the electrical measurement that is necessary to take into account when acquiring and analysing the *I-V curves* is that there is an offset in the current. There are two sources for the current offset in *I-V curves*, one is the offset of the preamplifier, which remains constant in time, and the other is the capacitive offset produced by the defect of the capacitance of the electrical circuit of measurement, and which is given by $I_{offset\_C} = C\frac{dV}{dt}$, and which, for our case, also remains constant because the voltage sweep rate is constant. To compensate the offset and obtain the real value of the current *I*, the *I-V curves* are corrected, and a constant I_{offet} value is added or subtracted to all the data in the *I-V curves,* I_{offet} is selected so we obtain I(0V) = 0.

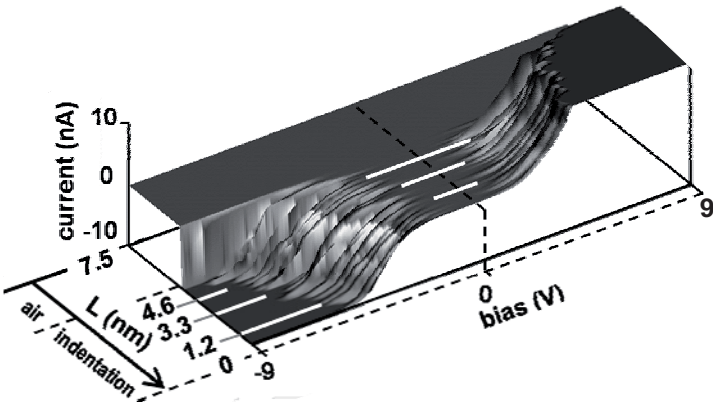

Fig. 1. 3D representation of the *I-V curves* acquired during a stepwise approach performed on a PM monolayer containing bacteriorhodopin using the *dynamic&steps with stiff probes* protocol. The current *I* is plotted as a function of the tip-substrate distance *L* and the applied bias *V*. The current is observed to grow when the *V* is increased and *L* reduced. Three *I-V curves* at *L* = 1.2, 3.3 and 4.6 nm are signaled and individually plotted in Fig 2.

7.2. Qualitative electrical analysis of the electrical measurements from the wild type purple membrane (bacteriorhodopsin membrane)

Fig. 1 shows a 3D linear representation of the typical structure of the *I-V curves* that it is obtained when one full stepwise indentation process is performed on a monolayer of PM, in this case PM containing bR. The 3D plot is made by representing the current flow *I* through the PM monolayer as a function of the tip-substrate distance *L* and the applied bias *V*. The 3D plot clearly shows a continuous evolution towards higher values of *I* when *V* is increased and *L* decreased. The evolution is soft and regular which indicates stable measuring conditions, fact remarkable considering the measurements are being performed on a

biological sample, traditional source of instable and noisy electrical measurements.

Fig. 2 shows three *I-V curves* extracted from the stepwise approach shown in Fig. 1, where each of the *I-V curves* takes place at different *L* distances (signalled in Fig.1). The three *I-V curves* have been plotted using two different representations to provide a better visualization of the physical situation: (a) log-linear and (b) Fowler-Nordheim representations. In order to highlight the agreement of the measurements with the established physical theory, next explained in section 7.4, the fittings of the theory to the data are plotted in Fig. 2 as continuous lines.

The first thing we observe in Fig. 2a and 2b is that the evolutionary trends observed, and previously commented, in Fig. 1 are confirmed with a higher detail. Nevertheless Fig. 2 expands the range of information available from Fig, 1 and provides new information not observable in Fig. 1, in particular Fig. 2a shows an exponential trend of the current *I* with respect the bias *V* during all the range of applied bias, and, what is more interesting, the exponential trend is divided in two separate regions depending on the applied bias *V*, which are separated by an elbow-like transition between them. The importance of this finding will be further discussed over the next sections.

This way, the new developed *Dynamic&steps with stiff probes* protocol, and the extended bias range achieved, has allowed us to observe a physical phenomenum, the transition between two conduction regimes, which would not have been possible if we would have been restrained to the $V < 1$ V bias range present in previous C-AFM *point contact current-voltage spectroscopy* protocols [1,2,3,4].

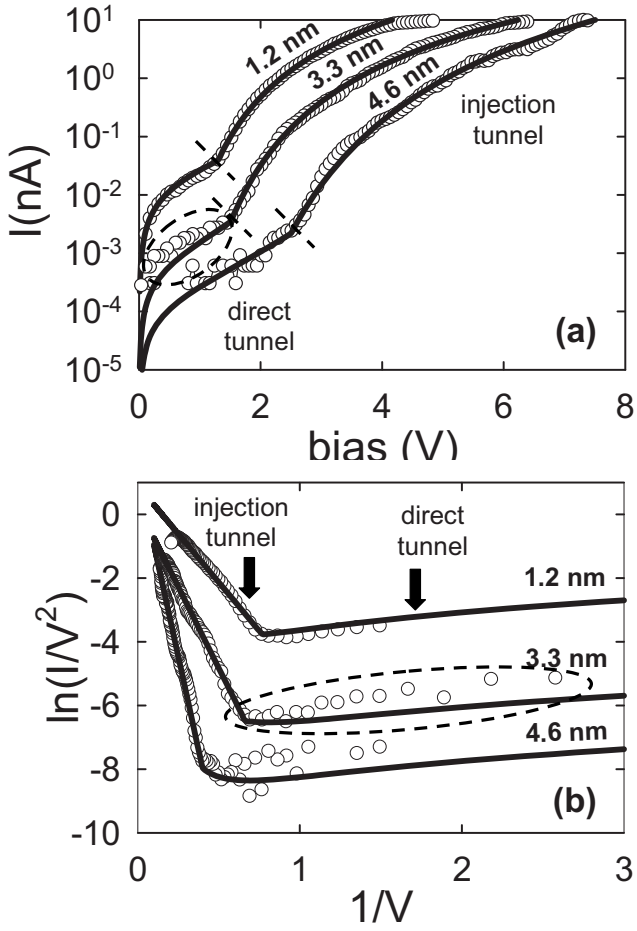

Fig. 2. (a) Log-linear and (b) Fowler-Nordheim representation of a selected set of current-voltage curves at different indentation depths for the Wild Type Purple Membrane containing bacteriorhodopsin. Continuous lines represent theoretical fittings to the experimental data (from the injection regime and the transition bias). Perfect fitting is observed in the injection tunnel regime. In the direct tunnel regime in some cases the curves are fitted automatically with no additional fitting parameter, but this is not the general case as shown in the regions signalled by a slashed ellipse. Nevertheless in all the curves the transition point between the two transport regimes is clearly observed.

7.3. Qualitative electrical analysis of the results from the bleached Purple Membrane containing bacterioopsin

Qualitatively there is no significant difference between performing the *point contact current-voltage spectroscopy* on a PM monolayer containing bR or bO. Both measurements on bR and on bO generate in the current *I* the same trends as a function of the applied bias *V* and tip-substrate distance *I*, furthermore the same mechanical behaviours are also observed. Fig. 3 shows a 3D plot for a measurement performed on a bO monolayer, it is clearly observed that there is not significant difference at simple view from the 3D plot performed on a bR monolayer in Fig. 1. It will be necessary to go into a quantitative in-deep study to observe some differences between the bR and the bO.

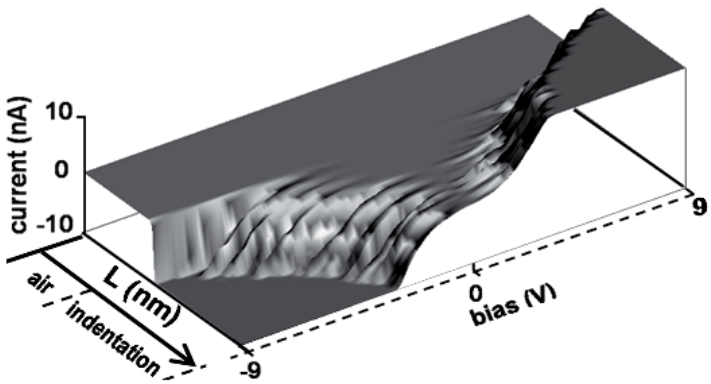

Fig. 3. 3D representation of the I-V curves acquired during a stepwise approach performed on a PM monolayer containing bacterioopsin

7.4. Electron transport theory

Due to the high degree of reproducibility and reliability of the measurements performed a quantitative analysis of the data can be attempted. For the present measurements, the *I-V curves* display all the features characteristic of non-resonant tunnel transport through a metal-insulator-metal (MIM) system, which indicates, as other authors previously suggested, see section 2.2.3, that the presence of the biomolecule between the probe and the substrate creates an energy barrier between the AFM probe and the substrate that prevents the direct crossing of the electrons from the AFM probe to substrate, forcing the electrons to cross through quantum tunnelling.

Simmons in his theory from the year 1963 derived a theoretical expression that enables the description of the tunnel transport through any energy barrier of any MIM system using an equivalent linear barrier model. In the model of Simmons the height of the barrier is the mean value of barrier height in the real system [5]. The general current voltage characteristics for tunnel MIM systems can then be expressed in terms of Simmons theory as:

$$I = \frac{qA}{2\pi h \bar{d}^2}\left[\bar{\phi} e^{-\frac{4\pi\sqrt{2m^*}}{h}\bar{d}\sqrt{\bar{\phi}}} - (\bar{\phi}+qV)e^{-\frac{4\pi\sqrt{2m^*}}{h}\bar{d}\sqrt{\bar{\phi}+qV}}\right] \quad (1)$$

where A is an effective electric contact area, q is the electron charge, m^* is the effective mass of the electron, V the applied voltage and h the Planck's constant. Moreover, $\bar{d}$ and $\bar{\phi}$ are the effective tunnel distance and the mean tunnel barrier height, respectively, which depend on both the metal-insulator contact barrier height ϕ_c, the inter-electrode distance L and the applied voltage, V. In the simplest case of a symmetric MIM system, assuming a linear voltage drop inside the insulator and neglecting space charge and image charge effects (see Fig. 4a) one can show that [5] :

$$\bar{d} = \begin{cases} L & , \quad qV < \phi_c \\ \dfrac{\phi_c}{qV} L & , \quad qV > \phi_c \end{cases}$$

and (2)

$$\bar{\phi} = \begin{cases} \phi_c - \dfrac{qV}{2}, & qV < \phi_c \\ \dfrac{\phi_c}{2}, & qV > \phi_c \end{cases}$$

The regime for $qV < \phi_c$ corresponds to the *direct tunnel* regime in which electrons tunnel directly from metal to metal, while the regime for $qV > \phi_c$ corresponds to the *injection tunnel* regime (or Fowler-Nordheim regime) in which electrons are injected first into the insulator and then arrive to the second electrode. By using Eqs. (1) and (2), the current voltage characteristics predicted by Simmons theory look like the ones shown in Fig.2, where we used the following parameters A=0.2 nm^2, m^*=0.04 m_0, L=5 nm, ϕ_c=2 eV. The curves have been plotted in linear-linear, log-linear and Fowler-Nordheim representations to facilitate the comparison with the experimental results.

Eqs. (1) and (2) can be written in a explicit form for the direct tunnel regime as [5]

$$I = \frac{qA}{2\pi h L^2}\left[\left(\phi_c - \frac{qV}{2}\right) e^{-\frac{4\pi\sqrt{2m^*}}{h} L\sqrt{\phi_c - \frac{qV}{2}}} - \left(\phi_c + \frac{qV}{2}\right) e^{-\frac{4\pi\sqrt{2m^*}}{h} L\sqrt{\phi_c + \frac{qV}{2}}}\right] \qquad qV < \phi_c \qquad (3)$$

while in the injection regime can be approximated by [5]

$$I = \frac{q^3 A V^2}{8\pi h L^2 \left(\frac{\phi_c}{2}\right)}\left[e^{-\frac{8\pi\sqrt{2m^*}}{h}\left(\frac{\phi_c}{2}\right)^{3/2}\left(\frac{L}{qV}\right)}\right] \quad qV > \phi_c \qquad (4)$$

For the range of parameters considered in the present paper the agreement between the approximate expressions in Eqs. (3) and (4) and the exact

ones in Eqs. (1) and (2) is excellent as shown by the symbols in Fig. 4b-d.

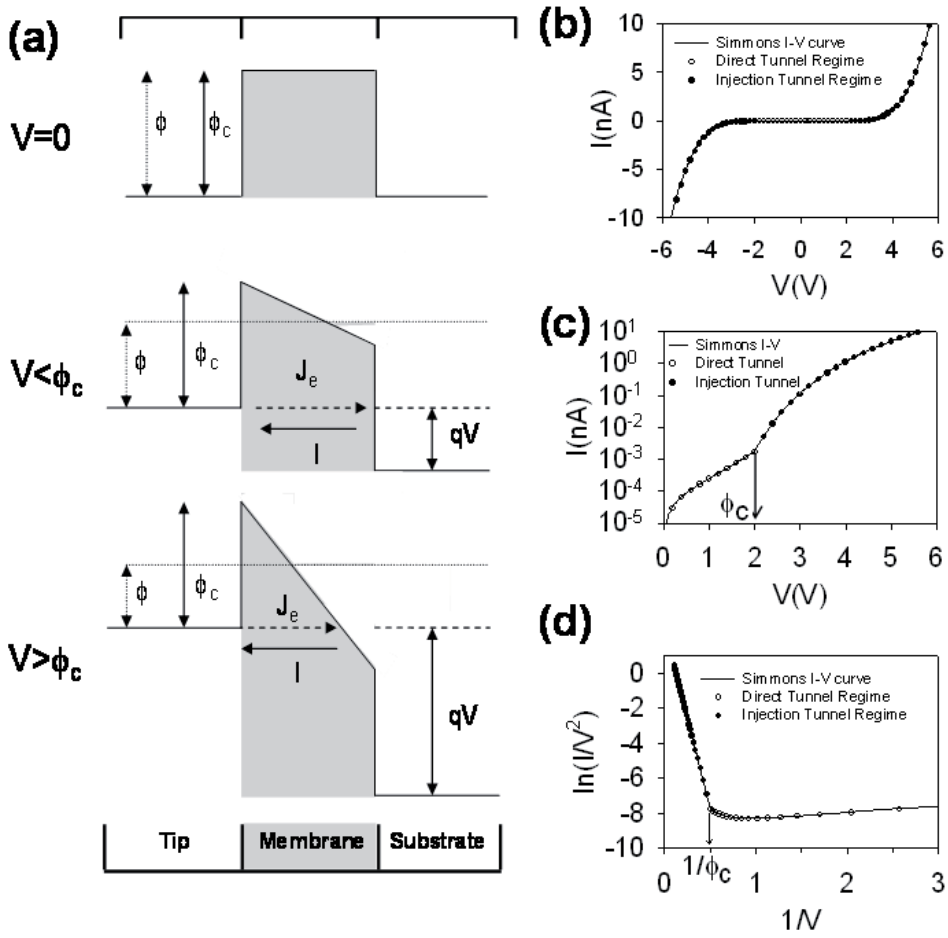

Fig. 4. (a) Schematic representation of the energy profile and electron transport in a MIM system under the linear voltage drop assumption. (b), (c) and (d) (continuous line) linear, log-linear and Fowler-Nordheim representations of the current-voltage characteristics predicted by Simmon's tunnel theory for MIM systems (Eqs. (1) and (2)). Empty circles represent the direct tunnel regime according to Eq.(3). Filled circles represent the injection tunnel regime according to the approximation in Eq. (4). Parameters are: A=0.2 nm^2, m*=0.04 m_0, L=5 nm, φ_c=2 eV

7.5. Parameter extraction protocol

From the previous theoretical framework it is possible to extract the parameters characterizing the electron conduction through the purple membrane in a quantitative way by using the following protocol derived in this PhD work.

First, the value of the contact barrier height ϕ_c is estimated from the crossover between the direct and injection tunnel regimes. Next, we extract the slope of the linear portion of the Fowler-Nordheim representation of the current-voltage characteristics, which according to Eq. (4) is given by

$$s = -\frac{8\pi\sqrt{2m^*}}{hq}\left(\frac{\phi_c}{2}\right)^{3/2} L \qquad (5)$$

From this value, and the estimated values of the contact barrier height and the inter-electrode distance L (evaluated as described before) we estimate the value of the electron effective mass, m^*. Finally, we estimate the only remaining parameter, the effective area, A, by making the experimental and theoretical current-voltage characteristics to match. We fine tune the estimated values to obtain the best fitting in all the current-voltage characteristic representations between the experimental and theoretical curves.

7.6. Quantitative electrical analysis of the wild type purple membrane (bacteriorhodopsin membrane)

Fig. 2 shows the quality of the fittings achieved using the extraction protocol for the various representations. The injection region shows excellent agreement for all the curves. In the direct tunnelling regime some curves are fitted automatically with no additional fitting parameter, but this is not the general case, as is seen in Fig. 2a and 2b in the region marked with a slashed ellipse. It is important to highlight that in all the cases it is possible to distinguish the transition between the

direct and the injection regimes and therefore to determine the contact barrier height by means of the proposed procedure.

The evolutions of the conduction parameters ϕ_c, m^* and A as a function of the inter-electrode distance L and voltage polarity are given in Fig. 5 for the case of PM monolayer, for the set of 3 independent measurements performed.

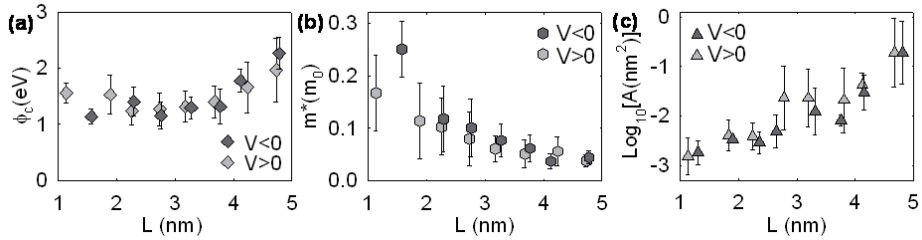

Fig. 5. (a) Contact barrier height, (b) effective electron mass and (c) the logarithm of effective area as a function of the inter-electrode distance L for the electrons injected from the substrate (V < 0) and from the tip (V > 0). The values are obtained using the extraction protocol of section 7.5 and correspond to three independent acquisitions on different membrane patches. Bars represent the standard deviation.

As can be seen the results obtained are reasonably reproducible. At the minimal deformation (L = 5 nm) the value of the height of the barrier ϕ_c is 2.2±0.6 eV, the effective mass m^* of the electrons in the barrier is 0.04±0.02 m_0 and the emission area A is 0.2 nm^2 (-0.7±0.7 in $\log_{10}$ units). Further reduction of L produces a lowering of the barrier height ϕ_c at a rate of 0.6±0.2 eV/nm until L = 3 nm where it stabilizes at a value of ~ 1.5±0.2 eV. Simultaneously the effective mass m^* increases in a 1/L-like trend, for L ~ 2.5 nm reaching 0.2±0.1 m_0, and A follows an exponential reduction which reaches ~0.002 nm^2 for L~1.5 nm (-2.9±0.6 in $\log_{10}$ units). The process presents minimal influence of voltage polarity, with only scarce asymmetry respect the bias polarity being found in effective mass m^*: higher values are found for the electrons injected from the substrate towards the tip (V < 0).

7.6.1. Results in the context of previous knowledge

The values of ϕ_c obtained agree with previous *I-V curves* measurements on biomolecules using C-AFM on small bias ranges (<1V), where only the direct tunnel regime is probed [1,2,3,4]. The low effective mass measured for the electrons in the PM monolayer is similar to the m^* observed in some semiconductors such as GaAs, InAs or InSb. This is one order of magnitude smaller than those found in other nanometric systems such as self-assembled monolayers and very thin silicon oxide films [6,7]. At this time, no previous measurements of m^* in biological material for comparison exist.

The trends in ϕ_c and m^* (see Fig. 5a-5b) as a function of the inter-electrode distance L are typical of metal-insulator-metal systems and have been well studied in oxide films [8,9] and respond to the sum of several effects from the idealizations of the barrier model, in particular the idealization of the potential drop at the interphase, the parabolicity of the band, the image charges, or the presence of defects. Fig. 6a shows the evolution of m^* as a function of the L predicted by *Städele et al.* [9]. Other works from *Zhao et al.* [3], on the theoretical calculations on the influence of protein atomic packing, predict the atomic packaging remains constant for $L < 3$ nm and, as a result, ϕ_c is also constant (see Fig. 6b-c), which is in full agreement with our results. Finally, the high symmetry of all the *I-V curves* indicates similar physical conditions in both interfaces.

With respect the effective contact area A, the values observed is in agreement with previous observations of field emission areas [10] in field emission devices, and its evolution observed towards smaller values when L is reduced agrees with extended FN theories for field emission devices with hemi-ellipsoidal electrode geometries [11], which agree with the shape of our AFM tip. The FN theory for hemi-ellipsoidal electrode geometries shows that effective contact area A is proportional to L^2, and therefore for our experiment predicts, as L goes from 5 to 1 nm,

a reduction in A by a factor of 24, factor is in rough agreement with our experimental values.

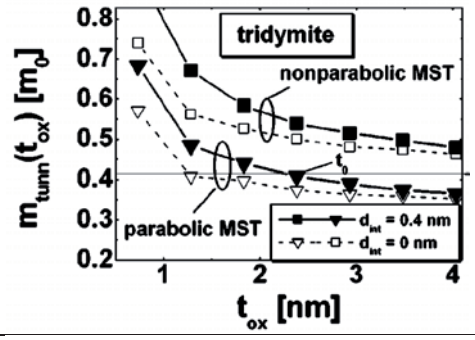

Fig. 6 (a), from *Städele et al.* [9] . Theoretical predictions for the dependence of the tunnel mass m^* (given in units of the free electron mass m_0) on oxide thickness t_{ox} , calculated using the tridymite oxide model for a parabolic and a non parabolic bandgaps. Please observe the high similarity with the results we have found in the PM.

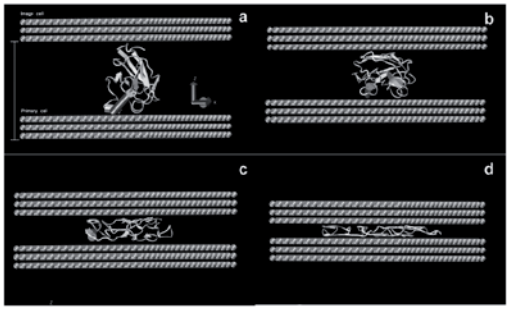

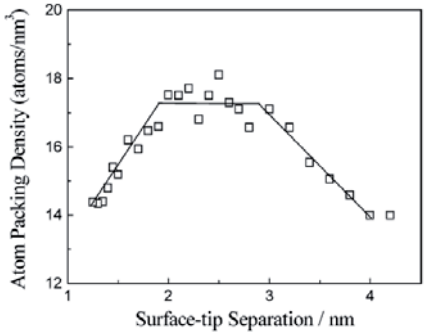

Fig. 6 (b)(left) and **6(c)**(right), from *Zhao et al.* [3]. **(6b)** Structure evolution of the azurin protein on a surface constructed at interfacial separation distances of (a) 4.0 nm, (b) 2.7 nm, (c) 1.7 nm, and (d) 1.0 nm. **(6c)** The atom packing density is increased as the inter-electrode distance L is reduced, but it easily reaches a limit provided by the repulsive forces at L = 3 nm.

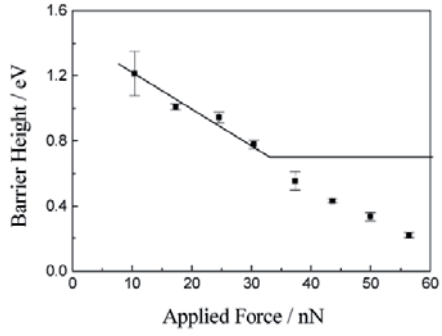

Fig. 6(d), from *Zhao et al.* [3] (solid line) Simulated evolution of the barrier height Φ upon protein compression. Once the limit atom packaging limit is reached the barrier height Φ remains constant. Please observe the high similarity with the results we have found in the PM.

7.6.2. Current density through an individual bacteriorhodopsin trimer

The excellent quantitative agreement of the conduction parameters with well established theoretical models again support the reliability of the proposed measuring methodology.

Based on this, it is possible now to estimate the current flow carried by the individual protein unit forming the purple membrane, the Bacteriorhodopsin trimer. We obtain a value of 50 pA per trimer considering a trimer area of ~ 25 nm^2 and the current density of ~ 2 pA/nm^2 measured at 1 V (see Fig. 2a). This current is several orders of magnitude higher than previous measurements using sub-millimetre electrodes (~$3x10^{-19}$ A per trimer) [12] but it is consistent with the C-AFM measurements of other protein systems [1,2,3,4]. The reason we propose for this discrepancy is that in the sub-millimetre electrodes the current flow is non-homogenous, but smaller in some spots of larger inter-electrode distance. C-AFM measurement is free from this uncertainty as we measure at the nanoscale, thus overcoming the problems of inter-electrode distance variations along the electrode and other potential sources of macro scale artefacts.

7.7. Quantitative electrical analysis of the results from the bleached Purple Membrane (bacterioopsin membrane)

Fig. 7 shows the quality of the fittings achieved using the explained extraction protocol of section 7.5 for the bleached Purple Membrane containing bacterioopsin bO in log-lineal representation. As in the case of Wild Type Purple Membrane containing bacteriorhodopsin bR, both the direct and the injection tunnelling regime shows good agreement with the theory, and only some slight mismatches are observed in some *I-V curves*, which nevertheless does not avoid determining the contact barrier height Φ and effective mass m^*. Therefore it can be concluded that the electron transport takes place by the same mechanism both for the bO and the bR, and that this mechanism is non-resonant tunnelling transport. This also renders valid all the analysis performed in section 7.6 for the case of the bR PM also to the case of the bO PM. It can then be concluded that the only possible difference that can be found in the electron conduction through bO and bR are the parameters of the conduction but not the conduction mechanism itself (at least for our 0% relative humidity studies). This idea is contrary to the one expressed by *Jin et al.* in their study of the PM at 60% RH using sub-millimetre electrodes [12] , where it was concluded that the presence of the retinal molecule in the bR protein activated a two step tunnelling mechanism not present in the retinal free bO protein.

In Fig. 8 the evolution of the conduction parameters Φ, m^* and A as a function of the tip-substrate distance L is shown both for the bR and the bO containing PM (the data for the bR PM one is the same as Fig. 5). As in the case of bR measurements, 3 independent measurements have been performed in the bO PM. The barrier height Φ and the emission area A show similar behaviour with L in both the bO and bR membranes in all the distance L range. Nevertheless, the barrier height Φ is approximately ~0.5 eV higher for the bO membrane than for the bR membrane in the distance range from ~ 5 nm to ~ 3.5 nm. For $L < 3.5$ nm there is not barrier height Φ difference.

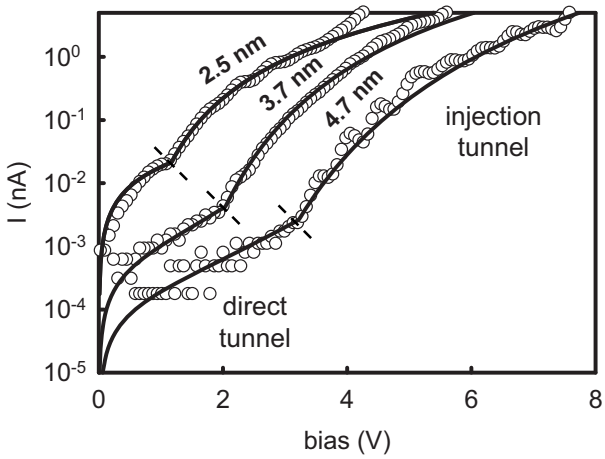

Fig. 7. Log-linear representation of a selected set of current-voltage at different indentation depths for the bleached Purple Membrane containing bacterioopsin. Continuous lines represent theoretical fittings to the experimental data (from the injection regime and the transition bias). The fitting is good both for the direct and injection tunnel regimes, and in all the curves the transition point between the two transport regimes is clearly observed.

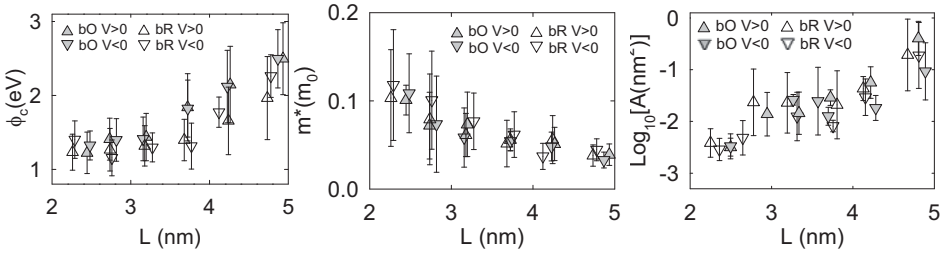

Fig. 8. Comparative graph of the evolution of the conduction parameters Φ, m^* and A as a function of the tip-substrate distance L at the bO and bR containing PM. The bR PM data is the same of Fig. 5. As in the case of the bR PM, 3 independent measurements have been performed on 3 PM patches. The bars represent the standard desviation.

The observed difference in barrier heights at bR and bO is probably due to the variation of structure of the membranes upon bleaching. In particular, as was determined by the high resolution AFM images of *Moller et al*. [13], when bR is transformed into bO during the bleaching process of the PM, the membrane suffers: (a) lost of the long distance

ordering that changes from a periodic lattice into a disordered assemble of trimers, and (b) significant increase in the inter-trimer distance.

The relation between the barrier height and the structural details of the proteins is further supported by the fact the difference in the barrier height for the bO and bR membranes disappears for $L < 3.5$ nm. Fact which in rough agreement with the atomic packaging limit determined by *Zhao et al.* [3], which sets for $L < 3$ nm a maximum compression limit, and thus indicating that for $L < 3$ nm the protein is so compressed that the structure of the protein is independent of original structural details and of its ordering. This way the convergence of the values of the barrier height from the bR and the bO membranes for $L < 3.5$ nm would be fully understandable.

With respect the effective mass m^*, the fact that both membranes show identical behavior and values for the effective mass m^* as a function of distance L could indicate that the ordering of the membrane, and its crystalline assembly of trimers, does not affect the value for the m^* of the electrons that cross the membranes. This fact would indicate that m^*, which physically is directly related to the structure of the energy bands of electrons in the membrane, depends exclusively on the structure of the trimer, fact which agrees perfectly with previous AFM and NMR observations, where it was concluded that the structure of the trimer remains practically unaltered between the bR and bO membranes [13,14], and thus explaining why the value of m^* remains unaltered in the bR and bO membranes; m^* is only dependant on the structure of the trimer not on the inter-trimer organization.

To assure the confidence in the results, it is important mentioning that the same types of conductive substrate and tip coatings are used in all the measurements, and thus the surface electronic structure at the electrode-membrane interface must be similar in all the measurement. This fact is further supported by the highly symmetry of the *I-V curves* in the bO and the bR membranes. And this fact further assures that the differences observed in the values of the barrier heights for the bR and

bO membranes must be inherent to a variation in the inner (electronic) structure of the membranes.

7.8. Mechanical aspects of the measurement

Experimentally it has been found that the mechanical behaviour of the bR and for the bO containing membranes is the same. Therefore the study of the mechanical behaviour during the setpwise approach is explained in a single section which can be applied indistinctively to both types of membranes.

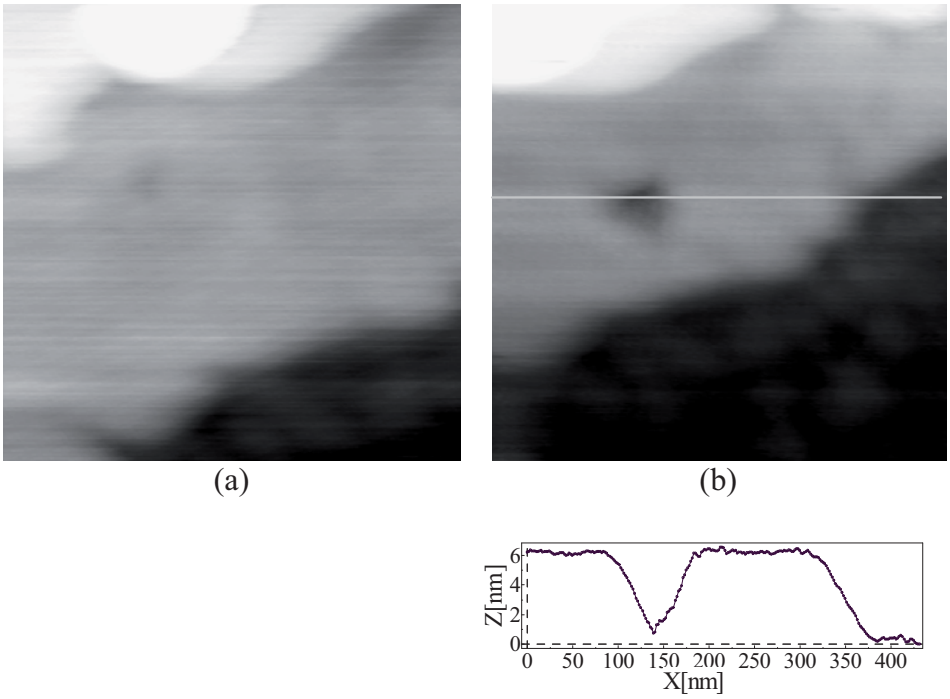

Fig. 9. (a) 336 x 336 nm^2 image of the PM monolayer prior to the electrical characterization, and (b) the same region after the electrical characterization process, a profile is also shown.

7.8.1. Topographic *dynamic mode* examination

Thanks to the topographic study of the area of the sample where the measurements were performed it is possible to know the mechanical conditions that were present during the measurement, and this way notice possible mechanical malfunctioning, as for example a sudden unexpected lateral movement. To perform the topographic evaluation *dynamic mode* is used. The topographic evaluation checks that everything has developed correctly in the measurement, in the case the measurement has been successful the PM monolayer shows on its surface a clear imprint of the pyramidal shape of the AFM tip (see Fig. 9a and 9b), where no lateral displacements are appreciated and deepness of the indentation is of 5 nm, i.e. the membrane thickness. When this type of imprint is not observed it is a sign of unexpected movements which have taken place. Finally, the imprint image is also a confirmation that the measurement has been performed in the spot we desired.

The topographic image also reveals us useful information about the mechanical properties of the membranes, from the clear imprinting of the AFM tip on the PM monolayer it is clear that the membrane behaves plastically in the dry N_2(g) environmental conditions of the study. This result agrees with similar observations by *Zhao et al*. on azurin protein system, where a plastic behaviour was observed when studying the azurin protein with the C-AFM [3]. Nevertheless in the case *Zhao et al*. the measurement was performed at 40-50% relative humidity, and the fact that both protein systems show plastic behaviour independently of the relative humidity seems to indicate that protein systems behave plastically when deformed at the nanoscale at least in a wide range of humidity.

7.8.2. Mechanical evolution

When performing an *I-V curve* on soft samples, concern exists over whether or not the whole curve is taken under constant deformation and applied force, due to the presence of the electrostatic forces related to the applied voltage. With the *dynamic&steps with stiff probes* protocol

this can be quantified in a precise way by analyzing the deflection-voltage curves simultaneously recorded in the 3D experiments.

Fig. 10 shows the evolution of the cantilever deflection as a function of the applied bias when the tip is in air and when in contact with the membrane (Fig. 10a and inset Fig. 10c) and the cantilever deflection as a function of the piezo displacement at 0 V applied (Fig. 10c) during the stepwise approach of the tip on a PM monolayer.

The first important aspect to note is that, due to the use of a stiff cantilever (~40 N/m), the applied bias produces, in all cases, a very small deflection of the probe (below 1 nm) and that the deflection of the cantilever when the tip is in the air (~ 1 nm) (Fig. 10(c) inset) is still further reduced when the tip is in contact with the membrane ~ 0.6 nm (Fig. 10a). These results show that very small deformations are produced on the membrane during an *I-V curves*, in spite of the wide voltage range used, thus supporting the use of stiff cantilevers to perform these measurements.

The reduction in the cantilever deflection when in contact with the membrane as compared to the deflection in air can be understood in terms of the mechanical response of the membrane. This mechanical response can be analyzed by reconstructing a force distance curve from the 3D image by selecting all points at 0 V applied. The result is shown in Fig. 10c. The evolution of the cantilever deflection (i.e. applied force) when the tip is in contact with the membrane shows two regions, a compressive region in which the cantilever bends much less than the piezo displacement increase and a non-compressive region where the cantilever bends in accordance with the piezo displacement. In the former case the tip essentially indents the membrane while in the later case it remains at a constant distance from the bottom electrode (this distance can obtained as $L = t_m - |\Delta z_p| + |\Delta d| \sim 5nm - 5nm + 1nm \sim 1nm$).

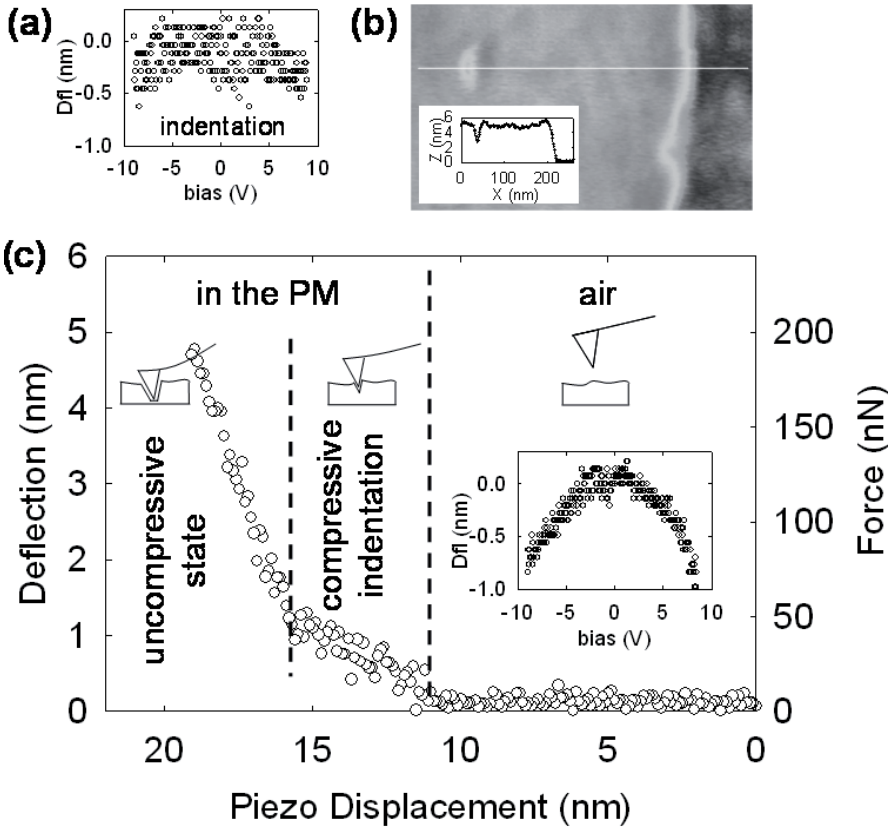

Fig. 10. Cantilever deflection as a function of the applied bias at a fixed piezo displacement for (a) the tip in contact with the PM monolayer and (inset (c)) the tip in the air. (b) Partial indentations performed in a PM monolayer and imaged in dynamic mode. The mark of the tip is observed thus showing the plastic nature of the PM in dry conditions. (c) Cantilever deflection (left axis) and applied load (right axis) as a function of piezo displacement as the tip goes from being in the air to in the PM. The tip in the PM goes through two linear regions of slopes ~10 nN/nm and 40 nN/nm corresponding respectively to a compressive and uncompressive region of the mechanical evolution of the sample.

In the compressive region the cantilever deflection shows a linear dependence with the piezo displacement with a proportionality constant k_{ef}~10 nN/nm. This finite value indicates that during its deformation the membrane generates a force opposite to the deformation which can sustain part of the cantilever applied force. The deformation force is also

shown to vary linearly with the membrane deformation at a rate of k_m~13 nN/nm. The relationship between both values and the spring constant of the cantilever (k_l~40 nN/nm), is

$$k_{ef}^{-1} = k_m^{-1} + k_l^{-1} \qquad (6)$$

as corresponds to the effective spring constant of two springs in series, see Fig. 11a.

In the uncompressive region, the force applied by the cantilever varies with the piezo displacement with a slope of ~40 nN/nm, thus meaning that the compressed membrane is able to sustain all the applied force by the tip. We note that in this region the *I-V curves* present a rectifying behaviour, this fact further proves that the tip is some distance away from the substrate, otherwise the *I-V curves* would be linear.

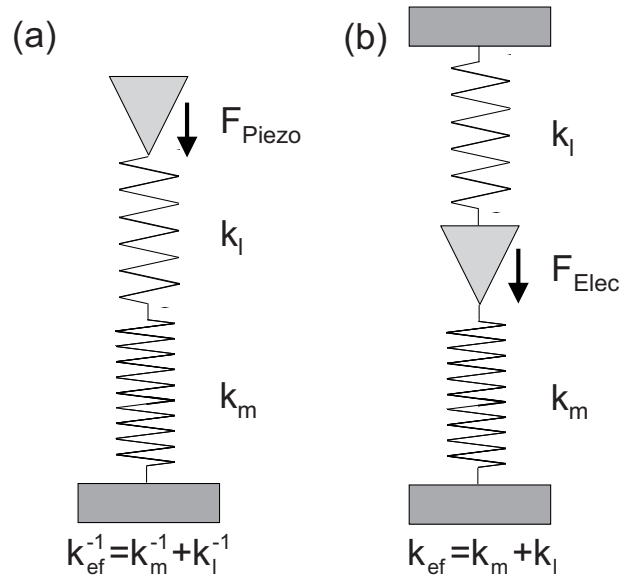

Fig. 11. Equivalent spring scheme of the AFM cantilever and PM patch for the situation when (a) the applied force is generated by the vertical piezo stage movement F_{Piezo} and the cantilever and membrane act in series, and (b) when the force is from electrostatic origin F_{Elec} and the cantilever and the membrane act in parallel.

In the presence of an applied voltage, an electrostatic force appears on the cantilever that tends to bend it further downwards. When the cantilever is in the air just before membrane contact the deflection observed for 9 V applied is ~1 nm, which corresponds to an electrostatic force of F_{elec}~40 nN. When in contact with the membrane, this force induces a deformation of the membrane which is smaller than the deflection of the cantilever in air due to the fact that the membrane is able to partially sustain this force. In the present case the deflection induced by the electrostatic force is equivalent two springs acting in parallel, see Fig. 11b, can be computed as

$$\delta_{Elec} = \frac{F_{elec}}{k_l + k_m} \sim 0.75nm \qquad (7)$$

in close agreement with the observed deflection during the experiments (see Fig. 10a). It is worth noting that if instead of a stiff cantilever a soft cantilever had been used in the experiments, i.e. with a spring constant ~2 N/m as used in previous studies of C-AFM on biomolecules [1,2,3,4,15], then the electrostatic deformation for the same voltage range would have been ~2.6 nm, thus preventing the use of these cantilevers for wide voltage range current-voltage characteristics.

7.9. References

[1] L. Andolfi, A. R. Bizzarri, and S. Cannistraro, "Electron tunneling in a metal-protein-metal junction investigated by scanning tunneling and conductive atomic force spectroscopies," Appl Phys Lett **89** (18), 183125 (2006).

[2] D. G. Xu, G. D. Watt, J. N. Harb et al., "Electrical conductivity of ferritin proteins by conductive AFM," Nano Lett **5** (4), 571-577 (2005).

[3] J. W. Zhao, J. J. Davis, M. S. P. Sansom et al., "Exploring the electronic and mechanical properties of protein using conducting atomic force microscopy," J Am Chem Soc **126** (17), 5601-5609 (2004).

[4] A. Stamouli, J. W. M. Frenken, T. H. Oosterkamp et al., "The electron conduction of photosynthetic protein complexes embedded in a membrane," Febs Lett **560** (1-3), 109-114 (2004).

[5] J. G. Simmons, "Generalized Formula for Electric Tunnel Effect between Similar Electrodes Separated by a Thin Insulating Film," J Appl Phys **34** (6), 1793-& (1963).

[6] B. Brar, G. D. Wilk, and A. C. Seabaugh, "Direct extraction of the electron tunneling effective mass in ultrathin SiO2," Appl Phys Lett **69** (18), 2728-2730 (1996).

[7] W. Y. Wang, T. Lee, and M. A. Reed, "Electron tunnelling in self-assembled monolayers," Rep Prog Phys **68** (3), 523-544 (2005).

[8] G. Lewicki and J. Maserjian, "Oscillations in Mos Tunneling," J Appl Phys **46** (7), 3032-3039 (1975).

[9] M. Stadele, F. Sacconi, A. Di Carlo et al., "Enhancement of the effective tunnel mass in ultrathin silicon dioxide layers," J Appl Phys **93** (5), 2681-2690 (2003).

[10] C. A. Spindt, I. Brodie, L. Humphrey et al., "Physical-Properties of Thin-Film Field-Emission Cathodes with Molybdenum Cones," J Appl Phys **47** (12), 5248-5263 (1976).

[11] J. D. Zuber, K. L. Jensen, and T. E. Sullivan, "An analytical solution for microtip field emission current and effective emission area," J Appl Phys **91** (11), 9379-9384 (2002).

[12] Y. D. Jin, N. Friedman, M. Sheves et al., "Bacteriorhodopsin (bR) as an electronic conduction medium: Current transport through bR-containing monolayers," Proceedings of the National Academy of Sciences of the United States of America **103** (23), 8601-8606 (2006).

[13] C. Moller, G. Buldt, N. A. Dencher et al., "Reversible loss of crystallinity on photobleaching purple membrane in the presence of hydroxylamine," Journal of Molecular Biology **301** (4), 869-879 (2000).

[14] S. Yamaguchi, S. Tuzi, M. Tanio et al., "Irreversible conformational change of bacterio-opsin induced by binding of retinal during its reconstitution to bacteriorhodopsin, as studied by C-13 NMR," Journal of Biochemistry **127** (5), 861-869 (2000).

[15] C. Gomez-Navarro, P. J. de Pablo, and J. Gomez-Herrero, "Electrical properties of long molecules: single-walled carbon nanotubes and DNA," Int J Nanotechnol **2** (1-2), 90-102 (2005).

Chapter 8. Nanoscale impedance microscopy mapping of the purple membrane

Summary: Chapter 8 puts into practice the AFM protocols explained in chapter 4 for the study of the electrical properties of biomolecules using Nanoscale Impedance Microscopy NIM. From the use of these protocols relevant physical information of the biomolecules will be obtained, in particular, its thickness and its dielectric constant.

8.1. Introduction

The overall opposition to the pass of an alternating current I_{AC} through an electric circuit is represented by the impedance Z. The impedance Z is dependant of three properties of the circuit: the alternating current resistance R_{AC}, the capacitance C, and the inductance L. For the usual AFM set-up the effect of the inductance L is minimal and can be ignored, which provides the following expression for the impedance: $Z = R - {}^{i}\!/_{\omega C}$, which is dependent of two parameters R and C, that as commented in section 3.2, the custom made amplifier implemented in the AFM set-up is prepared to measure separately.

The capacitance C describes the accumulation of electric charge in the different regions of the circuit as a response to an applied bias V, but this fact is more interesting that what it looks at first sight because the accumulation of the charges is directly related to the interaction of the electric field with the samples; this way the capacitance reveals information about the dielectric properties of the system, and how the system interacts with an electric field.

Therefore, the measurement of the capacitance C is a very important issue for the development of biosensors at the nanoscale. The most appropriate technology for the measurement of the capacitance at the nanoscale is the Nanoscale Impedance Microscopy (NIM). The use of NIM will not only allows mapping of the impedance distribution of the sample, i.e. the distribution of R and C, but to obtain quantitative information about the electrical properties of the biomolecules.

Nevertheless, nowadays NIM has not been yet applied for the electrical characterization of biomolecules. Several reasons are behind this lack of use, first the novelty of the technique dating from 2003 [1], but also the inherent technical difficulties in the measurement, we list, the extremely small capacitance variations that must be measured in the presence of large stray contributions [2], the long acquisition times per point required to achieve enough capacitance resolution that hinder the normal AFM operation and increase the effect of the drift, the inability of the *contact mode* typically used for AFM electrical measurements to electrically measure biological samples without damaging them, and finally the requirement of a good understanding of the electric interactions at the AFM-probe/sample/substrate system in order to extract quantitative information from the measurement.

8.2. The electric field distribution at the 'probe/sample/substrate' system.

The characterization of the electric fields present between the AFM tip and substrate has driven the attention of a broad group of AFM theoretical researchers because in spite of its resemblance to the parallel plate capacitor the 'AFM-probe/sample/substrate' system hides some unexpected behaviours.

In section 4.4 it was explained that the apex capacitance C_{apex} can be described in situations where the volume in-between the AFM probe and the substrate is filled with air using the analytical expression derived by *Hudlet et al.* [3] that modelizes the tip apex as a cone of opening angle θ that ends in a sphere relates of radius R, and associates the C_{apex} of the tip with the tip-electrode distance L. The ability of this expression to correctly describe the electric field distribution and the capacitance within the range of experimental error has been extensively corroborated by the multitude AFM tip calibrations performed in this work of thesis, as well as by the experiments performed by *Law et al.* [4].

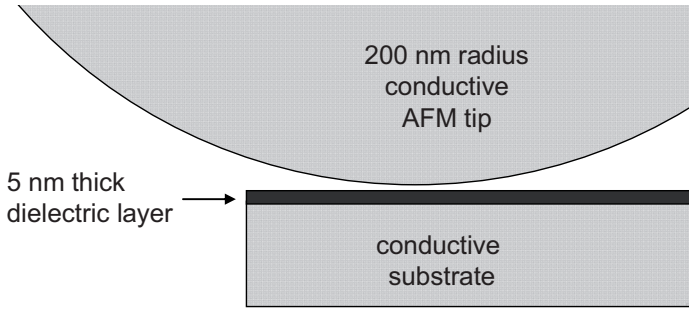

Fig. 1. Cartoon to scale of the tip-substrate system with a thin film in-between.

Nevertheless, the expression from *Hudlet et al.* is not appropriate when a dielectric object, as a biological sample, is placed between the AFM tip and the substrate, a new analytical expression is needed to describe this situation, and extract physical parameters of our samples from the measurement of the variation of C_{apex} in a simple and direct way. At the present time, the only analytical expression at this respect was published in 2007 by *Sacha et al.* [5] for the electrostatic force present between an AFM tip and a conductive substrate when on top of the substrate a thin film of dielectric material is present [5].

$$F_{apex}(z,h,R) = -\pi\varepsilon_0 V^2 \frac{R}{z + h/\varepsilon} \qquad (1)$$

where z is the distance from the tip apex to the surface of the dielectric film, h is the thickness of the dielectric film, and ε is the relative dielectric constant of the dielectric film. Eq. 1 has shown good fit to force simulations performed using the image charge of the electric field, *Sacha et al.* The energy of the electric fields between the tip apex and the substrate (or equivalently the apex capacitance, $U = \frac{1}{2} C_{apex} V^2$) is directly

related to the electrostatic forces by $F_{apex} = \frac{dU}{dz}$, therefore by using Eq.1 it is possible to obtain a new analytical expression for C_{apex} as follows:

$$C_{apex}(z,h) \equiv \int \frac{2F(z,h)}{V^2} dz + K(R) = -2\pi\varepsilon_0 R \ln\left(\frac{R}{z + h/\varepsilon}\right) + K(R) \quad (2)$$

At the current time our research group is further demonstrating the validity of Eq. 2. For this, first principles derivations and finite element simulations are being used. We have demonstrated that Eq. 2 is valid provided that $R(1-\sin(\theta)) >> z + h/\varepsilon$. This is a condition satisfied by the AFM configurations shown in Fig 1, an AFM tip of radius R of 100-200 nm over a biological membrane, which typically are of 2-20 nm thickness h. A new paper on the theoretical derivation of Eq. 2 is to be expected to be published soon.

Let us consider for comparison the situation equivalent to Fig. 1 but where instead of the AFM tip we had a parallel plate capacitor with a layer of dielectric deposited on top of one of the electrodes, the analytical expression for the system capacitance would be:

$$C_{ppc} = \varepsilon A / z + h\varepsilon \quad (3)$$

it is interesting observing that Eq. 3 does not present the logarithmic dependence of Eq. 2, fact which will produce in NIM measurements special features not present in a classic parallel plate capacitor.

From both situations, AFM tip and parallel plate, Eq. 3 and Eq. 2, it is clear that two parameters can be extracted from NIM measurements on dielectric samples, the thickness of the sample h and its relative dielectric constant ε .

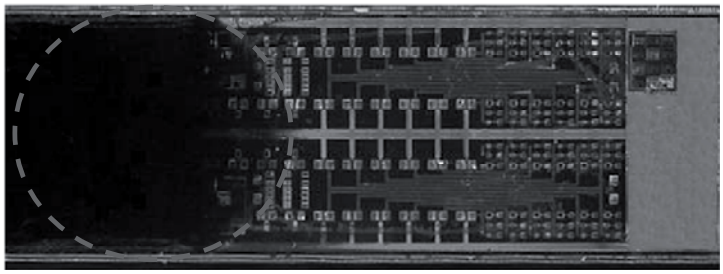

Fig. 3. Large area deposition of PM on an electrode for phototransceiver fabrication (from *Shin et al.* [6]), dashed line indicates the PM covered area.

8.3 Thickness measurement of nanoscale biological layers

As commented in chapter 1, biological membranes andbiomolecular self-assembled layers are being investigated as potential active materials in new micro- and nanoelectronic hybrid devices, typically the biological layers are deposited on top of the electrodes and cover the whole surface of the electrode, see Fig 3. In its development, a main issue concerns the non-destructive measurement of the biolayer thickness with sub-monolayer thickness vertical resolution and sub-micrometric spatial lateral resolution. Standard thin film characterization techniques such as optical ellipsometry, reflectance spectroscopy [7], and capacitance metrology [8,9] are not suitable for this purpose as they offer in all cases lateral resolution beyond the micrometer. A new technique which provides this information would be desirable.

Additionally this new technique will also find application for transistor gate oxides where the thickness measurement is critical and its accurate measurement constitutes a practical challenge.

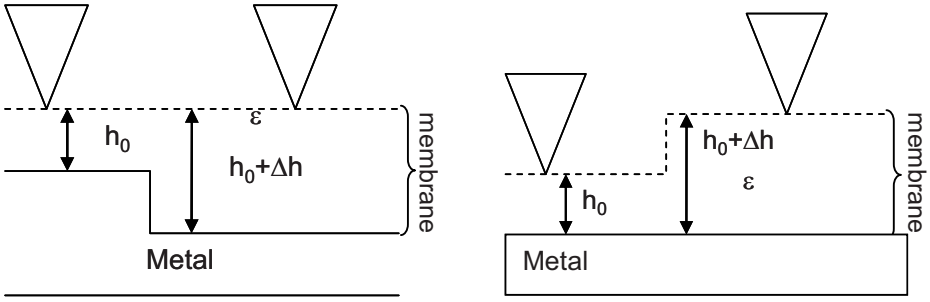

(a) (b)

Fig 4. Two situations of a dielectric layer on top of a metal substrate where NIM can be used to extract the thinner layer thickness h_0. A combination of both situations can also be considered.

The extraction of the thickness of a dielectric/biological layer can be performed using NIM, for this the AFM tip is scanned from point to point of the sample and the capacitance variations in C_{apex} are registered. Essentially two experimental situations can be considered, see Fig. 4, (a) the case where bottom electrode has been nanopatterned and the surface of the layer is flat, and (b) the case where the bottom electrode is flat and the layer presents in its surface topographic features as steps. Of course, a combination of both situations can also be considered.

By setting in Eq. 2 the distance from the tip apex to the surface of the dielectric film to zero ($z = 0$), the change in the measured capacitance between the two film thickness in Fig 4a and 4b can be expressed as:

$$\Delta C_{apex}(\Delta h, h_0) \equiv C_{apex}(0, h_0 + \Delta h) - C_{apex}(0, h_0)$$
$$\equiv -2\pi\varepsilon_0 R \ln\left(\frac{h_0 + \Delta h}{h_0}\right) \qquad (4)$$

Note that within this approximation the local capacitance due to a change in thickness is independent from the dielectric constant and only depends on the sample thickness, this is a surprising fact that is generated by the

presence of the logarithmic dependence in the AFM tip-substrate field distribution, and which does not takes place for standard parallel plate capacitor field distributions. Therefore Eq. (4) can interpret quantitatively the capacitance measurements of the situations depicted in Fig. 4 and extract the biolayer thickness from them.

For real NIM measurements, the measured capacitance in an AC CS-AFM experiment includes a contribution from the stray capacitance variation that can be approximated by a linear function of the profile changes, thus giving

$$\begin{aligned}\Delta C_{meas}(\Delta h, h_0) &\equiv \Delta C_{stray}(\Delta h, h_0) + \Delta C_{apex}(\Delta h, h_0) \\ &\equiv -M_{stray}\Delta h - 2\pi\varepsilon_0 R \ln\left(\frac{h_0 + \Delta h}{h_0}\right) \end{aligned} \qquad (5)$$

It is important to quantify the relative error in the thickness measurement. By assuming that the main sources of error come from the capacitance measurement, the tip radius calibration and the dielectric step height we then have

$$\frac{\delta h_0}{h_0} = \left(1 + \frac{h_0}{\Delta h}\right)\ln\left(1 + \frac{\Delta h}{h_0}\right)\left[\frac{\delta \Delta C_{apex}}{\Delta C_{apex}} + \frac{\delta R}{R}\right] + \frac{\delta \Delta h}{\Delta h} \qquad (6)$$

Values for the relative error measurements depend very much on the set-up and sample considered, typically: capacitance error 1-10%, tip radius calibration 1-10% and topographic measurement 1-2%. This gives an overall error around 4-30% when measuring a step equal to the film thickness. This relative error is reasonable in the lower limit (compatible with the best optical thickness characterization method by with much higher lateral resolution), thus indicating that highly sensitive measuring protocols can be followed to achieve meaningful quantitative results for the dielectric layer thickness variation.

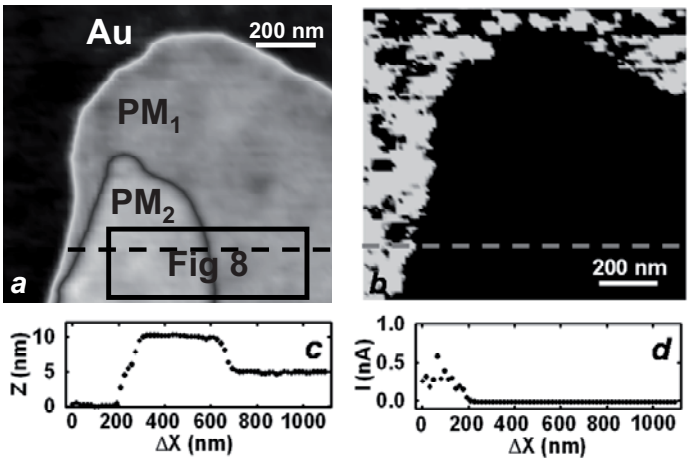

Fig. 5. Simultaneous topographic (including profiles) and conduction image of a PM patch formed by two PM monolayers, the top one is of smaller area and forms a step over the lower one similar to the situation of Fig. 4b. The current image shows that PM has an insulating electrical behaviour and thus the electrical interaction between the AFM tip and the substrate is purely capacitive. The rectangle shows the area where the topography and capacitive image of Fig. 8 is acquired.

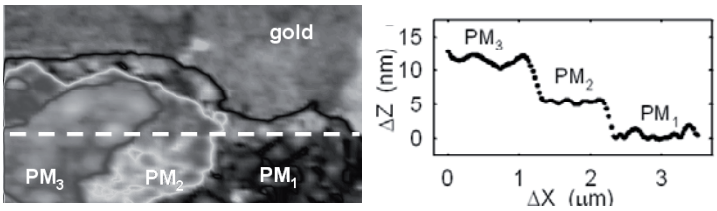

Fig. 6. Topography of another PM patch formed by three PM monolayers which form two steps over the bottom PM monolayer, a profile is shown.

8.4. NIM imaging on the purple membrane and thickness extraction: technical implementation

As model system of biological layer to test the thickness extraction protocol we used purple membrane (PM) layers. Chapters 6 and 7 showed that the PM constitutes a biological layer highly homogeneous and insulating at low applied bias, therefore the PM is compatible with a pure capacitive behaviour at low applied bias, and Eq. 5 can be directly applied.

Fig. 5 shows simultaneous conduction and topography images of a PM patch that we will use as model layer to test the thickness extraction protocol. The image has been obtained using jumping mode JM as described in section 4.3 with a 3 nN force and a dc bias of 100 mV. This PM path is composed of two piled PM monolayers being the top one smaller in area, and therefore forms a step in the surface of the sample equivalent to the situation described by Fig. 4b. Importantly for our sample we can access the thickness of the lower layer from the topographic image, this will be used to check the thickness extraction protocol, but it is not the general case for biosensors, see Fig. 3.

Fig. 6 shows a topographic image of another patch that will be used to test the thickness extraction protocol formed by three piled PM monolayers which create two steps over the underlying PM monolayer.

All the NIM measurements were performed under dry $N_2(g)$ conditions, an applied sinusoidal voltage of $0.7V_{RMS}$ amplitude and 92 kHz frequency, and 0 V dc bias, using conductive the diamond coated probes CDT-FMR from Nanosensors^{TM} with spring constant of 2.8 N/m. The measurements were performed with two different probes, one for the PM patches of Fig. 5 and another tip for the PM path of Fig. 6. Both probes have different geometrical structures, this was established by the structural characterization of the tip apex of each of the AFM probes using capacitance-distance curves as described in section 4.5. The calibration of the two probes is shown in Fig. 6 (figure previously used in section 4.5), the fittings are performed with a constant opening angle of

the cone of θ = 30º, the calibration gives for the apex radii R of the two probes values of: $R_{Fig.5} = 300 \pm 30\ nm$ and $R_{Fig.6} = 90 \pm 9\ nm$. Additionally, the capacitance-distance curves provide a stray capacitance of $c_{stray} = 0.19 \pm 0.05\ aF / nm$ for both probes.

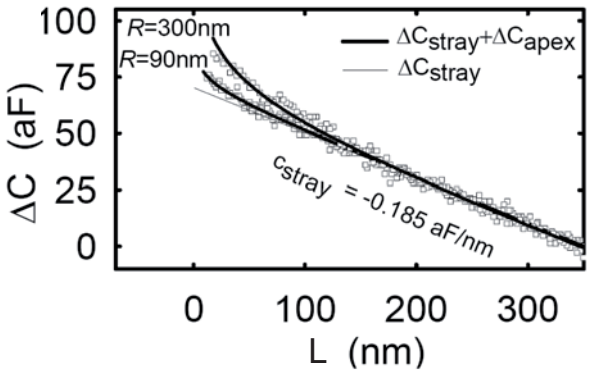

Fig. 7. Capacitance-distance curves of the two AFM probes used in Figs. 5 and 6, the dimensions of the probes obtained from the curves show respectively radii of 300 and 90 nm. The observed stray capacitance Z variation is of 0.19 aF/nm.

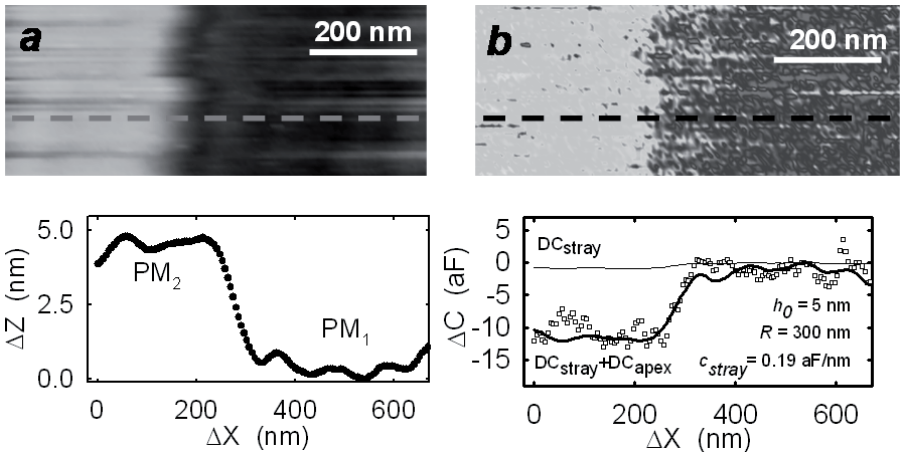

Fig. 8. Simultaneous topography and capacitance images of the rectangle signalled in Fig. 5. Good agreement is observed between topography and capacitance, a profile along one of the lines is shown.

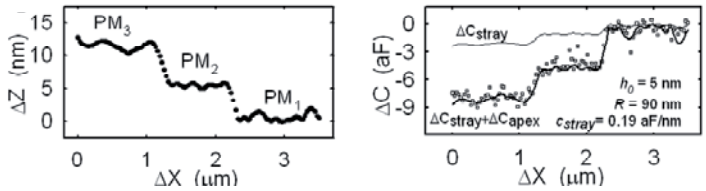

Fig. 9. Simultaneous topography and capacitance of the line signalled in Fig. 5. Good agreement is observed between topography and capacitance.

To measure the variation of the apex capacitance C_{apex} of the AFM probes they are scanned over the surface of the PM patches of Fig. 5 and Fig. 6 using jumping mode JM as described in section 4.3. This measurement represents the first NIM measurement on biological material.

Two different contact times T were used, each of them for a different reason, as next described.

In order to perform a capacitance map, the contact time T is set to its maximum operative limit, approximately at 143 ms/pixel, at this contact time T the JM is still capable of stable functioning and provides good enough resolution (below 3 aF) to map the C_{apex} variations. Fig. 8 shows simultaneous topography and capacitance mapping of the area signalled by a rectangle in topography image of Fig. 5. It is observed a direct correlation between membrane topography and capacitance, thus showing the ability of NIM in JM to image both properties simultaneously. This correlation between topography and capacitance is further evidenced through the profiles taken along one scanning line, in which a capacitance variation of a few attoFarads precisely tracks the topography profile of the monolayer PM_2 over the first layer PM_1.

If we are not interested in a map, but in performing a capacitance profile with the best possible resolution, the best option is to scan repeatedly the same line and average out the successive capacitance profiles. Thanks to the profile averaging the contact time per point T can be reduced, and thus the stability of the AFM scanning is improved. For example see Fig. 9

which has been obtained averaging out 9 consecutive scans taken at a scan speed of 56 ms/pixel on the PM patch imaged in Fig. 6. In the same way we did for the capacitance map of Fig. 8, we find an excellent correlation between topography and capacitance, the steps from PM_1 to PM_2 and PM_3 are clearly observable in the capacitance profile, and the resolution is better (around 1 aF) than in the capacitance map of Fig. 8.

One important aspect of the capacitance mapping on the PM is that, as in the case of the conduction C-AFM mapping, the integrity of the PM membrane patch has remained unaffected during all the imaging process, and we have been able to perform the capacitance imaging for hours without noticeable damage to the sample, fact which highlights the ability of Jumping Mode to perform simultaneous topographic and electric measurements without destroying or appreciably deforming the biological layers.

The C_{apex} variations can be interpreted in a quantitative way and hence used to accurately determine the membrane thickness of the underlying membrane with nanoscale lateral and vertical spatial resolution. Please note that from the topographic profiles of Fig. 8 and Fig. 9 it is impossible to obtain the thickness of PM_1.

To determine the underlying thickness we use Eq. 5, and introduce all the known parameters, stray capacitance rate c_{stray} and the tip radius R from the capacitance-distance curves, and thickness variation Δh from the topographic profile, to next fit the measured capacitance to Eq. 5 by adjusting the only remaining free parameter, and obtain the value the thickness of the first PM layer (PM_1), h_0.

Operating as described, we obtain $h_0 = 5.0 \pm 0.8\, nm$ and $h_0 = 5 \pm 1\, nm$ respectively from data in Figs. 8 and 9, showing an excellent agreement between theoretical and experimental data for both cases, see fitting lines in Figs. 8 and 9. The results show a great precision and the value of the thickness obtained by the capacitance measurement perfectly fits the 5 nm thickness of the bottom PM monolayer (PM_1) measured from the large area topographic image of Fig. 5 and Fig. 6. Also of high relevancy is the

fact that thanks to the calibration of the dimensions of the probe the extracted thickness is independent of its dimensions. In summary, these nice results open the door to the non-destructive measurement of the thickness of biological layers and other dielectric layers with a vertical resolution below 1 nm.

8.5. Characterization of the dielectric constant

The dielectric constant represents the response of the charges in a material to the application of an external electric field. This is an extremely important property that strongly describes the nature and behaviour of those (dielectric) materials which lack of free charges. In the dielectric materials the response to the external electric field is produced by the polarization of the different dipoles present inside the material which can rotate as an electric compass depending on the sense and direction of applied field.

The dielectric constant is a frequency dependant parameter, this dependence is produced because at higher frequencies the speed of the changes in the electric field 'leaves behind' successive polarization mechanisms which are not able to follow the electric field, this way the polarization response of the material to the applied field decreases as the frequency is increased, and consequently, its measuring parameter, the dielectric constant, decreases too.

Different techniques are available to measure the dielectric constant of materials. At high frequency (~10^{14} Hz), optical techniques enable the measurement of the dielectric constant in a wide number of circumstances including nanometric thin films. And at lower frequencies (< 10^{11} Hz) the measurement of the dielectric constant is performed by placing the dielectric material between two electrodes (in a similar way to our AFM tip/sample/substrate configuration) and using impedance or microwave analysers. These analysers work in the same way that our AFM set-up, and the NIM technique, they compare the applied bias in one electrode with the measured AC signals in the other electrode. Nevertheless,

technological difficulties have hindered the measurement of the dielectric constant of nanoscale objects at non-optical frequencies, and this measurement has only very recently performed by our group [10].

The basic technological difficulty is that the measurement of the dielectric constant requires from differential measurements, first the capacitance of the empty nanoscale capacitor cavity must be measured, and next it is necessary to introduce a dielectric object inside the capacitor and record the jump that takes place in the capacitance of the system, from this data it is possible to extract the dielectric constant of the sample. This is a simple sequence of measurements to perform at the macroscale, but it has not been possible to perform it at the nanoscale due to the difficulty of manipulating nanoscale objects. The recent technology of NIM and the flying method open the door to performing dielectric constant measurements at the nanoscale.

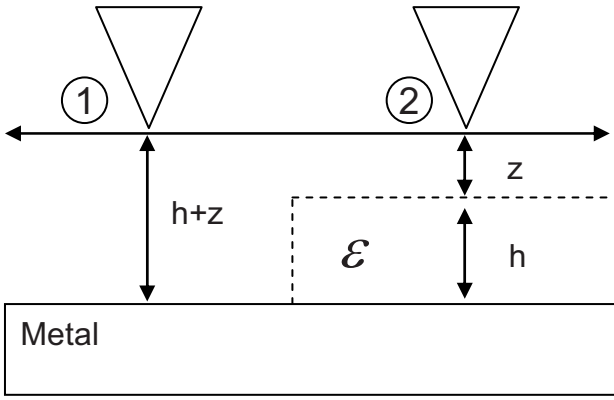

Fig. 10. Schematic of flying method, the parameters required for the extraction of the dielectric constant of the dielectric layer are shown.

A possible method to measure the dielectric constant is by using the flying method. The flying method consists in scanning the AFM tip over the border of the dielectric layer at constant distance from the substrate. Two situations are then given, see Fig. 10, (1) between the tip and the substrate only air is present, (2) between the tip and the substrate, a

dielectric material is present in addition to the air. Thanks to the measurement of the change in capacitance ΔC between the situations (1) and (2) it is possible to extract the dielectric constant of the material.

The dielectric constant can be extracted using Eq. (2). If the apex capacitance C_{apex} for situations (1) and (2) is subtracted, we obtain:

$$\varepsilon = \frac{1}{(e^{-\frac{\Delta C}{2\pi\varepsilon_0 R}} - 1)\frac{z}{h} + e^{-\frac{\Delta C}{2\pi\varepsilon_0 R}}} \qquad (7)$$

Equation which provides the dielectric constant of the material once the change in capacitance is known, in addition to the tip radius, the vertical tip position and dimensions of the dielectric object.

8.6. Dielectric constant measurement: technical details

The *Flying* mode measurements have been performed with the operating protocol described in section 4.4, a scan frequency of 0.065 Hz, 32 capacitance measurements acquired at each line, and applied bias amplitude of 3 V. In order to increase the resolution in capacitance several scans are averaged.

The calibration of the probe was performed using capacitance-distance curves as described in section 4.5, the results are shown in Fig. 11. The tip radius is estimated at R= 250±50 nm, for which the cone opening angle was set at θ=30º. The relative error of 50 nm is relatively big, even if Fig. 11 shows nice fittings, we do this because we have an experimental shortage of capacitance-distance curves, and in order to account for this lack of experimental radius verification, it has been set a considerable high error for the tip radius, which nevertheless, as will be later shown, does not significantly affect the extracted value of dielectric constant.

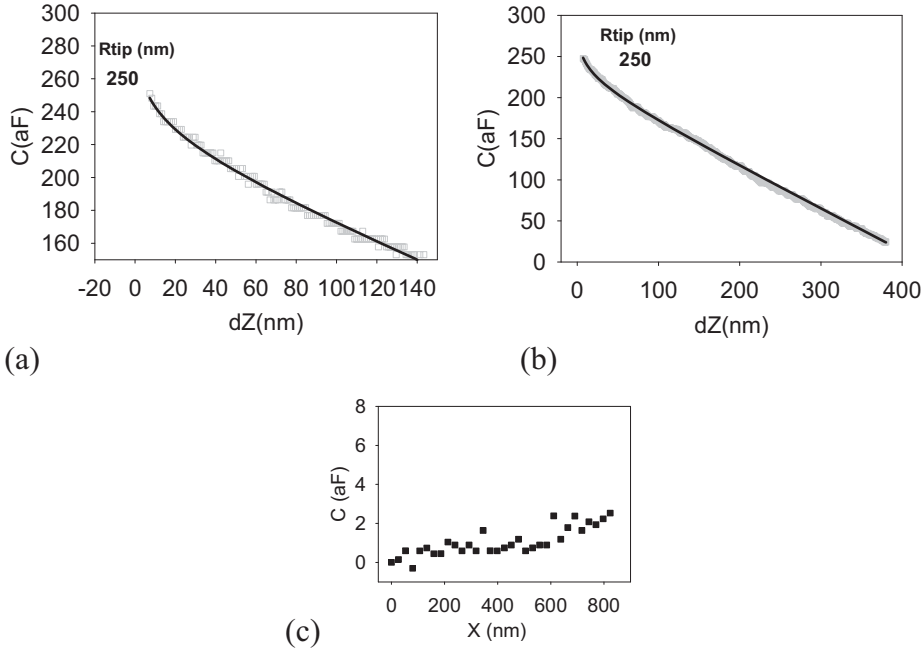

Fig. 11. Calibration of the AFM tip radius (opening angle θ set at 30º) for short (a) and longer (b) capacitance-distance curves. (c) Calibration of the lateral stray capacitance performed at 300 nm above the PM path (average of 9 sweeps).

The structural characteristic of the PM patch used for the dielectric constant measurements are shown in Fig. 12, acquired in *Dynamic*. It is observed that the PM patch consists of two PM layers with the top one of smaller area than the bottom one, therefore we can use the top layer to reference the vertical tip position, as explained in section 4.4. The white dashed line of Fig. 12 represents the path the AFM tip follows during the *Flying mode* measurement.

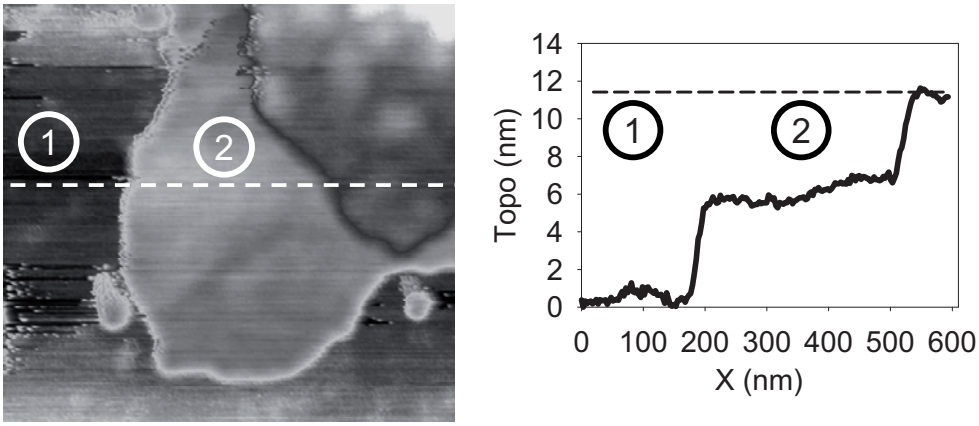

(a) (b)

Fig. 12. Topographic characterization of the PM patch selected for the *Flying* mode measurement, (a) image, (b) profile along dashed line of (a). The PM patch is composed of two layers, the top one of smaller area, this structural configuration enables us performing the *Flying* mode as detailed in section 4.4, using the top layer as a reference to position vertically the AFM tip,. The dashed lines represent the trajectory of the AFM tip during the *Flying* mode measurement in the XY (a) and XZ (b) planes, while the circled numbers relates to the situation of the tip during the measurement as described in Fig. 10.

The structural characteristic of the PM patch used for the dielectric constant measurements are shown in Fig. 12, acquired in *Dynamic*. It is observed that the PM patch consists of two PM layers with the top one of smaller area than the bottom one, therefore we can use the top layer to reference the vertical tip position, as explained in section 4.4. The white dashed line of Fig. 12 represents the path the AFM tip follows during the *Flying mode* measurement.

After a successful *Flying* measurement, and in order to characterize the stray capacitance variation ΔC_{stray}, the same tip motion is repeated at much higher distance from the substrate, about 300 nm, at this distance only stray capacitance varies (C_{apex}~0), once known the stray capacitance variation it is subtracted from the data of the *Flying* measurement.

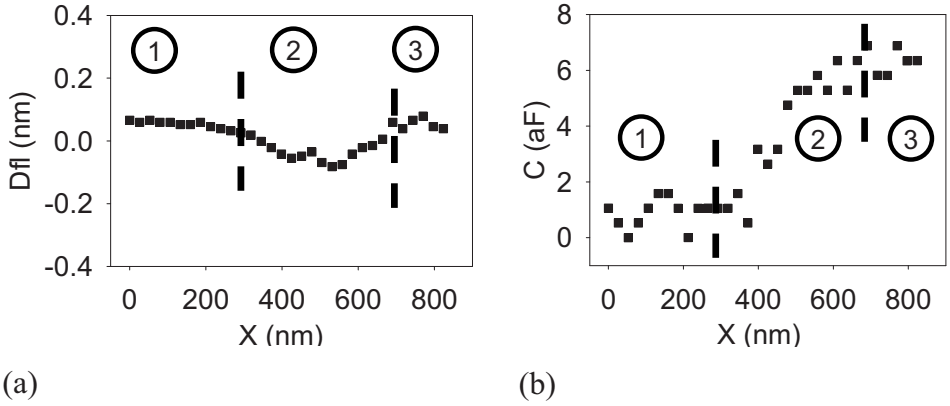

(a) (b)

Fig. 13. Evolution during the *Flying* measurement of (a) cantilever deflection and (b) apex capacitance (a) Minimal cantilever deflection is observed (variation < 0.2 nm), but the evolution of the deflection determines the position of the AFM tip during the measurement both horizontally and vertically; (1) tip over bare gold, (2) tip over the PM monolayer, and (3) tip is soft contact with the upper PM layer. (b) A jump in apex capacitance of ~4 aF is observed between the situations where the AFM tip flies over the PM monolayer and over bare gold substrate.

The data acquired from the *Flying* measurement on the PM monolayer shown in Fig. 12 is shown in Fig. 13, where Fig. 13a shows the cantilever deflection evolution, and Fig. 13b the evolution of the apex capacitance.

The monitoring of the cantilever deflection during the Flying measurement enables to track the position of the AFM tip in the horizontal X and vertical Z axes. Three different regions can be identified in the cantilever deflection plot as a function of the lateral tip position: (1) when the tip is exclusively over the air, without membrane in between the tip and the substrate, (2) when the tip is on top of the PM monolayer the cantilever bends slightly towards the substrate pushed by the attracting forces (Van der Walls and electrostatic) created by the PM monolayer on the AFM tip, and (3) when the AFM tip is touches (brush passes) the upper PM layer and the cantilever is pushed slightly backwards. Importantly, the monitoring of all the situations of the AFM tip is performed with a minimal cantilever deflection range of the order

of 0.2 nm, value so small it does not need to be considered for the dielectric constant extraction, given that is one order of magnitude smaller than the typical distance parameters *z* and *h* from Eq. 7 that are in the order of several nanometers.

On the other hand, the evolution of the apex capacitance during the *Flying* measurement clearly shows a jump of ~4 aF in capacitance not associated to the cantilever motion between the situations (1) and (2), this is between the situations when a monolayer of PM is present between the tip and the substrate and when it is not.

From the value of ΔC_{stray}= 4 aF the dielectric constant of the PM monolayer can be determined using Eq. 7, and a value of 1.8 is obtained. Nevertheless, it is necessary to establish an uncertainty range in the dielectric constant extraction, for this we consider the possible errors of measurement of parameters of Eq. 7. In the case of the tip radius we consider $R \in [200,300]nm$, for the PM monolayer thickness $h \in [5,6]nm$, for tip-membrane distance $z \in [3,5]nm$ and for the capacitance change $\delta C \in [3,5]aF$. These are quite wide range of errors which nevertheless produce a relatively small error in the dielectric constant of 0.7. Therefore we obtain that the dielectric constant of the PM monolayer using NIM and the *Flying* mode protocol turns out to be 1.8 ± 0.7 (in relative terms to the permeability of the void $\varepsilon_0 = 8.85 \times 10^{-12}$ F/m).

This result represents the first measurement of a dielectric constant at the nanoscale on a biological sample. And in the context of previous macroscale measurements the value of 1.8 ± 0.7 for the dielectric constant of a single PM layer in dry N_2(g) atmosphere is consistent with findings for dry proteins of estimated dielectric constants between 2 and 4, although it is in lower limit of macroscopic measurements. A possible reason is that the presence of residual water in the macroscopic measurements increased the observed dielectric constant, as was suggested for the case of the stacks of hundreds of dried PM monolayers by *Berntsen at al.* [11]. The nanoscale measurement is free from this uncertainty; the presence of water between the PM patch and the substrate

is ruled out by the high symmetry of the *I-V curves* measured which is incompatible with energy asymmetries at the tip-PM and PM-substrate interfaces, and as we know from the AFM studies of *Gil et al.* [12] that no water is present on the surface of materials once the relative humidity is decreased to 0%, therefore water cannot be present either between the PM and the substrate.

8.7. References

1 R. Shao, S. V. Kalinin, and D. A. Bonnell, "Local impedance imaging and spectroscopy of polycrystalline ZnO using contact atomic force microscopy," Appl Phys Lett **82** (12), 1869-1871 (2003).

2 L. Fumagalli, G. Ferrari, M. Sampietro et al., "Nanoscale capacitance imaging with attofarad resolution using ac current sensing atomic force microscopy," Nanotechnology **17** (18), 4581-4587 (2006).

3 S. Hudlet, M. Saint Jean, C. Guthmann et al., "Evaluation of the capacitive force between an atomic force microscopy tip and a metallic surface," European Physical Journal B **2** (1), 5-10 (1998).

4 B. M. Law and F. Rieutord, "Electrostatic forces in atomic force microscopy," Physical Review B **66** (3) (2002).

5 A. Verdaguer, G. M. Sacha, H. Bluhm et al., "Molecular structure of water at interfaces: Wetting at the nanometer scale," Chem Rev **106** (4), 1478-1510 (2006).

6 J. Shin, P. Bhattacharya, J. Xu et al., "Monolithically integrated bacteriorhodopsin-GaAs/GaAlAs phototransceiver," Opt Lett **29** (19), 2264-2266 (2004).

7 Tompkins, "Spectroscopic Ellipsometry..... New York: Wiley," (1998).

8 J. Graham, M. Kryzeminski, and Z. Popovic, "Capacitance based scanner for thickness mapping of thin dielectric films," Rev Sci Instrum **71** (5), 2219-2223 (2000).

9 A. Guadarrama-Santana and A. Garcia-Valenzuela, "Principles and methodology for the simultaneous determination of thickness and dielectric constant of coatings with capacitance measurements," Ieee T Instrum Meas **56** (1), 107-112 (2007).

10 L. Fumagalli, G. Ferrari, M. Sampietro et al., "Dielectric-constant measurement of thin insulating films at low-frequency by nanoscale capacitance microscopy," Applied Physics Letters **accepted** (2007).

[11] P. Berntsen, R. Bergman, H. Jansson et al., "Dielectric and calorimetric studies of hydrated purple membrane," Biophysical Journal **89** (5), 3120-3128 (2005).

[12] A. Gil, J. Colchero, J. Gomez-Herrero et al., "Macroscopic water deposits on polycrystalline gold measured by scanning force microscopy," Ultramicroscopy **86** (1-2), 1-9 (2001).

Chapter 9. Conclusions and perspectives

The main success of this work of thesis has been the demonstration of the excellent properties that the AFM technique has to become a custom-designed tool for the assistance in the development of electrical biosensors and other biohybrid devices in their route towards the miniaturization to the nanoscale (the importance of which was detailed in chapter 1). The AFM is capable of quantitative electrical characterizing in the nanoscale with a combination of information from AC and DC sources that combined enable to establish a complete and detailed picture of the electrical behaviour of each of the biomolecules in the biosensor, as well as on other important electrical components of the biosensors.

In the chapter 2 of this work of thesis it is reviewed the state of the art in the electrical characterization of biomolecules with the AFM, the main conclusion is that an optimal use of the AFM for the electrical characterization of biomolecules requires from novel adaptations of the commercial AFM set-ups and from a complete understanding of the physical phenomena present during the measurement. The critical point being to combine is the soft and brittle nature of biological samples with the electrical forces present during the electrical measurements.

The novel strategies implemented in the AFM to push forward the electrical characterization of biomolecules are explained in chapter 3 (set-up adaptations) and chapter 4 (operational protocols). Thanks to these strategies it will be possible to expand the number sources of electrical information at the nanoscale. In particular, protocols for the DC conductive imaging, force controlled wide bias range current-voltage curve acquisition, and nanoscale impedance microscopy have been implemented.

Selecting an appropriate test sample is a very important point of any technological development in characterization techniques, chapter 5 explains the special characteristics of the purple membrane which has driven us to select it as a test sample.

When the novel developments in AFM electrical characterization technology are put into practice on the purple membrane the usefulness of the technical approaches implemented is demonstrated. A host of new physical information on the purple membrane is obtained. Thanks to the DC maps shown in chapter 6 it has been discovered that the membrane presents nanoscale conductive defects never before observed. The force controlled wide bias range current-voltage curves shown in chapter 7 provide us with detailed information on the electron conduction mechanisms through the purple membrane, the conduction regime is identified and its governing parameters extracted, some of them never before measured on a biological sample as the effective mass. Finally, the first application of nanoscale impedance microscopy to the electrical characterization of biological samples, shown in chapter 8, reveals itself a highly useful tool that enables the measurement of the thickness of the membrane when not accessible by other methods, as well as the measurement of the dielectric constant of the membrane, magnitude that had also never before been measured at the nanoscale on a biological sample.

In order to obtain quantitative electrical characterization from the biomolecules it is necessary to count with a theoretical framework which transcripts the raw electrical data into physical information. For this purpose, chapters 7 and chapter 8 count with theoretical sections. In chapter 7, the electrical conduction mechanism is detailed and a parameter extraction protocol designed and implemented. In chapter 8, the electrical field distribution between the conductive AFM probe is described and the particularities for cases studied discussed.

Nevertheless, a research work is never complete, new perspectives open from where this work of thesis ends. This work of thesis can be considered a demonstration of principle. And as such, the work here shown has been restrained to dry air conditions which is the most favourable environment from the point of view of electrical measurements, but which is harsh for any biological activity. The biological justification of the experiments of this work of thesis has been possible only because of the extraordinary biological properties of the selected sample, the purple membrane that is capable of biological activity even in dry environments. Nevertheless, this is not the general case, and the vast majority of biomolecules require of wet physiological media to be biologically active. This situation will unequivocally drive us to new steps in the electrical characterization of biomolecules at the nanoscale, and towards the research in wet/liquid environments. New challenges will emerge and new technological developments will be required to adapt to the AFM systems to the wet environment, for instance the adaptation of the electrical AFM probes to wet/liquid environment work.

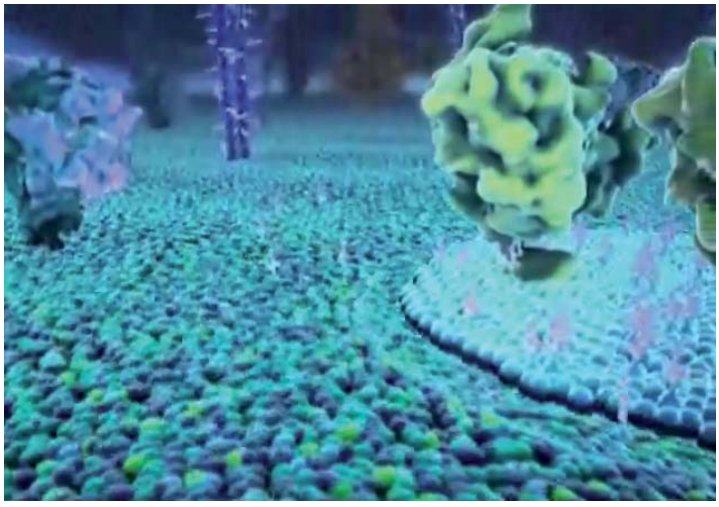

Computer recreation of the cell membrane with the different protein systems present in it, from *Biovisions at Harvard University*.

Apendix
Biological concepts on proteins and their electrical properties

A.1. Introduction to proteins

Proteins are frequently called the building blocks of life; they are the chief actors within the cell. With the exception of certain types of RNA, most other biological molecules are relatively inert elements upon which proteins act.

Proteins are large organic compounds made of amino acids arranged in a linear chain linked together by peptide bonds which fold into unique 3-dimensional structures. Their biological function is sustained on the structural conformation of the peptide chains as well as the proper sequence of aminoacids that form the chain. Proteins are not rigid, on the contrary reshaping forms part of their cycles of activity; different stages of their cycles are associated to different structural configurations.

There are only 20 types of aminoacids only differentiated by their side chain R which gives each aminoacid its particular properties. The rest is composed by an amino group (NH2), a carboxyl group (COOH) and a hydrogen atom linked through the central alpha carbon (Ca). A covalent bond links together the different aminoacids and holds the aminoacid chain together, see Fig. 1.

The structure of proteins is best understood if described at three levels of organisation; the amino acid sequence of a protein, or primary structure, the inner geometries found in all the proteins, or secondary structures (2°D), whose two most prominent cases are the alpha helix (α-helix) and the beta strand (β-strand), and finally, the folding and twisting of secondary structures, or tertiary structure, see Fig. 2 for an illustrative example.

From all the tasks proteins perform, cell signalling and signal transduction are the most interesting for sensor applications. All proteins

that deal with signals management are termed *receptor proteins*. Receptor proteins are the signal-receiving units of a cell. Even a single-cell organism cannot survive without receiving information from the 'outside world' (i.e. an amoeba will never find food if it is not directed by chemotaxis receptors or a rhodobcter bacterium would never survive had it not a receptor for light). Signalling is a key factor for life success in single and multicellular organisms, signals are exchanged between organs, cells, and even between organelles inside the cell but the reception of signals from outside is as well as important (vision, smell, taste, immunologic response,…). Receptors have arrived at high levels of specialization and efficiency. Three types of receptor proteins exist:

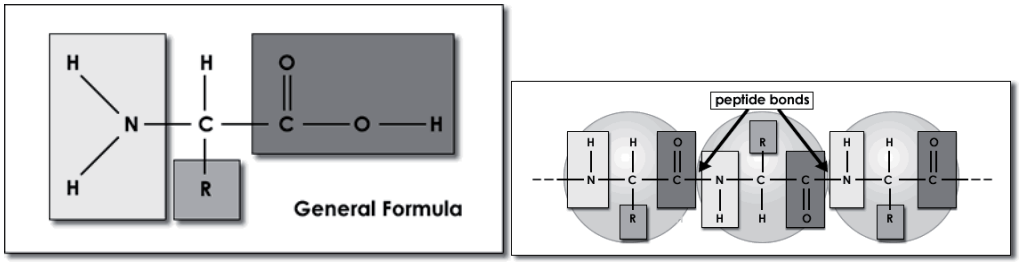

Fig. 1. Schematic representation of the composition of proteins


(a)

(b)

Fig. 2. Examples of the (a) secondary, and (b) tertiary structures of proteins using a phone cord.

- *Peripheral membrane proteins* which do not span the membrane but are adjacent to it.

- *Membrane proteins* embedded in the lipid bilayer of cell membranes, where signal transduction pathways are activated across the membrane in response to an activation by a binding molecule, ligand or physical stimuli. Many hormone receptors and neurotransmitter receptors are membrane receptors.

- *Intracellular proteins* are often present in the cell nucleus and play a role in gene expression.

One the most relevant proteins for our interest are *membrane proteins* which are specialized in outer signal reception. In particular, hydrophilic compounds which cannot pass the cell membrane because they are not soluble in a lipophilic fluid, and thus membrane proteins have two binding sites: one facing the exterior of the cell and another facing the interior of a cell. The way the membrane proteins work is the extracellular signal binds to the ligand-binding domain and induces a conformational change in the receptor that is transmitted through the membrane-anchoring domain onto the coupling domain localized at the inner face of the cell wall. Although the signal itself has physically not reached the interior of the cell, the signal message, by being converted to receptor form, leads to a cascade of intracellular biochemical consequences as if it had really entered the cell.

Membrane proteins are formed by polypeptide chains that cross the cell membrane from side to side. Some membrane proteins have a single polypeptide chain but it is much more common that they are composed of seven chains and known as Seven Transmembrane proteins (7TM) or as Guanine nucleotide-binding protein-coupled receptors (GPCRs) for the Guanine nucleotide which is linked to their cytoplasmic side and gets released upon signal reception. The importance of 7TM/GPCRs is enormous provided they are the sensory element in processes as important as smell, taste, vision, neurotransmission, control of blood pressure, viral infection or cell growth or embryogenesis within others. And it is such that it is very common that health disorders are associated to problems and malfunctioning of 7TM/GPCRs, as a matter of fact 30% of all approved drugs are designed to target 7TM/GPCRs proteins.

Some *peripheral membrane* and *intracellular* proteins present metal atoms in their structure, this very important sub-group of proteins is termed *enzymes*, these proteins act as catalysers to accelerate specific chemical reactions that rapidly transform a reactant molecule present in the surroundings into new chemical products. Thus e*nzymes* produce a chemical response to the presence of selective substances. The combined action of the set of enzymes present in the cells forms the metabolic pathways of living beings and determines the substances living organisms are made of. E*nzymes* are vital component for the correct functioning of life, any *enzyme* disorder is cause of a disease, and there are numerous drugs that target *enzymes* to avoid their malfunctioning. Thanks to their high chemical selectivity some *enzymes* has been used to fabricate chemical biosensors.

Proteins suffer from *convergent evolution*. Their structure of proteins linked to a specific task forces them adopt specific functional shapes, and it seems that there must not be so many of these shapes, as it is common to find proteins with no genetic relation sharing structural characteristics even if the number of possible configuration is 10^{130} is almost endless [1]. This is the case of bactereorhodopsin (bR) and rhodopsin, both photosensitive proteins with no genetic relation and no similarities in the

aminoacid sequence which share remarkable structural and functional similarities: i) they use a derivative of vitamin A, the retinal, to sense the light, and ii) locate it on the same place, being both iii) made of seven transmembrane α-helixes (7TM). In practical terms they are so similar that they are considered functional equivalents, and this is so to such level that the bR is commonly used to study how GPCR proteins work even if bR is technically not a GPCR.

A.2. Polarizability of proteins

The electrostatic forces are the glue on which protein tertiary structure is maintained. It is also an active force used by proteins with charge transport functions (ion pumping proteins and enzymes) to move the charges through them using sequential configurational changes that produce a wave of electrostatic potential on which the charges ride (and that could be detected by electrical measurements).

Most of the electrostatic forces in proteins come from dipoles which scatter along the protein chain, these dipoles, when placed in aqueous solution, self-arrange and fold the protein, forming the protein tertiary structure, placing the areas with less number of dipoles, the hydrophobic areas, inside the protein in a water free area of dielectric constant 2-4 ε_0, and the areas with higher number of dipoles, polar/hydrophilic areas, exposed to the exterior in a wet area of dielectric constant ~80 ε_0 [2 3 4]. The time response of the folding is 10^{-6}-10^{-7} s and is slower than that of the rest of biological material, being characteristic of protein complexity.

A.3. Electron conduction in proteins

Electron conduction in solids requires a continuous large number of strongly interacting atomic orbitals that form electronic band structures, and that the number of electrons in the bands do not completely fill it. These two conditions are ruled by the strength of the overlapping between the orbitals and the extent of the delocalization of the electrons in the orbitals. In the case of proteins, the covalent bonds that link the consecutive aminoacids only get the electrons delocalized to the first neighbor and a delocalization band across the protein is not formed (Fig. 3 shows the electron density calculations). This makes that the only possible mechanisms for electrons to move inside proteins is moving from energy minimum to energy minimum separated by energy barriers which they typically cross by quantum tunnel effects.

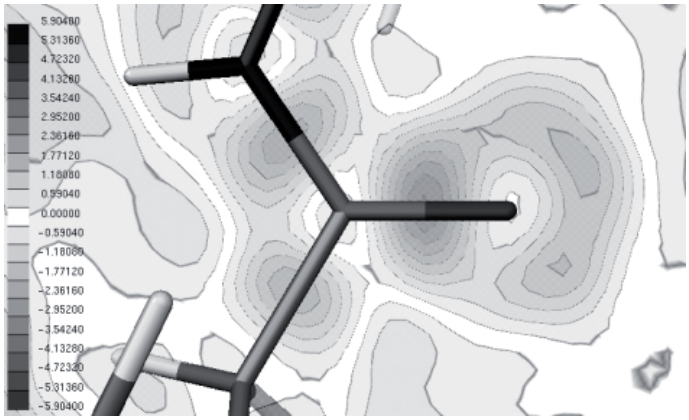

Fig. 3. Electron density in the plane of a peptide bond of the protein

Proteins harness the susceptibility (exponential dependence) of quantum tunnel to energy and distance variations to control the tunneling electron charge movement between the areas of the protein in close proximity, controlling both the rates and pathways of charge transport by small configurational changes. This approach is highly versatile, and it allows for a precise control of the long distance movement of electrons using a variety of cooperation effects between the local regions of the proteins,

the protein can then select the mechanism that best adapts to its needs and its environment. These transport routes are complex and are not yet well understood, but thanks to the use of SPM techniques and the study of Metal-Protein-Metal systems it has been possible to recognize several of these long distance transport mechanisms:

- *Direct non-resonant tunneling* has been recognized in two proteins systems, the redox proteins Plastocyanin[5] and the Azurin[6] that contain metal atoms in their structure. At this type of transport the wavefunction of the incoming electrons is maintained across the entire protein system, the protein acts as a single energy barrier, and controls the electron transport tuning the characteristics of the barrier, i.e. its shape and height.

- *Double stage tunnelling* through the protein system has been associated to the electron transport through the bacterorhodopsin (bR) [7], it has been suggested that there are two stages in the electron transport across this protein, one from first electrode to the retinol, and another from the retinol to the second electrode. This suggestion is a consequence of the strong dependence ~ 300 % of the electron flow crossing the bR on a small structural conformation changes of 0.3 nm, equivalent to about 6 % of the size of the proteins, which is hardly compatible with *non-resonant direct tunnelling*.

- *Poole-Frenkel* mechanism has been recognized on the redox proteins reverse transcriptase (RT) [8] and haemoglobin [9]. In this mechanism the electron trapped in energy minima in the protein are able to escape the minima by thermal emission, this creates a current flow based in the hopping of electrons from trap to trap when an electric field is present. An important aspect of this type of mechanism is that it is highly dependent on temperature, fact which could have important biological consequences.

-Three other types of conduction mechanisms *photovoltaic effect*, *tunnelling to surface vibronic and delocalized states*, and *semiconduction* have been associated to the electron transport in photosystem II redox proteins [10], a protein with an active function in photosynthesis. At this

time the precise model for electron transport sequence in the photosystem II is highly unknown, what is clear is that it is a fairly complex process.

A.4. References

1 T. F. Smith and H. J. Morowitz, "Between History and Physics," Journal of Molecular Evolution **18** (4), 265-282 (1982).

2 D. Rosen, "Dielectric Properties of Protein Powders with Adsorbed Water," Transactions of the Faraday Society **59** (489), 2178-& (1963).

3 S. Bone and R. Pethig, "Dielectric Studies of the Binding of Water to Lysozyme," Journal of Molecular Biology **157** (3), 571-575 (1982).

4 S. Bone and R. Pethig, "Dielectric Studies of Protein Hydration and Hydration-Induced Flexibility," Journal of Molecular Biology **181** (2), 323-326 (1985).

5 L. Andolfi, A. R. Bizzarri, and S. Cannistraro, "Electron tunneling in a metal-protein-metal junction investigated by scanning tunneling and conductive atomic force spectroscopies," Appl Phys Lett **89** (18), 183125 (2006).

6 J. W. Zhao, J. J. Davis, M. S. P. Sansom et al., "Exploring the electronic and mechanical properties of protein using conducting atomic force microscopy," J Am Chem Soc **126** (17), 5601-5609 (2004).

7 Y. D. Jin, N. Friedman, M. Sheves et al., "Bacteriorhodopsin (bR) as an electronic conduction medium: Current transport through bR-containing monolayers," Proceedings of the National Academy of Sciences of the United States of America **103** (23), 8601-8606 (2006).

8 S. A. Campbell, J. R. Smith, H. Jungblut et al., "Protein imaging on a semiconducting substrate: A scanning tunnelling microscopy investigation," Journal of Electroanalytical Chemistry **599** (2), 313-322 (2007).

9 D. Sarkar and T. N. Misra, "Direct-Current Electrical Characteristics of Hemoglobin Doped with Beta-Carotene," Journal of the Chemical Society-Faraday Transactions **88** (1), 53-56 (1992).

[10] P. B. Lukins, "Direct observation of semiconduction and photovoltaic behaviour in single molecules of the Photosystem II reaction centre," Chem Phys Lett **321** (1-2), 13-20 (2000).

[11] J. Shin, P. Bhattacharya, Y. Hao-Chih et al., "Low-power bacteriorhodopsin-silicon n-channel metal-oxide field-effect transistor photoreceiver," Opt Lett **Vol. 32** (5), 500 (2007).

List of publications

I. Refereed journal publications

'Nanobiosensors based on individual olfactory receptors' V. Akimov, E. Alfinito, J. Bausells, I.V. Benilova, **I. Casuso**, A. Errachid, G. Ferrari, L. Fumagalli, G. Gomila, J. Grosclaude, Y. Hou, N. Jaffrezic-Renault, C. Martelet, E. Pajot-Augy, C. Pennetta, M.A. Persuy, M. Pla-Roca, L. Reggiani, S. Rodriguez Segui, O. Ruiz, R. Salesse, J. Samitier, M. Sampietro, A.P. Soldatkin, J. Vidic, G. Villanueva 2007 **Analog Integrated Circuits and Signal Processing** (accepted)

'Nanoscale electrical conductivity of the purple membrane monolayer' **I. Casuso**, L. Fumagalli, J. Samitier, E. Padrós, L. Reggiani, V. Akimov, G. Gomila 2007 **Physical Review E** 76 041919.

'Electron transport through supported biomembranes at the nanoscale by conductive atomic force microscopy' **I. Casuso**, L. Fumagalli, J. Samitier, E. Padrós, L. Reggiani, V. Akimov, G. Gomila 2007 **Nanotechnology** 18 465503.

'Nondestructive thickness measurement of biological layers at the nanoscale by simultaneous topography and capacitance imaging' **I. Casuso**, L. Fumagalli, E. Padros, G. Gomila 2007 **Applied Physisics Letters** 91 063111.

'Immobilization of olfactory receptors onto gold electrodes for electrical biosensor' **I. Casuso**, M. Pla-Roca, G. Gomila, J. Samitier, J. Minic, M. A. Persuy, R. Salesse, E. Pajot-Augy 2007 **Materials Science and Engineering C** (accepted)

'AC and DC electrical imaging of biosamples at the nanoscale by Atomic Force Microscopy', **I. Casuso**, L. Fumagalli, G. Ferrari, M. Sampietro, E. Padrós, J. Samitier, G. Gomila 2007 **Journal of Physics. Conference Series** 61 185.

'Deflection-voltage curve modelling in atomic force microscopy and its use in DC electrostatic manipulation of gold nanoparticles', J. Toset, **I. Casuso**, J. Samitier, G. Gomila 2006 **Nanotechnology** 18 15503.

'Nanoscale capacitance imaging with attofarad resolution using ac current sensing atomic force microscopy', L. Fumagalli, G. Ferrari, M. Sampietro, **I. Casuso,** E. Martínez, J. Samitier G Gomila 2006 **Nanotechnology** 17 4581.

'Advances in the production, immobilization, and electrical characterization of olfactory receptors for olfactory nanobiosensor development', G. Gomila, **I. Casuso**, A. Errachid, O. Ruiz, E. Pajot, J. Minic, T. Gorojankina, M.A. Persuy, J. Aioun, R. Salesse, J. Bausells, G. Villanueva, G. Rius, Y Hou, N. Jaffrezic, C. Pennetta, E. Alfinito, V. Akimov, L. Reggiani, G. Ferrari, L. Fumagalli, M. Sampietro, J. Samitier 2006 **Sensors and Actuators B-Chemical** 16(1-2) 66-71.

II. Book chapters

'Probing electrical transport properties at the nanoscale by current-sensing atomic force microscopy' L. Fumagalli, **I. Casuso**, G. Ferrari, G Gomila, 2007 **Applied Scanning Probe Methods**, Springer.

III. Conference communications

April 2007, Barcelona, Spain. **Poster communication** *'Impedance imaging of biosamples at the nanoscale by Atomic Force Microscopy'*. AFM Biomed Conference.

September 2006, Murcia, Spain, **Poster communication** *'AFM DC+AC electrical characterization of Purple Membrane (PM) for biosensor applications'*, Spanish congress of Tunnel and Atomic Force Microscopies.

July 2006, Basel, Switzerland, **Oral communication** '*DC and AC electrical characterization of biological samples by AFM*', ICN+T 2006.

June 2006, San Francisco, USA, **Oral communication** '*DC and AC electrical characterization of biological samples by AFM*', NanoBio 2006.

February 2006, Linz, Austria, **Oral communication** '*Electrical characterization of bio-sensitive elements by AFM'*, Advances in Single-Molecule Research for Biology & Nanoscience.

September 2005, Oviedo, Spain, **Poster communication** '*AFM imaging of lipidic nanosomes containing Olfatory Receptors for biosensor applications*', Trends in Nanotechnology 2005.

March 2005, Barcelona, Spain, **Poster communication** *'AFM DC electrical characterization of Purple Membrane (PM) for biosensor applications'*, 2nd NanoSpain Workshop.

September 2004, Vic, Spain, **Oral communication** *'Electrical Conduction Through Bacterio-Rhodopsin Layers'*, Spanish congress of Tunnel and Atomic Force Microscopies.

March 2004 San Sebastian, Spain, **Oral Communication**, *'Advances towards the development of scanning probe microscopy for the electrical characterization of biological samples'* 1st NanoSpain Workshop.

September 2003, Salamanca, Spain, **Poster communication** *'Atomic Force Microscopy for Electrical Characterization of Biological Samples'*, Trends in Nanotechnology 2003.